UNIVERSITÀ DEGLI STUDI DI CAMERINO

School of Advanced Studies

DOCTORAL COURSE IN

COMPUTER SCIENCE AND MATHEMATICS

XXXV cycle

MONITORING OF CULTURAL HERITAGE BUILDINGS IN SEISMIC AREA

PhD Student
Leonardo Cipriani

Supervisor
Prof. Andrea Dall'Asta

Co-supervisor
Prof. Fabrizio Gara

Co-supervisor
Prof.ssa Laura Ragni

Summary

Introduction

I.1 Research context

Architectural heritage groups a wide number of historical constructions such as churches, towers, buildings, bridges, and fortresses, and all of them represent a focal point of the community's cultural identity. Along the centuries, indeed, a series of actions have been done to preserve their integrity and consequently to enhance the value of the cultural heritage for humanity.

Unfortunately, as stated in [Doglioni et al. 1994] [3], [Canuti et al. 2016] [1], [Despotaki et al. 2018] [2], and [Pavia et al. 2021] [4], such architectural cultural heritage is characterized by both structural and typological vulnerabilities often responsible of their poor performance to actions related to extreme events, like earthquakes, being it usually designed for gravity actions. Therefore, the analysis of the seismic vulnerabilities represents a relevant step for choosing and designing proper retrofitting and preservation strategies.

An integrated approach is required to know these sources of vulnerability, and different disciplines provide essential contributions: historic investigations of the construction evolution; geometric and material surveys of the constructions; in situ experimental testing and characterization of the materials; structural modelling and seismic analysis. Given the intrinsic difficulties that structural engineers must face when modelling heritage buildings, non-invasive experimental testing methods are valuable tools to provide support in the identification of the structural characteristics of a building. Among the various possibilities for non-invasive experimental tests, this PhD thesis refers to these ones that can characterize the response of the structure under service conditions, commonly referred as Operational Analysis (OA). As common practice these tests are separated in dynamic and static tests. Regarding dynamic tests, the technique and methodology of Operational Modal Analysis (OMA), e.g. [Brinker and Ventura – 2015] [5], [Ranieri and Fabbrocino – 2014] [6], is a very effective tool for structural identification and for model updating to support model-based simulations for the prediction of the seismic response of heritage constructions as well as for the calibrations of advanced seismic upgrading interventions. As regards instead the static tests, e.g. [Kita et all. 2018] [37], [Cavalagli et all. 2017] [43], [Ramos et all. 2012] [38] and [Lorenzoni et all. 2015] [44], together with the dynamic tests, they give a better interpretation of how the structure has been behaves under earthquakes or extreme events making in light the deficiency of the structural system in order to make a more realistic finite element model (FEM) of the structure.

In a wider comprehensive view, these analysis techniques provide a better knowledge of the structural response of cultural heritage in their operational conditions, helping in characterizing their seismic

response by the evaluation of the modal properties' changes (i.e., dynamic response), and in characterizing the evolution of kinematic mechanisms such as the over-turning mechanisms (i.e., static response). These results, inside the optical of structural health monitoring, can make in light outcomes both in modal properties and in displacement measures that can suggest potentials phenomenon of damage that may arise.

For this reason, the design of embedded monitoring systems that provide either a real-time and periodic information about the structural integrity and performance is a necessary activity to provide an insight on the structural health state of cultural heritage and to characterise the seismic response.

I.2 Objectives of the PhD Thesis

This PhD Thesis seeks to design an embedded monitoring system that acquire both dynamic physical and static quantities to identify the structural response over-time, either in operational conditions, and during seismic events including potentially destructive ones, to develop an automatic data analysis process that assesses the properties that describe the response of the structure such as modal properties which natural frequencies, modal shapes and modal damping integrated with static monitoring measures such as displacement measured across the cracks.

The innovative procedures developed within this work aims at automatically selecting the seismic evets input that can give a modification on the structural response within the data acquired through continuous monitoring, exploiting information available from the Italian National Institute of Geophysics and Volcanology (INGV) relevant to seismic events.

Specifically, the objectives of this PhD thesis are:

- to select the most effective monitoring system by considering specific problems concerning historical buildings and the available post processing data techniques to automize the analysis process.
- to set up a real-time process that continuously acquire data from different types of sensors and save them in a cloud server for the successive analyses.
- to select the seismic events occurred that may have changed the structural response, evaluating the in site expected shaking intensity through a calibration of a specific attenuation law based on data available from Italian National Institute of Geophysics and Volcanology (INGV) relevant to seismic events.to develop a tool that processes the acquired data using an efficient identification algorithm coupled with a clustering analysis.

- to validate the developed tools in two case-studies the Portico da Varano of Ducal Palace, and the Santa Maria in Via Church, both located in the city of Camerino, severely stroked by the 2016 central Italy seismic sequence.

I.3 Organization of the PhD Thesis

This dissertation is divided into four chapters. Chapter 1 introduces the theoretical bases concerning the dynamic problem of a structural system and a list of the available dynamic identification methods. The various steps to follow for developing the Stochastic Subspace Identification algorithm, where the data are driven by the output covariance, the SSI/Cov, and the basis to perform a clustering analysis are presented. Finally, the subchapter 1.4, aims at describing the necessary fixed points to be analysed in order to describe the response of a historical building.

In Chapter 2 the main and fundamental steps, necessary to design and to install an embedded monitoring system, are described.

In Chapter 3 the analysis path followed by process that has been developed and the proposal for a new approach to characterize the structural response to low energy earthquakes is described.

In Chapter 4 the two case-studies analysed are presented. The first is the Portico da Varano, an architectural element of the Ducal Palace in Camerino, in which the tool developed within this PhD Thesis has been applied and validated. The second is the Santa Maria in Via Church in Camerino, analysed in cooperation with the DICEA department of Università Politecnica delle Marche.

1 Overview of Structural Health Monitoring

1.1 Introductory concepts

The term structural health monitoring (SHM) refers to the process of implementing a damage detection strategy that involves the observation of a structure over time using periodically spaced dynamic response measurements, the extraction of damage-sensitive features from these measurements and the statistical analysis of these features [Farrar and Worden – 2013] [7]. The output of this process is a periodically updated information regarding the ability of the structure to continue to perform its intended function, considering the inevitable ageing and degradation of materials as well as the daily and seasonal changes in the environmental conditions. In addition, after an unusual event, such as an earthquake, SHM could be used for rapid condition screening, to provide, in near real time, objective data-base reliable indications on the performance of the system during the event and its integrity.

For his preliminary development, SHM inherits methodologies and approaches in the field of modal testing, i.e., experimental determination of the vibration response of a monitored structure as a ground base to verify models and predictions of its dynamic properties (natural frequencies, mode shapes and damping ratios) and relevant geometric, loading, inertial, and mechanical material parameters to them correlated [Ewins – 2000] [8]. These techniques give more attention to the analysis of the dynamic response of a structure as opposed to its static response, given the involvement of a larger set of parameters (inertial properties, stiffness, damping) at a global level while static response measurements can only be correlated to stiffness, mostly at a local level.

However, how described in some literature studies [Kita et all. 2018] [37], [Cavalagli et all. 2017] [43], [Ramos et all. 2012] [38] and [Lorenzoni et all. 2015] [44] to acquire a detailed knowledge of the response of the damaged cultural heritage buildings, is necessarily to integrate the dynamic response with the static ones to find a correlation between the parameters that describes the dynamical response with the static measure, i.e., the opening and closing of cracks and the environmental conditions.

The following sections deal primarily with the theoretical basis of OMA, the procedure for the post processing data, the related issues for the monitoring of historical buildings and the effects of environmental conditions on the acquired data.

1.2 Dynamic Monitoring

1.2.1 Definition of the dynamic problem

The basic model used to describe the dynamic behaviour of a civil structure is the Linear Sigle Degree of Freedom (SDOF) model (Figure 1a) [9], where the response in the time domain, is described by a second order differential equation.

$$m\ddot{y}(t) + c\dot{y}(t) + ky(t) = f(t) \tag{1.2-1}$$

were $y(t)$ is the coordinate that describes the displacement of the system, $f(t)$ is the external excitation and m, c, and k are the the mass, damping and stiffness respectively of the system.

The obtained results can be used to describe more complex multi degree of freedom (MDOF) models (Figure 1b) [9], by considering the system as a superposition of a number of SDOFs using the modal decomposition approach. The equation of motion of a Multi Degree of Freedom (MDOF) system characterized by *n* degrees of freedom can be expressed as

$$\mathbf{M}\ddot{\boldsymbol{Y}}(t) + \mathbf{C}\dot{\boldsymbol{Y}}(t) + \mathbf{K}\boldsymbol{Y}(t) = \boldsymbol{F}(t) \tag{1.2-2}$$

where $\mathbf{M}$, $\mathbf{C}$, $\mathbf{K} \in \mathbb{R}^{nxn}$ are the mass, damping and stiffness matrices, $\boldsymbol{F}(t) \in \mathbb{R}^{nx1}$ is the excitation force and $\boldsymbol{Y}(t) \in \mathbb{R}^{nx1}$ is the response of the system at continuous time, n is the number of masses that constitutes the system.

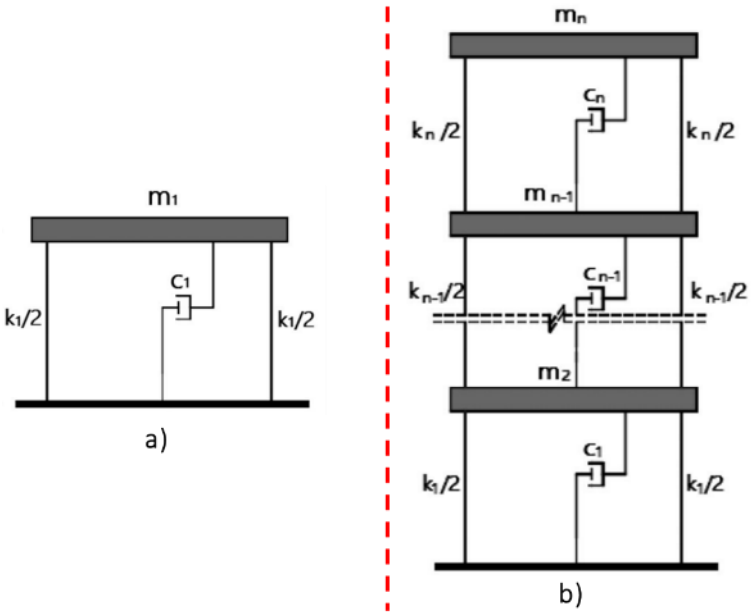

Figure 1: Simple representation of a) SDOF model b) MDOF model

Starting from Equation (1.2-2) and operating some mathematical derivations, it is possible to transform the second order differential equation of motions into a set of first order differential equations by expressing the problem in the state space representation.

Rewriting the system of differential equation in canonical forms

$$\ddot{\mathbf{Y}}(t) + \mathbf{M}^{-1}\mathbf{C}\dot{\mathbf{Y}}(t) + \mathbf{M}^{-1}\mathbf{K}\mathbf{Y}(t) = \mathbf{M}^{-1}\overline{\mathbf{B}}\boldsymbol{u}(t) \tag{1.2-3}$$

where the vector force $\boldsymbol{F}(t)$ is factorized into the product of matrix $\overline{\mathbf{B}}$, which defines the location of inputs, and the vector $\boldsymbol{u}(t)$ describing the time variation.

Introducing the state vector $\boldsymbol{s}(t) = \begin{Bmatrix}\dot{\mathbf{Y}}(t)\\ \mathbf{Y}(t)\end{Bmatrix}$ of the system, the equation of motion (1.2-3) can be rewritten as

$$\dot{\boldsymbol{s}}(t) = \mathbf{A}_c\boldsymbol{s}(t) + \mathbf{B}_c\mathbf{u}(t) \tag{1.2-4}$$

where

$$\mathbf{A}_c = \begin{vmatrix}-\mathbf{M}^{-1}\mathbf{C} & -\mathbf{M}^{-1}\mathbf{K}\\ \mathbf{I} & \mathbf{0}\end{vmatrix} \tag{1.2-5}$$

$$\mathbf{B}_c = \begin{vmatrix}\mathbf{M}^{-1}\overline{\mathbf{B}}\\ \mathbf{0}\end{vmatrix} \tag{1.2-6}$$

In the Equation (1.2-4), so called observation equation, matrix $\mathbf{A}_c$ and $\mathbf{B}_c$ represents the state matrix and the input matrix respectively; in the notation, the subscript c denotes continuous time. This representation of the dynamical problem is very common to relate the response of a dynamic system with the measured outputs [Ranieri and Fabbrocino – 2014] [6].

In practical applications only a limited number of DOF are monitored and, therefore, the output measurements (accelerations, velocity or displacements) are evaluated in $l<n$ locations. Under these assumptions, the observation equation can be defined as

$$\boldsymbol{y}_l(t) = \mathbf{C}_c\{\boldsymbol{s}(t)\} + \mathbf{D}_c\{\boldsymbol{u}(t)\} \tag{1.2-7}$$

where $\mathbf{C}_c$ is the output influence matrix, and $\mathbf{D}_c$ is the direct transmission matrix define by

$$\mathbf{C}_c = \left|\mathbf{C}_v - \mathbf{C}_a\mathbf{M}^{-1}\mathbf{C} \quad \mathbf{C}_d - \mathbf{C}_a\mathbf{M}^{-1}\mathbf{K}\right| \tag{1.2-8}$$

$$\mathbf{D}_c = \mathbf{C}_a\mathbf{M}^{-1}\overline{\mathbf{B}} \tag{1.2-9}$$

Matrices $\mathbf{C}_a$, $\mathbf{C}_v$ and $\mathbf{C}_d$ describes the location of the acceleration sensors, velocity sensors, and displacement sensors, respectively.

The mathematical tools to evaluate the experimental dynamical properties of a dynamic system, aims to assess the state matrix of the system $\mathbf{A}_c$ that contains all the system properties that control the dynamical response of the system.

1.2.2 Methods for Dynamic Identification

Dynamical identification methods can be grouped into two families, the experimental modal analysis (EMA) and the operational modal analysis (OMA), on which the main differences are on how the external forces are considered in the state space model of the dynamic system.

The first of these dynamical identification methods, the experimental modal analysis (EMA) [Ewins – 2000] [8], [Maia and Silva – 1997] [10], are the traditional identification techniques that extract modal parameters rely on the input and output data. Here, the structures are excited by one or several external loads, given by artificial excitation thought by hammers, shakers, hanging masses, jacks, and the modal parameters of the system can be identified from the input–output data by an Output/Input relation that returns the response function called Frequency response Function (FRF) in the frequency domain. The developed algorithms to evaluate the modal properties of the structures from EMA analysis can be developed in the time domain or in the frequency domain. Each of these approaches differ by the type of analysis, such as single input – single output (SISO), single input – multiple output (SIMO) and multiple input – multiple output (MIMO) and by the field estimate (local or global).

Among the algorithms defined in the frequency domain, that represent the earliest methos developed, there is the peak amplitude method (PPM), the circle-fit method (CFM), the Nonlinear Least Squares Frequency Domain (LSFD) and the Rational Fraction Polynomials (RFP) [Ewins – 2000] [8] and [Brincker and Ventura – 2015] [5]. On the other side, among the algorithms defined in the time domain are the logarithmic decrement method, the least square complex exponential methos

(LSCEM) [Brown et all – 1979] [12], the eigensystem realization algorithm (ERA) [Juang and Pappa – 1985] [11] and the autoregressive-moving average model (ARMA) [Box et all – 2008] [13].

However, experimental modal analysis is not suited for large civil engineering structures because it is unpractical and too expensive to use an artificial excitation given the size and mass involved and the required power consumption. For this reason, interest moved towards identification algorithms able to extract the modal parameters from structural response data under operational conditions, i.e., uncontrolled dynamic input. Such approach is defined operational modal analysis (OMA). In the technical literature there are various OMA algorithms developed in time domain and in frequency domain [Rainieri - Fabbrocino – 2014], [Brincker and Ventura – 2015], [V. Gattulli – 2016] [14].

The most common techniques utilized in OMA are: natural excitation technique (NExT) [James et all – 1995] [15]; random decrement technique (RDT) [Brincker and Amador 2022] [16] ; frequency domain decomposition (FDD) [Brincker et all - 2001] [17], polyreference least-squares frequency-domain estimates (p_LSCF) [Guillaume et all. - 2003] [18], the wavelet transform [Lardies and Gouttebroze – 2002] [19] to make a time-frequency analysis, and well know and largely used method, the stochastic subspace identification (SSI) [Van Overschee and De Moor – 1996] [20] , [Peters and de Roeck – 1999] [21], [Zhang et all. - 2012] [22], [Rainieri and Fabbrocino – 2014] [6], [Brincker and Ventura – 2015] [5], in Figure 2 is shown an outline of the available SSI algorithms.

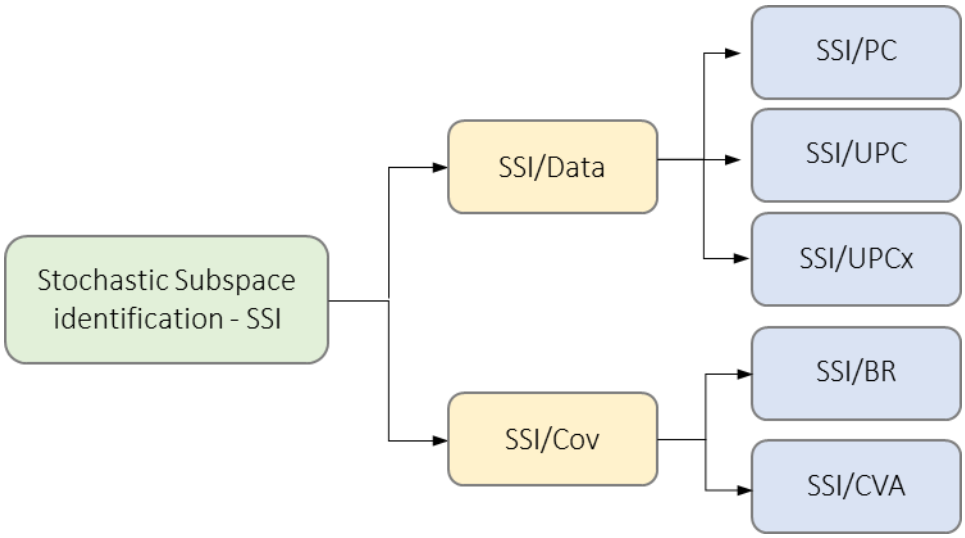

Figure 2: Outline of the available SSI algorithms

OMA has received an incremental interest and found many applications in the past decade because the measurements can be carried out under operational conditions without service interruptions, opening the way to continuous permanent monitoring, including the analysis of different scenarios before and after extreme events could occur, such as earthquakes, gaining information on possible damage conditions.

To this purpose, for SHM of cultural heritage buildings, subsequently discussed in Chapter 4, an automated OMA procedure was developed where the identification procedure is made by the SSI/Cov algorithm.

1.2.3 SSI/Cov – Review

As preliminary operation, the representation of the dynamical problem in the state space model by variables in state space defined in Equation (1.2-4) and Equation (1.2-7) are for a continuous-time state-space model. An important property of this model is the existence of an infinite number of state-space representation for a given system and each one is referred to as a realization [Rainieri, G. Fabbrocino – 2014] [6].

The experimental test yield measurements taken at discrete time instant therefore allows to establish only one of these realizations indeed the continuous-time state-space model has to be converted to discrete-time state-space model (Equation (1.2-4) and Equation (1.2-7)), where for a given sampling period Δt, the continuous-time equations can be discretized and solved at all discrete time instants $t_k = k\Delta t, k \in N$

$$\boldsymbol{s}_{k+1} = \mathbf{A} \cdot \boldsymbol{s}_k + \mathbf{B} \cdot \boldsymbol{u}_k \tag{1.2-10}$$

$$\boldsymbol{y}_k = \mathbf{C} \cdot \boldsymbol{s}_k + \mathbf{D} \cdot \boldsymbol{u}_k \tag{1.2-11}$$

where $\boldsymbol{s}_k$ is the discrete-time state vector, $\boldsymbol{u}_k$ is the sampled input, $\boldsymbol{y}_k$ is the sample output. In the Equations (1.2-10) matrices **A** and **B** represents the discrete state matrix and the discrete input matrix respectively, while in the Equation (1.2-11) matrices **C** and **D** represents the discreate output matrix and the direct transmission matrix. Between these discrete quantities and the continuous the relationship are

$$\mathbf{A} = e^{\mathbf{A}_c \cdot \Delta \boldsymbol{t}} \tag{1.2-12}$$

$$\mathbf{B} = (\mathbf{A} - \mathbf{I}) \cdot {\mathbf{A}_c}^{-1} \cdot \mathbf{B}_c \tag{1.2-13}$$

$$\mathbf{C} = \mathbf{C}_c \tag{1.2-14}$$

$$\mathbf{D} = \mathbf{D}_c \tag{1.2-15}$$

For a detailed treatise of this seen [Rainieri and Fabbrocino – 2014] [6], [Peeters and De Roeck – 1999] [21].

1.2.3.1 State Space Model with Stochastic Variables

The model described above is a deterministic model where the response of the system is driven by a deterministic input. However, deterministic model is not able to exactly describe real measurements, where the experimental data are affected by noise. For this reason, stochastic components must be necessarily included to describe the uncertainties due to the actual measurement data.

More in detail, in the discrete-time state-space model it is added the process noise $\boldsymbol{w}_k$, intended to consider the disturbance and model inaccuracies and the measurement noise, and $\boldsymbol{v}_k$, to considering the sensor inaccuracies.

Introducing the stochastic components in the Equations (1.2-10) and Equation (1.2-11), the discrete-time state-space model with the stochastic components assumes the form

$$\boldsymbol{s}_{k+1} = \mathbf{A} \cdot \boldsymbol{s}_k + \mathbf{B} \cdot \boldsymbol{u}_k + \boldsymbol{w}_k \tag{1.2-16}$$

$$\boldsymbol{y}_k = \mathbf{C} \cdot \boldsymbol{s}_k + \mathbf{D} \cdot \boldsymbol{u}_k + \boldsymbol{v}_k \tag{1.2-17}$$

In the context of Structural Health Monitoring, where the structure behaviour evaluation is performed by OMA, the terms that describe the input are not considered (immeasurable input). Therefore, the response of the system is generated only by the two stochastic processes and the following discrete-time stochastic state-space model is obtained:

$$\boldsymbol{s}_{k+1} = \mathbf{A} \cdot \boldsymbol{s}_k + \boldsymbol{w}_k \tag{1.2-18}$$

$$\boldsymbol{y}_k = \mathbf{C} \cdot \boldsymbol{s}_k + \boldsymbol{v}_k \tag{1.2-19}$$

In the Equation (1.2-18) the state matrix $\mathbf{A}$ transforms the current state of the system $\boldsymbol{s}_k$ in the next state $\boldsymbol{s}_{k+1}$, while in Equation (1.2-19) the product of the observation matrix $\mathbf{C}$ with the state vector provides the observable part of the dynamics of the system and the response vector $\boldsymbol{y}_k$ is given by the observable part of the state plus the measurement noise.

The noise components, processes and measurement noise, are both immeasurable and they are assumed to stationary white noise processes with zero mean, and with covariance matrices defined by

$$\mathbf{E}\left[\begin{pmatrix}\boldsymbol{w}_p\\ \boldsymbol{v}_p\end{pmatrix}\cdot\begin{pmatrix}\boldsymbol{w}_q^T & \boldsymbol{v}_q^T\end{pmatrix}\right]=\begin{pmatrix}\mathbf{Q} & \mathbf{S}\\ \mathbf{S}^T & \mathbf{R}\end{pmatrix}\cdot\boldsymbol{\delta}_{pq} \tag{1.2-20}$$

$$\mathbf{R}_i=\mathbf{E}[\{\boldsymbol{s}_k\}\{\boldsymbol{s}_k\}^T] \tag{1.2-21}$$

were $\boldsymbol{\delta}_{pq}$ is the Kronecker function ($\boldsymbol{\delta}_{pq}=1$ if $p=q$, 0 otherwise), and the matrices $\mathbf{Q}\in\mathbb{R}^{n\times n}$, $\mathbf{S}\in\mathbb{R}^{n\times l}$ and $\mathbf{R}\in\mathbb{R}^{l\times l}$ are the covariance matrices of the noise sequence. In the space dimension *n* is the number of states or the model order value, *l* is number of outputs, *p* and *q* are two arbitrary time instants. With this assumption in the OMA analysis the system response, in the state-space model is represented by a zero mean Gaussian process and the output covariance matrices Equation (1.2-21), carry all the information to describe the process.

The exhaustive treatise about the Stochastic Subspace Model, the analytical relation to evaluate the covariance matrices of the noise sequence and fundamental relations between all quantities are thorough described in [Rainieri and Fabbrocino – 2014] [6] and [Van Overshee and De Moor – 1996] [20].

1.2.3.2 Definition of the Toeplitz matrix

The definition of the Toeplitz matrix is the main step that leads at the evaluation of the state matrix **A**. The SSI-Cov method identifies a stochastic state-space model from the output data by the assess a covariance output matrix that under the assumption of a Gaussian stationary white noise with zero mean the covariance output matrix is equal to the output correlation matrix (1.2-22).

$$\left[\widehat{\boldsymbol{R}}_i\right]=\frac{1}{N-i}\cdot\left[\boldsymbol{Y}_{(1:N-i)}\right]\left[\boldsymbol{Y}_{(1:N)}\right]^T \tag{1.2-22}$$

where $\left[\boldsymbol{Y}_{(1:N-i)}\right]$ is obtained from the $l\times N$ output data matrix $[\boldsymbol{Y}]$ by removal the last *i* samples, vector $\left[\boldsymbol{Y}_{(1:N)}\right]$ is obtained from $[\boldsymbol{Y}]$ by removal the first *i* samples, $\left[\boldsymbol{Y}_{(1:N-i)}\right]$ is the unbiased estimate of the correlation matrix at time lag *i*, *N* is the numbers of points of the time series and *l* are the numbers of signals output.

The estimated correlations at different time lags are grouped into a Toeplitz matrix

$$\left[\mathbf{T}_{1|i}\right] = \begin{bmatrix} \left[\hat{R}_i\right] & \left[\hat{R}_{i-1}\right] & \cdots & \left[\hat{R}_1\right] \\ \left[\hat{R}_{i+1}\right] & \left[\hat{R}_i\right] & \cdots & \left[\hat{R}_2\right] \\ \vdots & \vdots & \ddots & \vdots \\ \left[\hat{R}_{2i-1}\right] & \left[\hat{R}_{2i-2}\right] & \cdots & \left[\hat{R}_i\right] \end{bmatrix} \tag{1.2-23}$$

which has $l_i \times l_i$ dimensions and each correlation matrix has dimensions $l \times l$.

The time lag value *i* and the model order value *n* are parameters that influence the size of the Toeplitz matrix because for the identification of a system of order *n*, the number of block rows *i* must fulfil the following condition:

$$l_i \geq n \tag{1.2-24}$$

The order of the system is not a priori known; an estimation of order can be obtained from the number of modes in the frequency range of interest by counting the number of peaks in the trace of the PSD matrix. Anyway, in the practical applications it is recommended to use a value of model order major about the number of peaks identified in the frequency range of interest to obtain a better resolution in the subsequential stabilization diagram.

1.2.3.3 Evaluation of the state matrix A

To established if the system is Observable (a state of the system is observable if the knowledge of input and output over a finite time interval completely determines the state) and Controllable (a state of a system is controllable if it can be reached from any initial state of the system in a finite time interval by some control actions) the rank of Toeplitz matrix must be equal to the model order value.

Evaluating the Singular Values Decomposition SVD of the weighted Toeplitz matrix

$$svd\left[\mathbf{W}_1\mathbf{T}_{1|i}\mathbf{W}_2\right] = [\mathbf{U}][\mathbf{\Sigma}][\mathbf{V}]^T \tag{1.2-25}$$

is possible to assess Observability and Controllability matrices. In the Equation (1.2-25), $\mathbf{W}_1$ and $\mathbf{W}_2$ are two weight matrices, which their formulation depends by the chosen algorithm [Van Overschee and De Moor – 1996] [20]. In the Equation (1.2-25), **T** is a non-singular matrix that determines one of the infinite equivalent realizations of the state-space model, **Σ** is a squared matrix of $n \times n$ dimention containing only the positive singular values arranged in descending order, while **U** and **V** are orthogonal matrices of $li \times n$ and $n \times li$ dimensions. In our application, the weighted matrices are equal to identity matrix $\mathbf{W}_1 = \mathbf{W}_2 = \mathbf{I}$, because the SSI/Cov BR (Balanced Realization) has been chosen as representative model of the system.

Therefore, based on what previously introduced, by splitting the SVD of the weighted Toeplitz matrix, is possible to evaluate the Observability [$\mathbf{O}_i$] and the Controllability [$\mathbf{\Gamma}_i$] matrices

$$\mathbf{O}_i = \mathbf{U} \cdot \mathbf{\Sigma}^{1/2} \cdot \mathbf{T} \tag{1.2-26}$$

$$\mathbf{\Gamma}_i = \mathbf{T}^{-1} \cdot \mathbf{\Sigma}^{1/2} \cdot \mathbf{V}^T \tag{1.2-27}$$

To the developed of tis algorithm, related at our case of study, has been chosen the [J.H. Yi, C.B. Yun – 2004] relation to define the controllability matrix is

$$\mathbf{O}_i = \mathbf{U} \cdot \mathbf{\Sigma}^{1/2} \cdot \mathbf{W}_1^{-1} \tag{1.2-28}$$

were the matrix **T** (Equation (1.2-26)) is assigned equal to the weighted matrix $\mathbf{W}_1$. Subsequently, it is possible to assess and evaluate the state matrix of the system **A** by an analytical expression

$$\mathbf{A} = \mathbf{O}_i^{1^+} \cdot \mathbf{O}_i^2 \tag{1.2-29}$$

that is related by the assessment of the pseudo inverse matrix of $\mathbf{O}_\mathrm{i}^1$**,** the observability matrix without the last l rows and the $\mathbf{O}_\mathrm{i}^2$ matrix, the observability matrix without the first l rows**.**

1.2.3.4 Stabilization Diagram

In this section we will talking about of the identification algorithm main outcome, that is the Stabilization Diagram plot. This one is a chart representation where the dynamical properties (i.e., natural frequencies, damping ratios and modal shapes) values are viewed as poles and physical to noise poles separation are made by mathematical rules on frequencies, damping ratio and modal shapes.

Eigenvalue Decomposition (EVD) of the state matrix **A** of the system is employed for natural frequencies assessment. Under the assumption that the discrete-time state model are related with their continuous-time, described in [Magalhães – 2010] [24] and [Magalhães and Cunha – 2011] [23], it can be applied the same rule by the continuous-time model to evaluate the dynamical resonant frequencies of the system.

$$\mathbf{A} = e^{\mathbf{A}_c \cdot \Delta \boldsymbol{t}} \tag{1.2-30}$$

where **A** is the time-discrete state space model matrix, $\mathbf{A}_\mathrm{C}$ is the time-continuous state space model matrix, and $\Delta\mathbf{t}$ is the time vector of the sampling interval.

More in detail, the modal properties of a continuous-time model is made by EVD of the $\mathbf{A_c}$ state space matrix hat gives the complex eigenvalue matrix $\boldsymbol{\Lambda_c}$ (1.2-32) where their sub-matrix $\boldsymbol{\Lambda}$ contains the $\boldsymbol{\lambda_k}$ eigenvalue related with the structure frequencies $\boldsymbol{\omega_k}$ and modal damping ratios $\boldsymbol{\xi_k}$

$$\mathrm{EVD}(\mathbf{A_c}) = \boldsymbol{\Psi} \cdot \boldsymbol{\Lambda}_c \cdot \boldsymbol{\Psi}^{-1} \tag{1.2-31}$$

$$\boldsymbol{\Lambda}_c = \begin{bmatrix} \boldsymbol{\Lambda} & 0 \\ 0 & \boldsymbol{\Lambda}^* \end{bmatrix} \Rightarrow \boldsymbol{\Lambda} = \begin{bmatrix} \ddots & & \\ & \lambda_k & \\ & & \ddots \end{bmatrix} \tag{1.2-32}$$

$$\lambda_k = -\xi_k \cdot \omega_k + i\omega_k \cdot \sqrt{1 - {\xi_k}^2} \tag{1.2-33}$$

where $\boldsymbol{\Lambda}^*$ is the complex conjugate matrix.

About discrete-time model, the modal frequencies operation evaluation, follow the same continuous-time model can be evaluate by

$$\mathrm{EVD}(\mathbf{A}) = e^{\boldsymbol{\Psi}\cdot\boldsymbol{\Lambda}_c\cdot\boldsymbol{\Psi}^{-1}\cdot\Delta\boldsymbol{t}} = \boldsymbol{\Psi} \cdot e^{\boldsymbol{\Lambda}_c\cdot\Delta\boldsymbol{t}} \cdot \boldsymbol{\Psi}^{-1} = \boldsymbol{\Psi} \cdot \boldsymbol{\Lambda}_c \cdot \boldsymbol{\Psi}^{-1} \tag{1.2-34}$$

where the eigenvalue sub-matrix assumes the form $\boldsymbol{\Lambda} = \begin{bmatrix} \ddots & & \\ & \mu_k & \\ & & \ddots \end{bmatrix}$

Eigenvalues μ_k of eigenvalue matrix $\boldsymbol{\Lambda}$ are related with the ones of continuous model by the following relation

$$\lambda_k = \frac{ln(\mu_k)}{\Delta t} \tag{1.2-35}$$

Then, from all eigenvalues λ_k only the elements with a positive imaginary part are taken to evaluate the structure natural frequencies f_k

$$f_k = \frac{Abs(\lambda_k)}{2\pi} \tag{1.2-36}$$

Finally, to have a complete modal properties structure description, the damping ratios are evaluated by the expression

$$\xi_k = -\frac{Re(\lambda_k)}{Abs(\lambda_k)} \tag{1.2-37}$$

and multiplication of the controllability matrix **C** with the eigenvector matrix **Ψ** related with positive imaginary part eigenvalue matrix **Λ** gives the observable components of modal shapes **ϕ**

$$\boldsymbol{\phi} = \mathbf{C} \cdot \boldsymbol{\Lambda}^{+} \tag{1.2-38}$$

where $\boldsymbol{\Lambda}^{+}$ is the state space matrix eigenvalue with positive imaginary part.

Is better to note that in this way, a state space model of order **n** provides modal parameters for **n/2** modes.

How shown in Figure 3, all these results can be collected in a matrix **P** where each element or pole contains dynamical properties information of the structure which are natural frequencies $\boldsymbol{f_k}$, damping ratios $\boldsymbol{\xi_k}$ and modal shapes **ϕ**.

$$\mathbf{P} \in \mathbb{R}^{n/2 \times n/2} = \begin{vmatrix} P_{1,1} & P_{2,1} & \cdots & P_{a,1} \\ 0 & P_{2,2} & & \\ \vdots & 0 & \ddots & \\ 0 & \cdots & 0 & P_{a,b} \end{vmatrix}$$

n/2 (horizontal) and n/2 (vertical) — where n/2 is the model order value

$\mathbf{P}_{a,b}$ with a = 1,...,n/2 and b = 1,…,x is the pole where take with himself the modal dynamical properties of the system.

Indeed, for each element $\mathbf{P}_{a,b}$ $\boldsymbol{f} = \begin{Bmatrix} f_1 \\ \vdots \\ f_b \end{Bmatrix}$ is the frequencies vector $\boldsymbol{\xi} = \begin{Bmatrix} \xi_1 \\ \vdots \\ \xi_b \end{Bmatrix}$ is the frequencies vector and $\boldsymbol{\phi} = \begin{Bmatrix} \phi_{11} \\ \vdots \\ \phi_{b,c} \end{Bmatrix}$ is the modal shapes vector with c = 1,...,l (number of sensors)

Figure 3: Representation of Identification algorithm outcome

Given that the system model order value is overestimate due to noise and model inaccuracies, not everything poles are related to real physical vibrational modes but also to spurious modes (e.g., noise modes or mathematical ones) without physical meaning, indeed with some expression that established the frequencies (1.2-39), damping ratio (1.2-40) and modal shapes (1.2-41) stable rule

$$\frac{|f(n) - f(n+1)|}{f(n)} < 0.01 \tag{1.2-39}$$

$$\frac{|\xi(n) - \xi(n+1)|}{\xi(n)} < 0.05 \tag{1.2-40}$$

$$1 - MAC(\{\boldsymbol{\phi}(n)\} - \{\boldsymbol{\phi}(n+1)\}) < 0.02 \tag{1.2-41}$$

It is possible to make a poles separation between physical to spurious ones for increasing model orders, this is the Stabilization Diagram.

In relationship (1.2-41) the stability information about modal shapes is given to a index that lies between 0 and 1 called Modal Assurance Criterion (MAC) defined by

$$MAC(\boldsymbol{\phi}_n^1, \boldsymbol{\phi}_n^2) = \frac{|\{\boldsymbol{\phi}_n^1\}^T\{\boldsymbol{\phi}_n^2\}|^2}{(\{\boldsymbol{\phi}_n^1\}^T\{\boldsymbol{\phi}_n^1\}) \cdot (\{\boldsymbol{\phi}_n^2\}^T\{\boldsymbol{\phi}_n^2\})} \tag{1.2-42}$$

$MAC(\boldsymbol{\phi}_n^1, \boldsymbol{\phi}_n^2) = 1$ perfect correlation between two vectors (stable)

$MAC(\boldsymbol{\phi}_n^1, \boldsymbol{\phi}_n^2) = 0$ inconsistent coherence between two vectors (no stable)

that give a quantitative comparison of modal vectors [Pastor at all – 2012] [25] and [Ranieri and Fabbrocino – 2014] [6]. In the Equation (1.2-42) $\boldsymbol{\phi}_n^1$ is the n-th vibrational mode of configuration 1 and $\boldsymbol{\phi}_n^2$ is the n-th vibrational mode of configuration 2.

More in detail the stabilization diagram construction is made by the comparison of the poles associated with a specific model order value (n+1) with other ones (n) obtained from a one-order lower model, only the poles that fulfill the stable criteria (1.2-39), (1.2-40) and (1.2-41), are labeled as stable. Physical vibrational mode of the structure is identified by the vertical alignment of stable poles how shown in Figure 4.

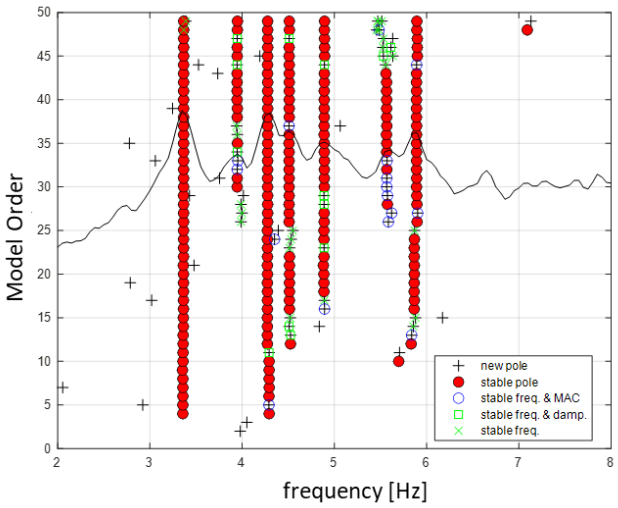

Figure 4: Stabilization Diagram from an OMA test – Portico da Varano, Camerino Ducal Palace.

About threshold values defined in stable expressions frequency, damping ratio and modal shape, they are not fixed values but can be specialized by the authors according to the structure type under analysis.

The MAC indices also give another relevant information about two different modal shapes coupling level Figure 5 a), indeed in an ideally configuration a perfect correlation is expected along the MAC matrix diagonal Figure 5 b).

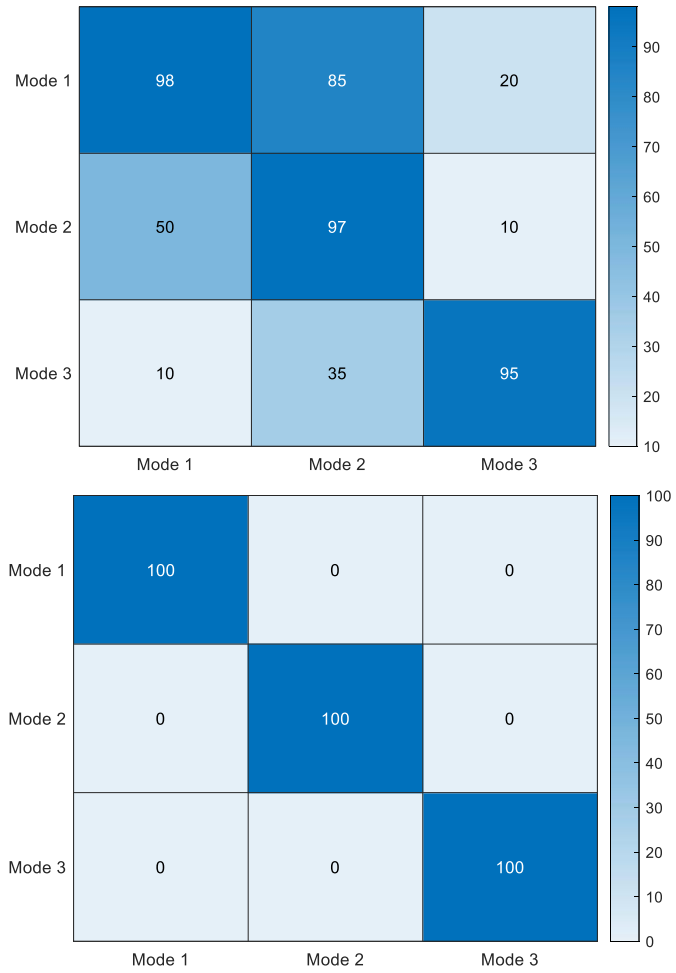

Figure 5: a) MAC matrix between modal shapes with hight coupling level b) MAC matrix between modal shapes without coupling, perfect correlation.

1.2.4 Clustering analysis

The reading of the Stabilization Diagram (Figure 4) to select the structural vibrational modes, usually is done by the technical Data analyst, but in order to a long term structural health monitoring, the target is to automate this decision making procedure given the higher number of measure data.

Inside this field, many scientists [Cabboi et all. 2017] [26], [Magalhaes et all. 2009] [27], [Ubertini et all. 2013] [28] have been developed different approaches taking advantage from the available Machine Learning procedures such as the "Clustering Analysis" that, applying specific comparison rule to a big set of data is possible to divide them in a series of bins, named cluster; each cluster is a big data subset that bring with it different properties identified by the data set.

With the term "Machine learning" [Talabis et all. 2015] [31] , you want to describe a series of operations or actions to acquiring skills (e.g., predict energy consumption, uncovering a hidden process and distinguishing the physical property to noise) from a data set. There are a lot of Machine Learning approaches that can be grouped in two families, the Unsupervised learning, where the process try to find recurrent behaviour or variables that a more relevant from a data set without labels values, the Supervised learning, where the process try to build a statistical models able to reproduce the labels and can make new predictions for these labels starting from a data set that describe instances with labels.

Clustering Analysis [Novoselsky and Kagan 2021] [29], [Saxena et all. 2017] [30] is an unsupervised learning that allows to discover hidden structures in a data set through a grouping data in clusters after the data similarity evaluation. Each cluster, as to be representative, should exhibit a high internal homogeneity (within the cluster) and high external heterogeneity (between the cluster).

Following a briefly description of the most common methodologies used to carry out a cluster analysis:

- K means clustering, a non-hierarchical procedure that asked to a prior definition of the number of clusters, k, is a computationally procedure very efficient, is able it is very at identifying clusters (Figure 6) [web link: K-means Clustering with Scikit-Learn - FreedomVC].

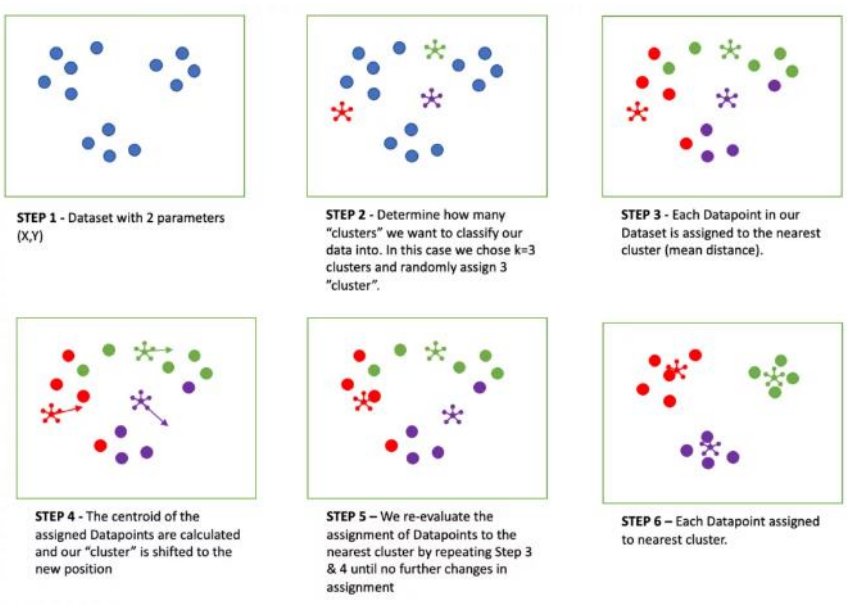

Figure 6 K means clustering.

- hierarchical clustering, a family of algorithms based on the construction of a hierarchy of a tree-like structure. At the beginning, each object is considered a cluster. In subsequent steps, the two closest clusters (or individuals) are combined into a new aggregate cluster, thus reducing the number of clusters by one in each step. Eventually, all individuals are grouped into one large cluster Figure 7 from [Magalhaes et all. 2009] [27]. Here we can choose two ways to perform a hierarchical clustering analysis:
    - agglomerative cluster analysis a bottom-up agglomeration methodology where clusters have sub-clusters, and so on. It starts where every object forms its own cluster and iteratively merges cluster into larger and bigger clusters. For the merging step, it finds the two clusters that are closest to each other and combines the two to create one cluster (Figure 7) [Magalhaes et all. 2009] [27]

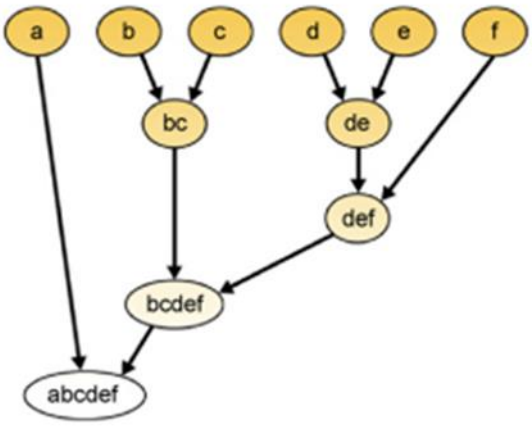

Figure 7: hierarchical agglomerative clustering

- divisive cluster analysis a top-down clustering methodology. The starting point is to consider that each object is part of a cluster, then in each subsequently step, this one cluster is divided in subsequent cluster till only clusters of individual objects stay and the desired cluster is obtained (Figure 8) [source: Hierarchical Divisive Clustering (dataaspirant.com)] This methodology is almost like the agglomerative approach except that it starts from the only cluster that consists of all the objects.

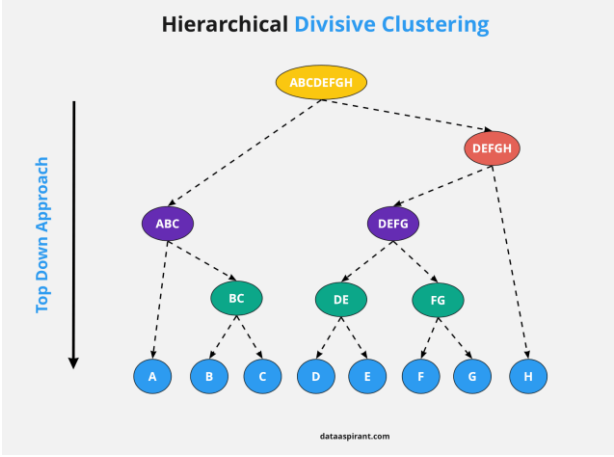

Figure 8: hierarchical divisive clustering

- density based clustering, namely DBSCAN, can be used to identify clusters of any shape in a data set containing noise and outliers. Unlike to K-means clustering, this approach does not require the specification about the number of clusters to be generated (Figure 9) [web link: Density-based Clustering (Spatial Statistics)—ArcGIS Pro | Documentation].

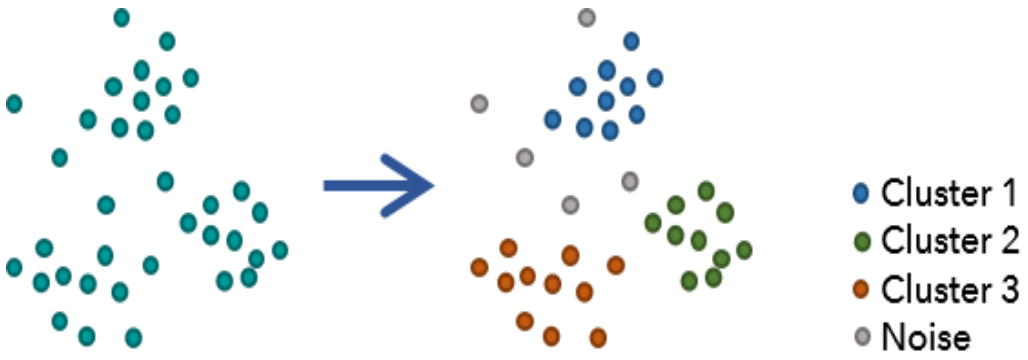

Figure 9: density-based clustering.

Control parameter used to define if an element can be related with an element of a cluster, is the proximity index that is a distance measure, a function that define the similarity and the difference between the labels. In literature there are different types of distance measure (e.g., Euclidian distance, Mahalanobis distance, Minkowski distance, Hamming distance, Jaccard distance) and choice between one distance to other, is function of the problem to resolve.

In our case, the decision making about which stable pole are representative of a physical mode of the structure are made by an agglomerative hierarchical clustering analysis with single Linkage criteria for merging clusters.

In a general point of view, the possible linkage criteria used between two sets of observation A and B for merging clusters are:

- Complete Linkage Clustering, this method is also called as the maximum linkage, and it considers the maximum distance between any object of one cluster to any other object of second cluster.

$$D(C_i, C_j) = max\ d(x, y), x \in C_i, y \in C_j$$

- Single Linkage Clustering, this method is also called as the minimum linkage, and it considers the minimum distance between any object of one cluster to any other object of second cluster.

$$D(C_i, C_j) = min\ d(x, y), x \in C_i, y \in C_j$$

- Average Linkage Clustering this method is also called as the unweighted Pair Group Method with Arithmetic Mean and it considers the average distance from any member of one cluster to any member of the other cluster.

$$D(C_i, C_j) = \frac{1}{n_i, n_j} \sum_{x \in C_i, y \in C_j} d(x, y)$$

The procedure applies a hierarchical clustering analysis of the stable poles, so, starting from the stabilization diagram results, that is the stable poles identification (Figure 10), the split operation from stable poles that describing a physical mode from other, is made following these steps:

- step n.1: evaluate the similarity between all the pairs of stable estimated modes by a specialized metric distance for this purpose how proposed in [Magalhaes et all. 2009] [27]

$$d_{i-j} = \left| \frac{f_i - f_j}{f_i} \right| + (1 - MAC_{i,j}) \leq d^*$$

where f_i and f_j are the natural frequencies of the i-th vibrational mode and the j-th vibrational mode while, the MAC parameter, quantifies the difference in term of modal shape and d* is a threshold value defined by the operator.

- step n.2: apply the Single Linkage Clustering criteria to link and menage the stable poles in many clusters by assigned a threshold value d* to the intercluster distance,

$$d^* = 0.5$$

- step n.3: assigned a lower bound, Nc, at the number of elements inside the cluster to define if the consistency of the cluster is good.

$$Nc = 20$$

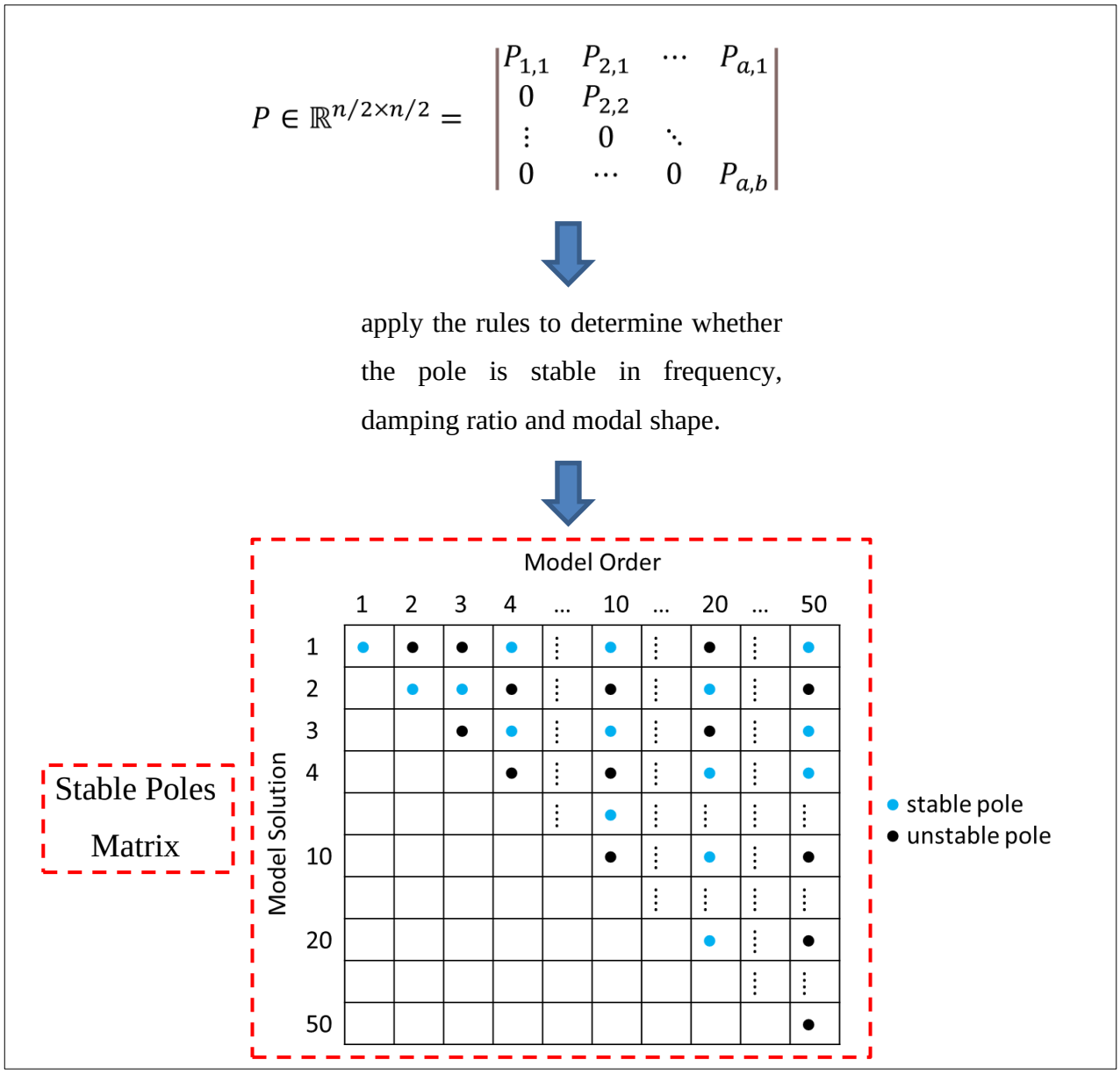

Figure 10: steps followed to define the stable/unstable poles.

A good graphical representation of the clustering analysis steps, starting from the Stable Poles Matrix, is presented in [Marongelli and Gentile 2019] [32] where the authors shown the path of the cluster's definition (Figure 11).

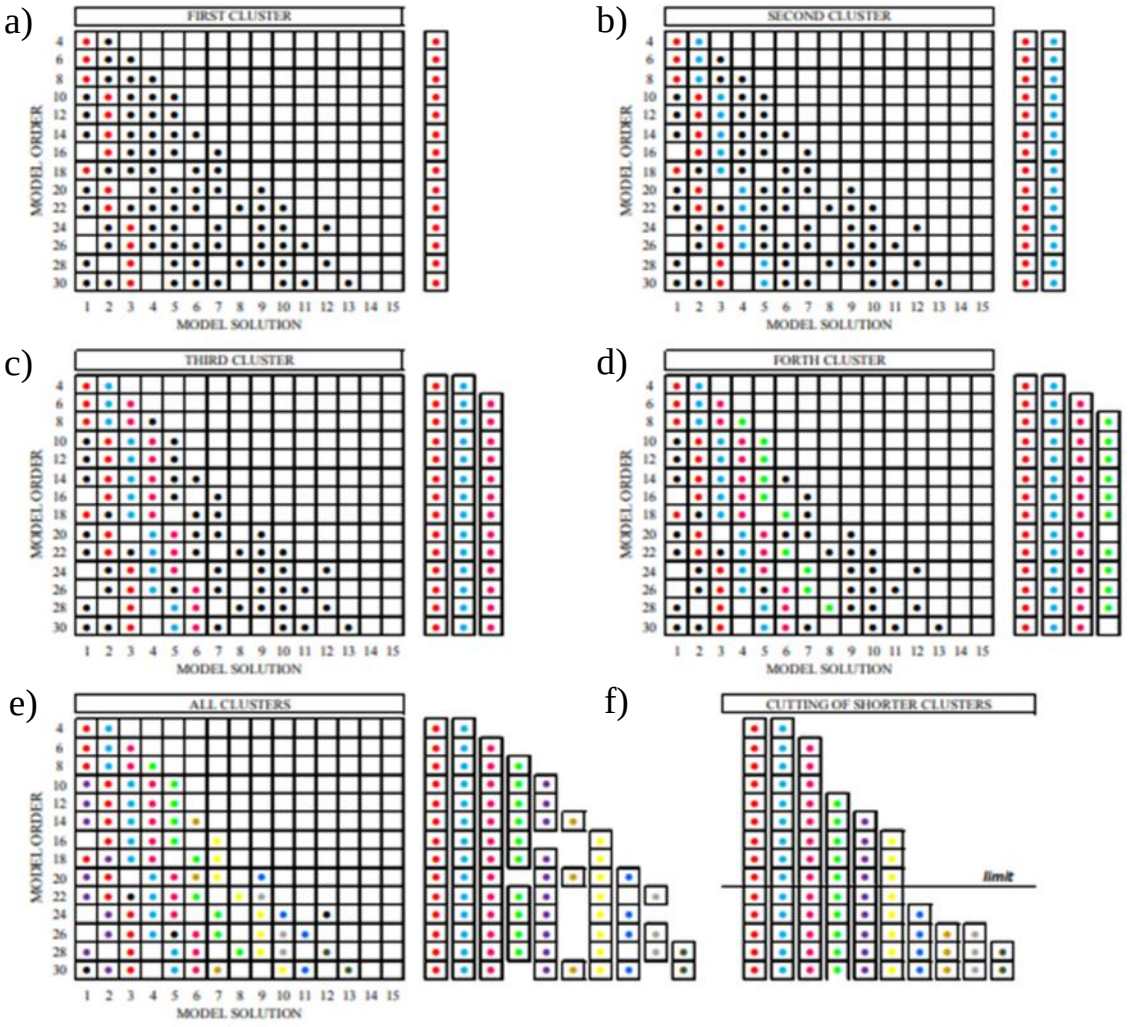

Figure 11: Clustering Analysis Process: (a)-(e) construction of clusters (f) cutting of weak clusters.

1.3 Specific topics for historic buildings

This PhD thesis is focused on the structural knowledge issues of the historic buildings that belong to cultural heritage of the country. Generally, these buildings are characterized by subsequent incorporation of surrounding buildings and, during time, are subjected of a series of ordinary maintenance intervention and structural retrofit intervention that usually lead to complex geometries embedding different materials and construction techniques.

The process of structural knowledge is comprehensive of the actions to identify the vulnerabilities of the structure [Morici et al. - 2020] [35], to get the behaviour under dynamic actions [Masciotta et al. - 2017] [34]; [Ubertini et al. – 2017] [36]; [Gentile et al. – 2019] [33]; and [Kita et al. - 2018] [37], assess the level of safety, and eventually design proper retrofit interventions [Pavia et al., 2021] [4]. Both experimental tests, such as non-destructive tests and dynamical tests, and geometry surveys are necessary since they are the only way to acquire input data for performing an accurate structural evaluation. A general scheme about in-situ and laboratory available tests is shown in Figure 12 [Ramos et al., 2012] [38].

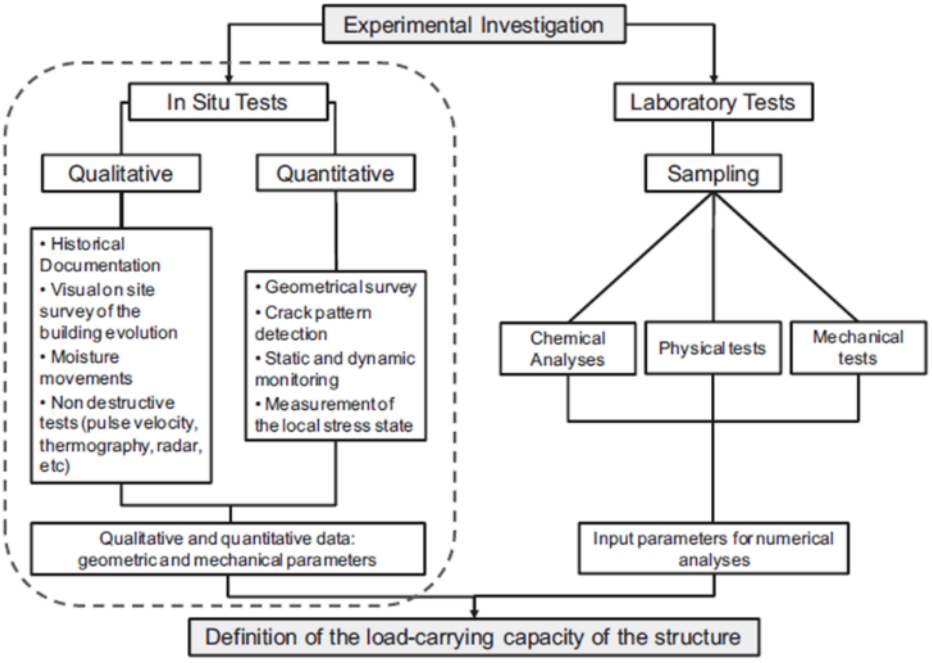

Figure 12: Overview about available in-situ and laboratory tests [Ramos et all 2012].

The goodness of structural health monitoring, finalized to evaluate and monitor the behaviour of the structure in time, are influenced from these knowledge activities. Aa reliable finite element model permits to relate the experimental results to numerical ones, after a response model calibration. Therefore, the interpretation of experimental results able to give a state of health of the structure are influenced by several issues:

1 detailed finite element model (FEM) of the structure.

2 monitoring of the state of the cracks.

3 environmental conditions.

1.3.1 Finite element Model of the structure

The finite element model “FEM” of the structure is a necessarily instrument to analyze the monitoring collected data and understand if a damage or a decay of mechanical properties occurred. Therefore, the knowledge activities of the buildings, that include the researching of historical documentation about the buildings and their subsequent modifications over time, the conducting of a geometrical survey, the assessing of the material deterioration extension and the identifying of the various structural typologies. As an example, one can bring up the “Gabbia tower in Mantova, Italy” Figure 13 [Saisi et all. 2015] [42] where the authors make in light the discontinuity of the buildings.

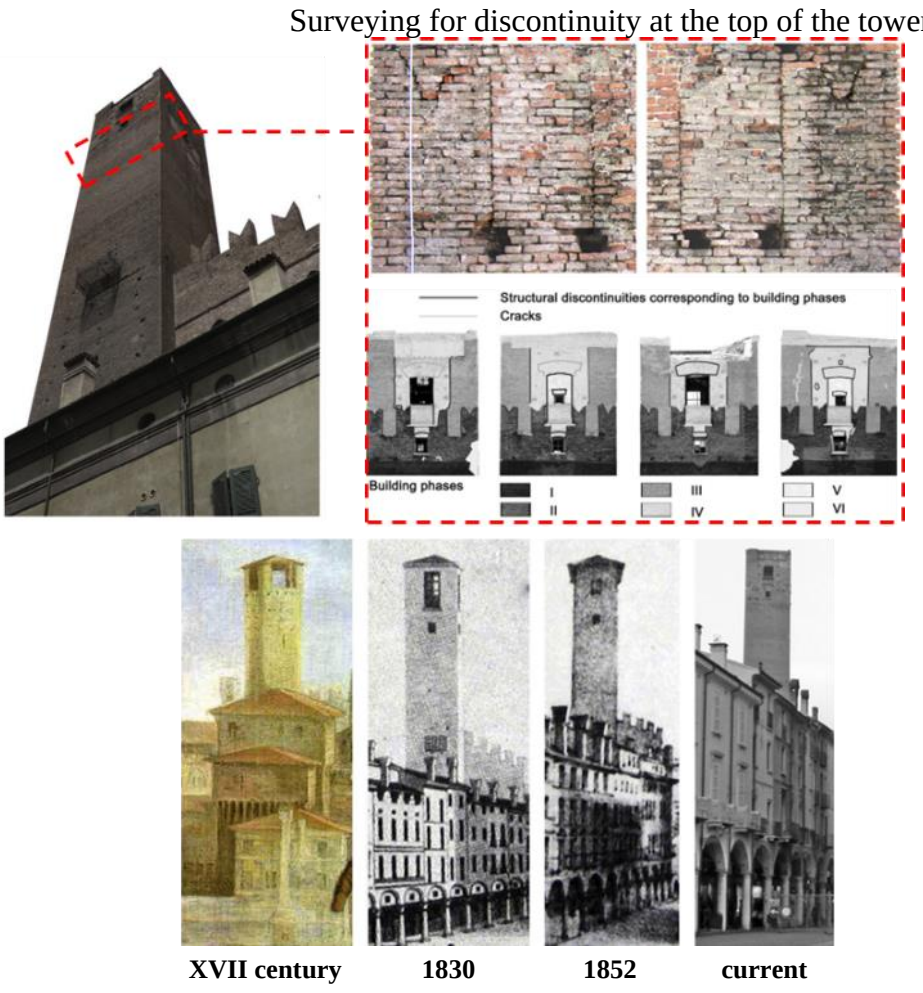

Figure 13: Gabbia tower in Mantova [Saisi et all. 2015].

These preliminary activities of knowledge are closely necessary to obtain an accurate structural model of historical buildings [Cabboi et all. 2017] [39], [Foti et all. 2011] [40], [Ramos et all. 2010] [41] and [Ubertini et all 2017][36]. This commonly involves employing a macro elements model, a structural modelling technique that breaks down complex systems into high-level components. This approach is particularly useful when dealing with intricate, extensive systems as it enables developers to prioritize the macro-level design and structure before getting into the specifics of each individual component. An example of this, is shown in Figure 14 [Ramos et all. 2010][41] where the tower has been modelled with a 3D brick element to better represent the corners stiffness and the geometry of the upper part of the tower where each region has different modulus of elasticity to taking into account the discontinuity and the different materials typologies.

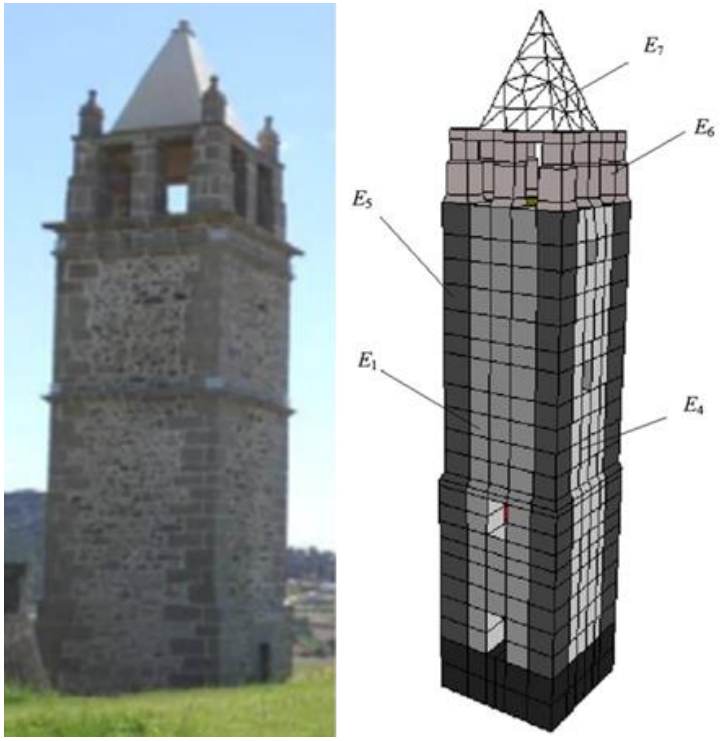

Figure 14: Mogadouro Clock Tower [Ramos et all. 2010][41]

In general, the response of the structural model does not match the experimental response in terms of natural frequencies, damping ratios, and modal shapes. However, this discrepancy in the model's response can be corrected by updating the model after conducting a sensitivity analysis of the model parameters that significantly impact the model's response. To update the model, the values of the parameters that affect the model response are altered, taking into account the changes in natural frequencies and modal shapes of the main modes of vibration in the structure. Figure 15 [Ramos et all. 2012] [38]shows an example of the modal updating results.

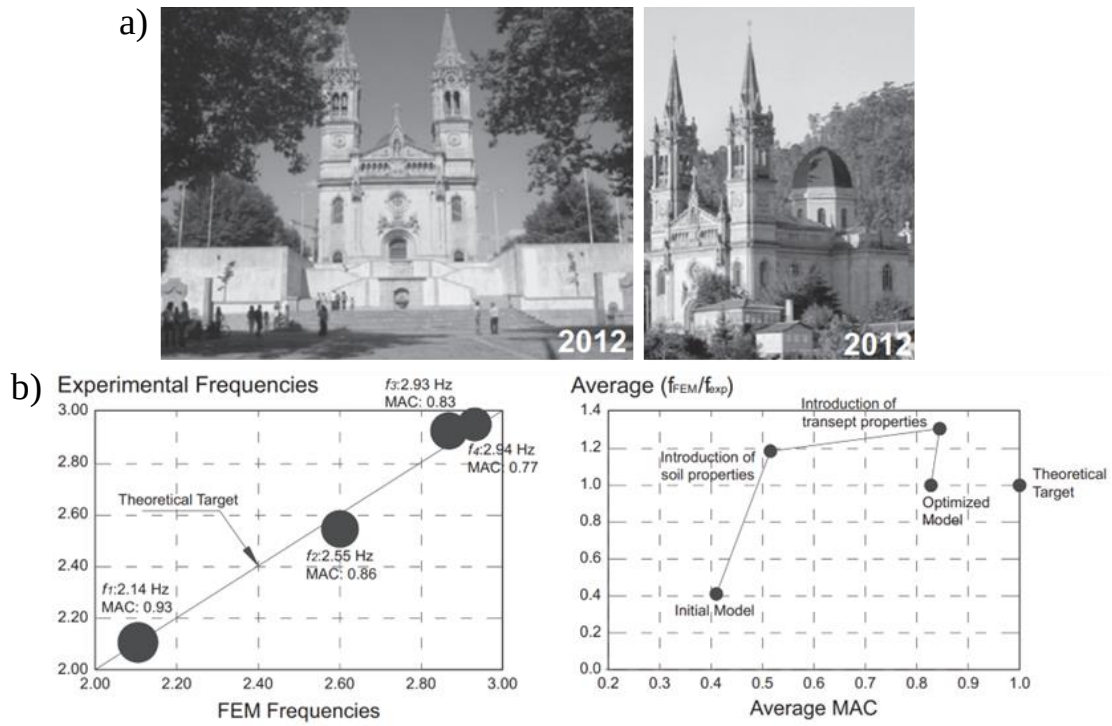

Figure 15: a) view of Saint Torcato Church, b) results of the modal updating process [Ramos et all. 2012].[38]

This result is useful because we have a model that can track the development of the structural response, evaluate the eventual state of damage, and simulate different damage scenarios so it can be assess threshold limits for the monitored parameters that define a damage in the structure.

1.3.2 Cracks survey and monitoring

The survey and monitoring of cracks in historical buildings is a crucial aspect of structural health monitoring. It is important to identify any cracks early on to prevent further damage to the building's structure and preserve its historical value. The survey involves a thorough examination of the building's exterior and interior, including its foundation, walls, and columns, to identify any visible cracks or signs of damage. This purpose is obtained with a series of preliminary operation such as a critical visual inspection of the building to identify the main mechanism that inducted the current state of damage, and an external façades geometrical survey with laser-scanner instrument or a topography survey to evaluate possible out of plumb or tipping mechanisms. These operations are essentially to design a static and dynamic monitoring of the structures with the aim to control the evolution in time of the damage. In [Kita et all. 2018] [37], [Cavalagli et all. 2017] [43], [Ramos et all. 2012] [38] and [Lorenzoni et all. 2015] [44] are discussed some consideration on these issues, such as the evaluation of the nature of the forces that have inducted the current crack patterns by a series of nonlinear structural analysis, the decision making about the sensors position after the identification of the mainly mechanisms of failure Figure 16, the operative methodologies linked both

the area interested to the mechanism of failure Figure 17 and the high-quality architectural of the building Figure 18.

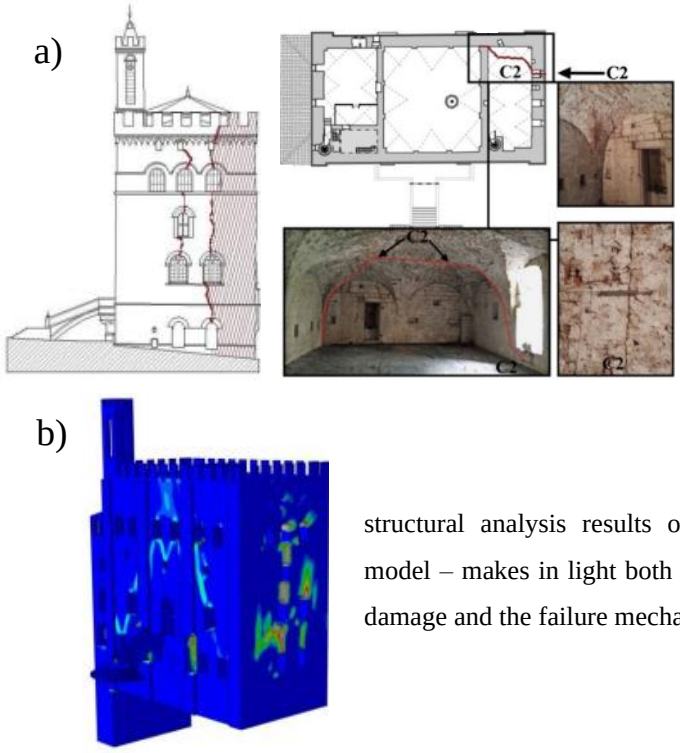

structural analysis results of the 3D element model – makes in light both the current state of damage and the failure mechanisms.

Figure 16: a) crack patterns and monitoring of Palazzo Consoli, b) results of structural analysis [Cavalagli et all. 2017] [43]

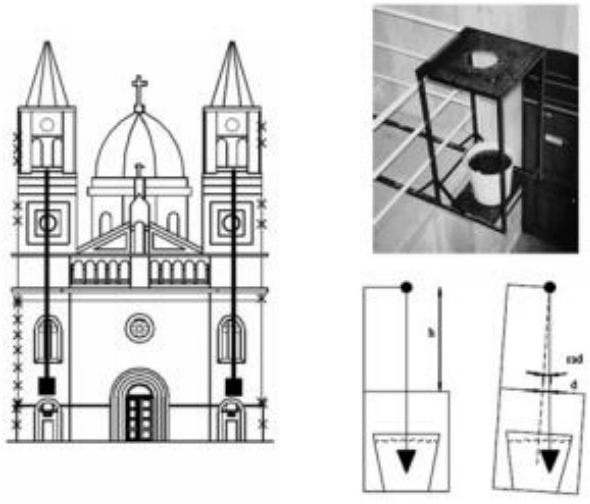

Figure 17: Saint Torcato Church – scheme of the tilt monitoring system [Ramos et all. 2012] [38]

Figure 18: Conegliano Cathedral – crack survey with contactless sensor [Lorenzoni et all. 2015] [44]

1.3.3 Environmental Condition

The Environmental and Operational Conditions (EOCs) plays a key role in the detection of the state of damage that can be occurred in architectural heritage [Sohn – 2006] [67]. More in detail how explained in [Keshmiry et all. – 2023] [66] these EOCs changes the structural response in terms of modal properties both to the change of the physical state of structural component (environmental conditions) and to the instantaneous frequency fluctuation (operational conditions such as nonstationary excitation). An overview of the mechanisms by which various EOCs can influence modal properties is shown in Figure 19.

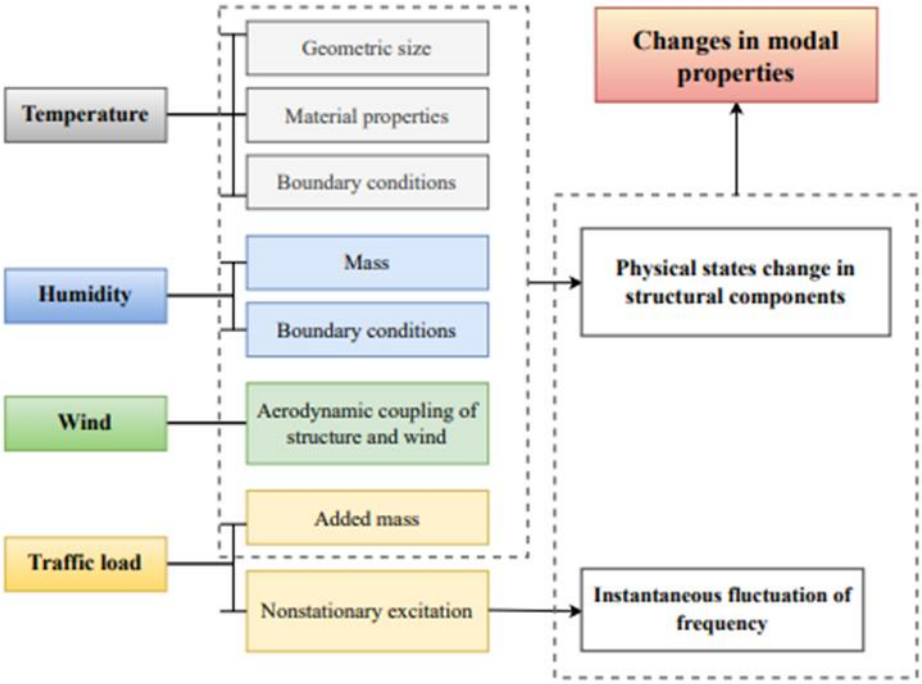

Figure 19: Overview of mechanisms EOCs – [Keshmiry et all. 2023]]

Inside the field of the damage assessment of the dynamical systems, the effects of the environmental conditions can significantly influence the reliability and the robustness of damage assessment methodologies and limit their performance.

In details, how analysed in various structural systems, the environmental factors (i.e., temperature, humidity, and wind velocity) produce effects on the structural response both to the dynamical properties such as natural frequencies, modal damping, and modal shape and to the local kinematic mechanisms such as cracks.

With major attention to the temperature effects on cultural heritage buildings, they differ from the expected behaviour of buildings characterized with a structural organism in reinforced concreate (RC) or stell where an increasing of temperature involve a stiffness loss with a decrease of the vibrational natural frequencies. In detail, the temperature variations in cultural heritage buildings lead to a response related both to the type of buildings (i.e., churches, renaissance buildings, and bell tower) and the boundary conditions such as metallic elements (e.g., tie-rods) or improvement interventions that influenced the response of the structure.

In [Azzara et all. – 2018] [70], [Garcias-Matias. E and Ubertini. F – 2020] [69], [Cabboi et all. – 2017] [68] and [Ubertini et all – 2018] [71] are treated some historical bell tower and the results shown that the natural frequencies identified along the monitoring period are influenced by the temperature variations, where an increasing of the temperature involve an increase of the natural frequencies. An example of this behaviour is shown in Figure 20, that represent the results of a monitoring system installed in the San Ferdinando bell tower in Lucca [Azzara et all. – 2018] [70]

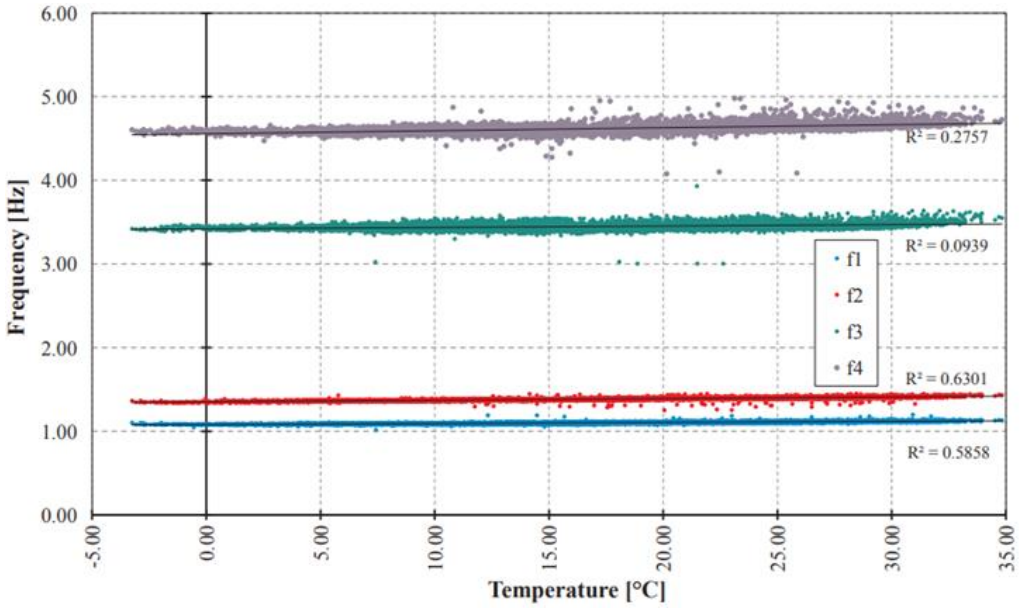

Figure 20: San Ferdinando bell tower – natural frequencies vs temperature.

Otherwise in [Kita et all. – 2019] [75], [Gentile et all. – 2019] [74], [Garcias-Matias. E and Ubertini. F – 2022] [73], [Ceravolo et all. – 2021] [72], [Zonno et all. - 2019] [76] and [Masciotta et all. – 2017] [34] are treated some churches, cathedrals, and renaissance buildings. Here, unlike the bell tower, the results shown that the natural frequencies identified along the monitoring period are influenced both to the temperature and to humidity variations and the trend seems to have a different behaviour related to typology of structure and to the boundary conditions. More in detail how shown in [Kita et. all – 2019] [75], that describe the results obtained from the SHM of the Palazzo Consoli in Gubbio, a negative sign of the frequency-temperature correlation coefficients observed. This trend can be related to the moderate state of structural damage and by various metallic reinforcements, such as the tie rods installed to reduce the lateral thrust of the majestic barrel vault of the Arengo hall. In detail how shown in Figure 21, the observed decrease in natural frequencies due to temperature increases could be conceivably attributed to temperature-induced slackening of such metallic reinforcements, resulting in a global softening effect, that could be enhanced by the existing macro-cracking conditions.

In Figure 22 are shown the trends between the crack amplitude and the temperature; the results confirmed that crack amplitudes are largely dominated by temperature changes where a decreasing temperature cause a global contraction of structural masonry volumes, resulting in opening of cracks. On the contrary, increasing temperatures result in crack closing.

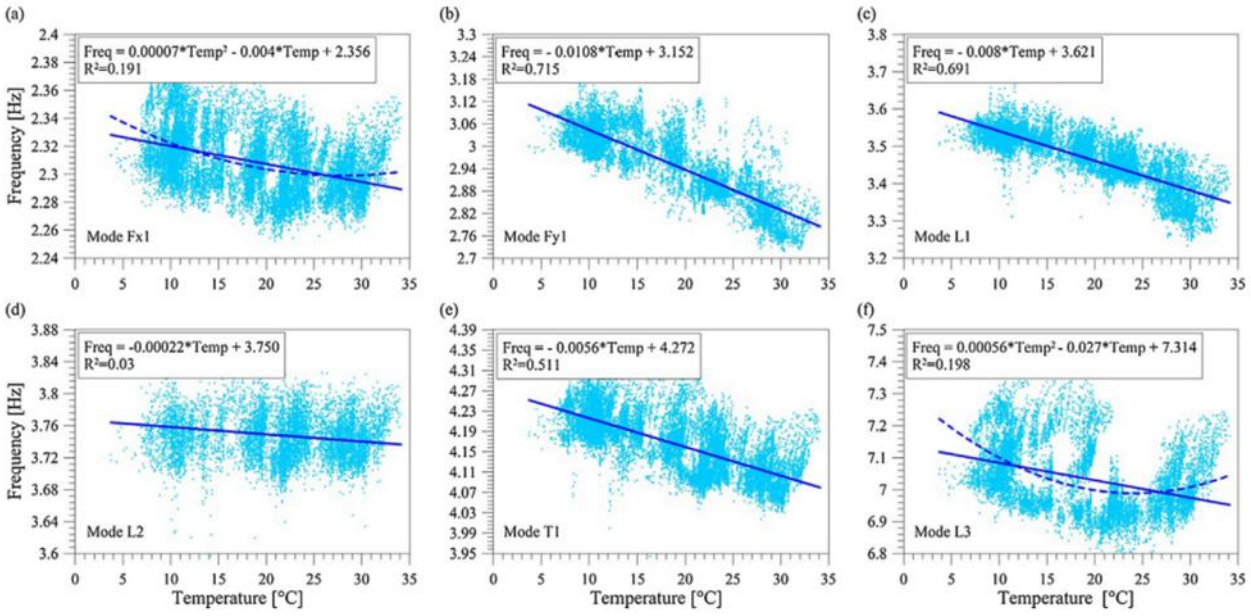

Figure 21: Palazzo Consoli Gubbio – natural frequencies vs temperature.

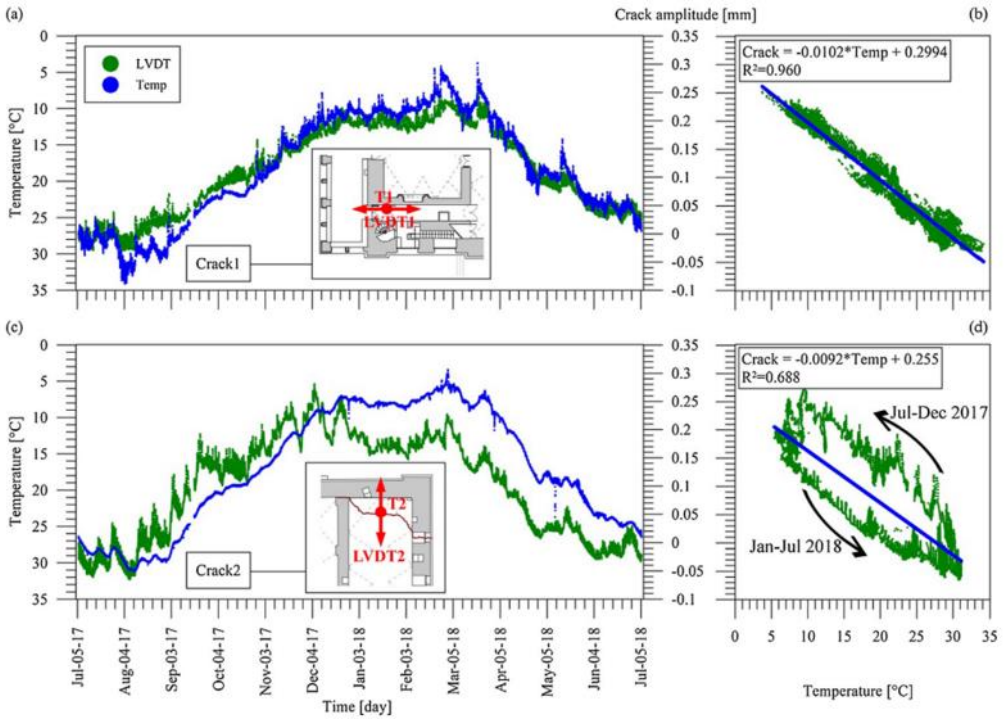

Figure 22: Palazzo Consoli Gubbio – crack amplitude vs temperature.

The effect of the humidity variation on the identified natural frequencies identified can be prevalent that temperature effects as shown in [Zonno et all. – 2019] [76]. In Figure 23 is shown that the relative humidity and the absolute humidity have a stronger influence on the variations of the modal parameters with a different intensity for each analysed mode. The influence of these parameters in the long-term dynamic behaviour is likely to be a combination of a dual phenomenon: an increase in volume with the consequent closure of the micro-cracks in the adobe structure (and therefore an increased system stiffness), and a change on the surrounding foundation soil conditions.

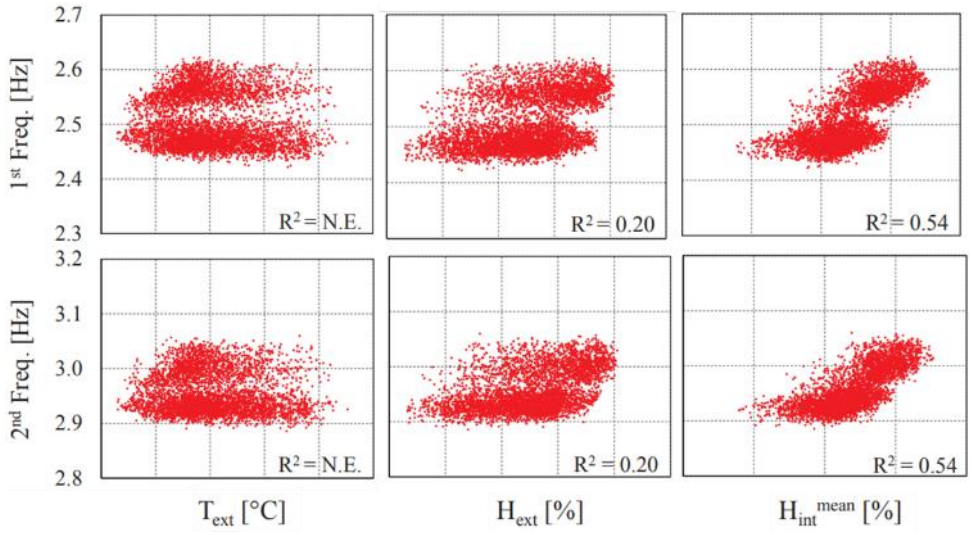

Figure 23: San Pedro Apostol in Andahuaylillas – correlation coefficients between natural frequencies vs temperature and humidity. N.E. denotes correlation coefficient less than 0.1.

Therefore, in order to establish a tool to detect the anomaly in the structural parameters taken as target for monitor the response of the structure along time, from the results shown above is clear that is needed to remove the environmental effects from the natural frequencies identified. This is performed applying statistical models at data to filter out the environmental effects from the natural frequencies monitored [Sohn. H. – 2007] [67], [Worden et all. – 2002] [78] and [Keshmiry et all. – 2023] [66]. Models largely used are the Multiple Linear Regression (MLR) models [Kita et all. – 2019] [75] the Principal Component Analysis (PCA) model [Garcias-Matias. E and Ubertini. F – 2022] [73], [Azzara et all. – 2018] [70], [Ceravolo et all. 2021] [72] and [Cabboi et all – 2017] [68] and the filtering of the data with a Kalman filter [Erazo et all. – 2018] [77]. In Figure xx and Figure xx are shown the MLR and the PCA model results from Palazzo Consoli in Gubbio [Kita et all. - 2019] [75] and [Garcias-Matias. E and Ubertini. F – 2022] [73].

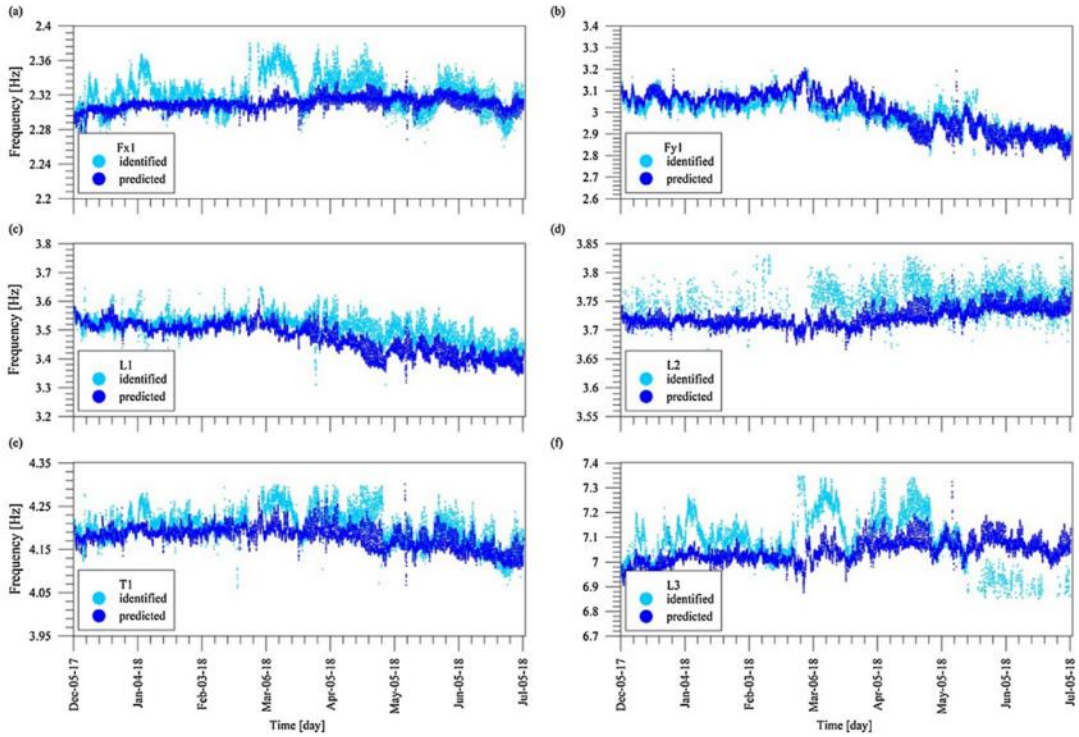

Figure 24: Palazzo Consoli Gubbio – application of the Multiple Linear Regression (MLR) to relate the response with the environmental parameters.

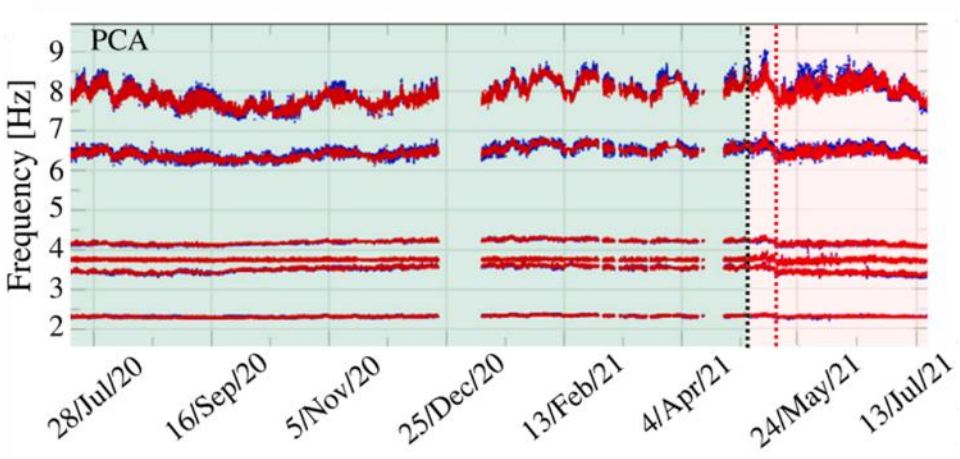

Figure 25: Palazzo Consoli Gubbio – application of a Principal Component Analysis (PCA) to relate the response with the environmental condition.

2 Design of monitoring systems

Ambient vibration tests as well as experimental tests with external input are the main dynamic tests family to identify and assess the dynamic behaviour of structures. With the aim to obtain a reliable estimation of the response, the design of the Monitoring System is a preliminary activity of paramount importance, together with the choice of the best identification algorithm [Gharehbaghi et all. – 2021] [45], [Brincker and Ventura – 2015] [5].

A monitoring system is characterized both a hardware and software component. The hardware component groups: a) the sensors chosen in account of the physical quantity to measure; b) the technology used to transmit the acquired measure from the sensors to the acquisition unit, in detail cable transmission or wireless (Wi-Fi) transmission; c) the acquisition modules that convert the signal from analogic to digital (A/D conversion) and they differ by the types of measure, i.e., dynamic of static and d) the acquisition unit that synchronize all the typologies of sensors in the measure chain. Instead, the software component adjusts the necessaries acquisition features to take the data.

Therefore, the necessary stages to design a Monitoring System can be summarized in the following six points:

1. The choice the typologies of sensors according to the physical measurements that need to be acquired. Within such step there are some issues that need to be considered as the sensitivity of the sensors, their measurement range, and the operational conditions of the sensors.
2. The installation and placement of the sensors. Such operations, indeed, can affect the response of the sensors, but above all the quality of the measurements of the physical quantities.
3. The identification of the best position for the sensors, considering the noise level and the expected response of the system under investigation.
4. The choice of the acquisition system, in terms of board resolution, operating temperature and environmental conditions (e.g., inside, or outside).
5. Programming the software for the measurement chain.
6. The set-up for the acquisition of the parameters, as the choice of the sample frequency, of the number of samples, and of the duration of the acquisition of the parameters.

In the next sub-sections these points will be analysed in detail.

2.1 The choice of sensors typologies

According to the physical quantities to be measured (e.g.: acceleration, velocity, pressure, displacement, environmental conditions, etc.), there is a wide choice of available sensors, as shown

in Figure 26. Within each family of sensors, there is a subgroup of instruments that are able to measure the same physical quantity and that differ among each other based on the capacity to convert the mechanical quantity measured into an electrical one. Moreover, the choice can be also driven by the expected behaviour and typology of structures to be monitored and on the infield conditions.

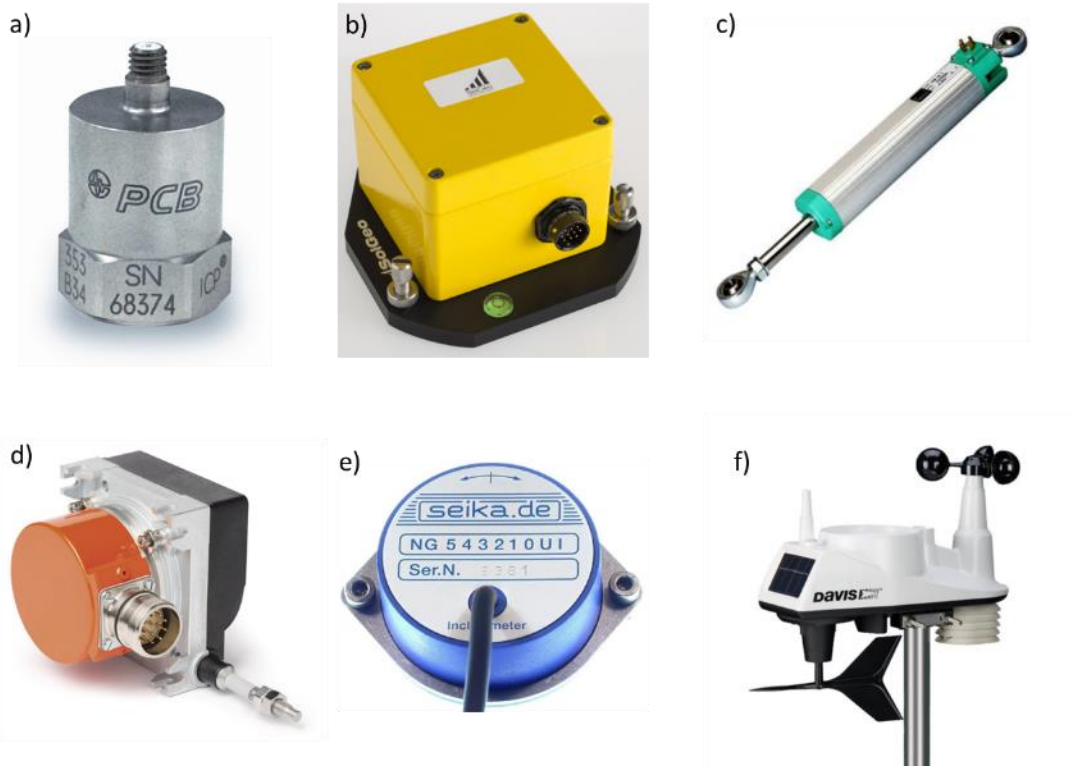

Figure 26: Types of sensors mainly used for the SHM of cultural heritage buildings: a) Accelerometer b) Velocimeter c) Linear Velocity Displacement Transducer (LVDT) d) Thread displacement transducer e) Inclinometer f) Weather station.

Within the family of accelerometers that are sensors largely used for the Structural Health Monitoring (SHM) of the dynamical properties of structures, there are different typologies of sensors like piezoelectric accelerometers, force balanced accelerometers, Micro Electro Mechanical System (MEMS) accelerometers, seismographs, or geophones, as reported in Figure 27. For instance, aiming at identifying the dynamic properties of buildings belonging to cultural heritage, the three types of accelerometers largely used are: piezoelectric, balanced and MEMS. The piezoelectric and force-balanced ones are better than the MEMS due to their higher sensitivity and resolution and, above all, to their low level of noise, which is a feature related to the electronic of the sensor. The level of noise is a very significant characteristic for the structural monitoring of the cultural heritage buildings under ambient vibrations actions. Differently from other typologies of building in which the human activity is a source of excitation, such kind of buildings is generally characterized by massive structures where

the impact of the anthropic activity is very low. Consequently, if sensors with a high level of background noise are used, it can happen that the environmental excitation may be lower than the sensor background noise resulting in a misleading frequency spectral analysis.

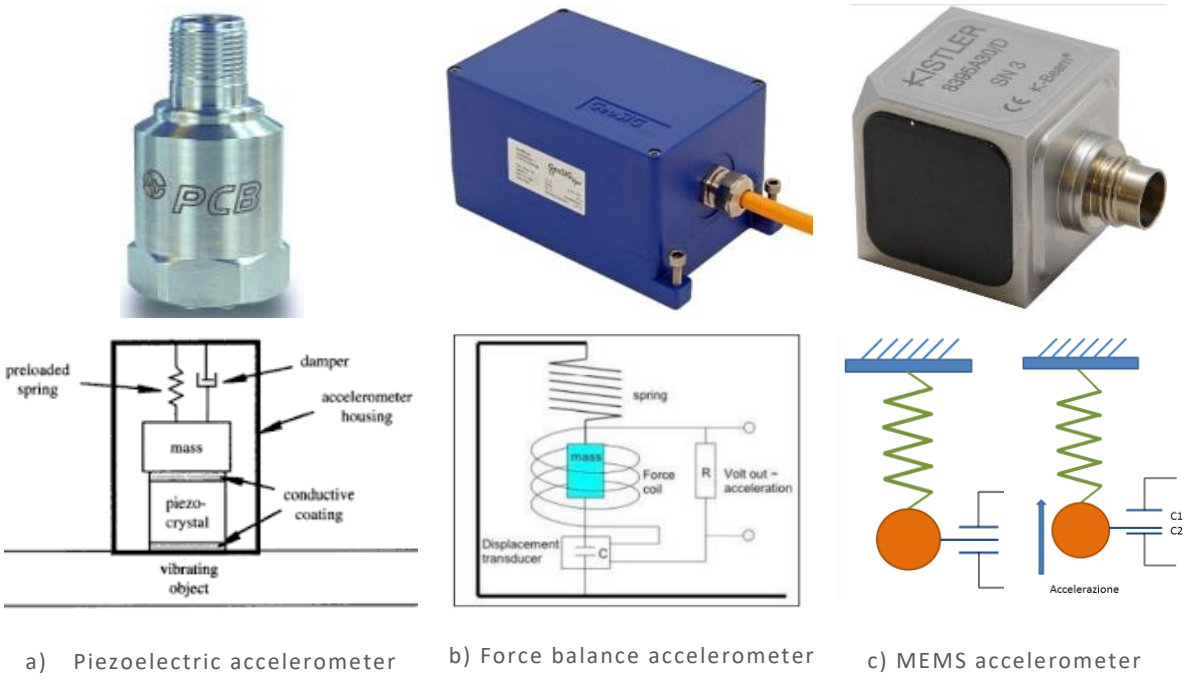

Figure 27: Most widely used accelerometers for dynamic tests.

The sensitivity is another key property of the sensors that influences the resolution of the physic quantity to be measured. It is related to the electrical measure obtained by the sensor, and it is suitable to considerer such parameter when choosing the acquisition module. When using a sensor (e.g., an accelerometer sensor) with sensitivity s = 10 V/g and input range +/- 0.5 g, indeed, the measure range requested by the acquisition module is +/- 5 V to fully exploit the resolution of the acquisition module.

For what concerns the resolution [Ranieri and Fabbrocino, 2014] [6], it represents the characteristic of a sensor that induces the smallest incremental and detectable change in the output of the physical quantity to be measured. It is usually expressed in terms of both percentage of the full-scale range, and minimum-maximum values of the physical quantity that can be measured by the sensor. Generally, such property is only given for digital output accelerometers, or systems that incorporate an analogue to digital converter. If the output is analogue, the resolution is given by the acquisition module in terms of bit resolution. It is better, indeed, to have an acquisition module that provides a higher value of bit resolution because in the Analogue to Digital (AD) conversion, the signal is better depicted.

Finally, regarding the dynamic range [Brincker and Ventura 2015] [5] of a measurement system, it can be defined as the ratio between the maximum instantaneous value of the signal and the minimum detectable value of the signal.

$$D = 20log\left(\frac{y_{max}}{y_{min}}\right) \text{[dB]} \quad (2.1\text{-}1)$$

This ratio represents the smallest signal that we can measure in the frequency band, and it is strongly influenced by the denominator (y_{min}) that, in turn, is deeply affected by the magnitude of undesired electrical noise, and by the quantization of the measurement by the AD converter. Basically, the smaller the frequency band, the smaller the noise and thus the larger the dynamic range.

2.2 Installation and placement of the sensors

During the design of a monitoring system or, more in general, during the performance of in-situ experimental tests there are two important aspects that must be considered: the type of connection between the sensors and the surface of structural elements, and the choice of the better placement of the sensors to understand the expected behaviour.

Regarding the first one, it is worth to remember that any connection does not have to condition the response of the sensors. If the target is to capture the dynamic behaviour of a building in terms of natural frequencies and modal shapes, indeed, the sensors must not be connected through deformable supports, or to supports that act like filters of the acquired signals, otherwise the spectral frequencies resulting from the analyses of the signals could be influenced by the behaviour of the connections. Moreover, each type of sensor interacts differently with the surface in which it is installed.

More in detail the connections of accelerometers, some of them are shown in Figure 28 and in Figure 30, can be seen as springs having an own stiffness k that are set in series with the accelerometers. The higher is the value of the stiffness and the lower is the frequency range reduction.

Usually, the different systems of connection are:

- Stud mount (30 kHz)
- Mounting pad (8 kHz)
- Adhesive mount (thin 8 kHz)
- Flat magnet (2 kHz)

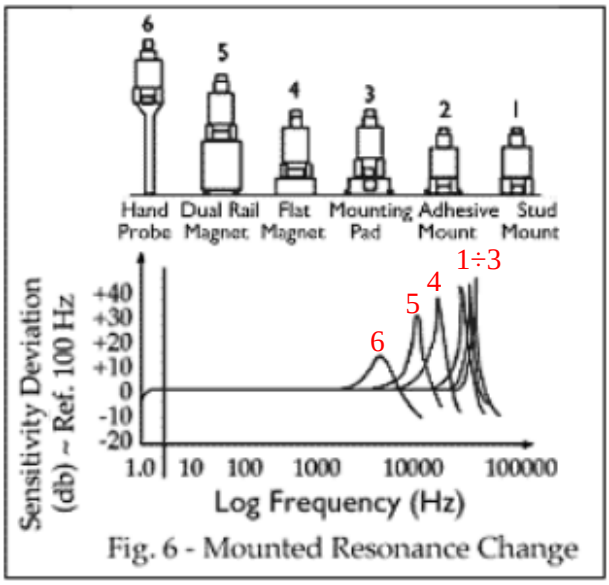

Figure 28: type of connections for Piezoelectric Accelerometers

The connection of displacement sensors, instead, is more affected by the type of surface. If the structure to be monitored has a homogeneous surface, which means that it can be seen as a continuous body, then the displacement sensors can be directly connected on the surface, and they will measure the evolution of the kinematic behaviour under investigation. Different is the case of structures characterized by heterogeneous materials on the surface (e.g., an ancient masonry wall). If the target is to measure the evolution of the cracks, indeed, and the sensor is installed directly on the surface, the displacements measured are due to the local displacements of the brick or of the mortar. For this reason, it is preferable install the sensors through a steel plate that involves a larger number of surface elements. An example of this solution is shown in Figure 29, where a measurement system characterized by LVDT (linear voltage displacement transducer) aims to monitor the evolution of the vaults cracks, is installed in one of the case of studies analyses in this thesis, that is the Portico da Varano of the Ducal Palace of Camerino.

Measure the evolution of the vault cracks

n.2 thin steel plate directly connected on the vault and a trasducer system installed on the steel plates

Figure 29: example of the installation of a displacement transducer in a masonry vault

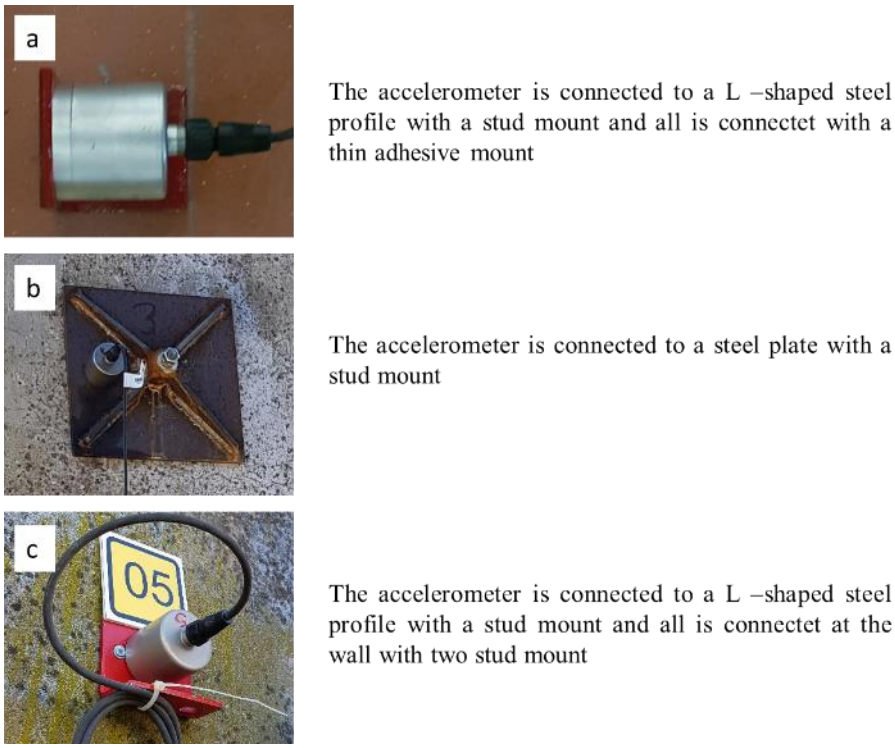

Figure 30: three examples of possible Accelerometer connections

Finally, to enhance the quality of the acquired measures and to correctly identify the behaviour of the structure under investigation, it is necessary to properly design the sensors position. This operation can be done through the following alternative strategies:

1. A strategy based on the sensibility and expertise of the operator concerning the prediction of the expected structural behaviour of the building under investigation. The behaviour depends on many factors, as the type of structure, its geometry, and the behaviour of horizontal slabs (i.e., deformable or infinitely stiff in their plane), which in turn can strongly influence the performance of the building, especially when subjected to horizontal loads. Such strategy and the assumed location of the sensors is validated a posteriori through the post-processing of the signals acquired.
2. A strategy based on a novel approach aiming at identifying the best position of the sensors through analytical evaluations. This last consists in performing the optimal sensors position algorithm that, starting from a FEM model of the structure under investigation, can identify the ideal points where positioning the sensors.

2.3 Check the quality of the data.

How better explained in [Brincker and Ventura – 2015] [5] an operation that will be a good practice before leaving the test site in order to check how well the monitoring system has been planned are to check clipping phenomena on the acquired signal for each sensor and to evaluate the signal to noise ratio.

Regard the first one, this permit to check if there are phenomena or signal levels that goes outside both the sensor measure range and the analogy-digital converter (ADC) measure range (Figure 31). It can be checked easily from a visual analysis of the acquired signal.

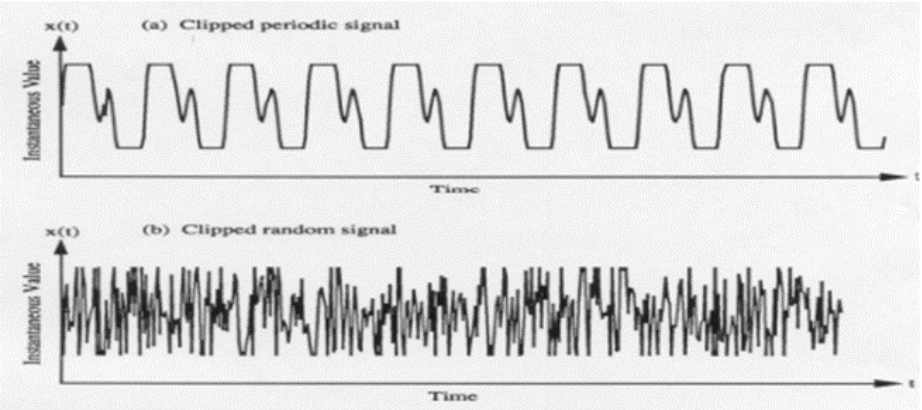

Figure 31: Periodic and random signal clipping

Instead, the second one is related to the physical characteristic of the sensor, the background noise. It is a measure of the strength of the signal acquired relative to background noise, which is an undesired signal. The ratio is typically expressed in decibels (dB) and it can be zero, a positive number or a negative number. A SN ratio over 0 dB indicates that the signal level is greater than the noise level. Generally, the higher the ratio, the better the signal quality and it should be controlled in every in situ experimental tests. The SN analytical expression is:

$$SN = 20log\left(\frac{y_{max}}{\sigma_n}\right) \tag{2.3-1}$$

where σ_n is the Root Mean Square (RMS) value of the background noise and y_{max} is the maximum instantaneous value of the signal that can be transmitted by the system without distortion. In Operational Modal Analysis (OMA) it is not recommended to use data with a signal to noise ratio smaller than 30-40 dB.

The simplest way to evaluate the signal to noise ratio is to perform a Frequency Domain Decomposition (FDD) on the measured data and to make a plot of the singular values of the Spectral

Density (SD) matrix as a function of the frequency. The distance between the maximum values of the modal peaks and the minimum singular value is a measure of the signal to noise ratio in each frequency band.

The SD matrix is the Fourier transform of the Correlation Function (CF) matrix. It's represented the cross-correlation matrix of the output data (2.3-2).

$$\boldsymbol{R}_y(\tau) = E[\boldsymbol{y}(t)\,\boldsymbol{y}^T(t+\tau)] = \boldsymbol{A}\,\boldsymbol{R}_q(\tau)\,\boldsymbol{A}^T \tag{2.3-2}$$

Where τ is the time separation between two-time instances, $\boldsymbol{A}$ is the mode shape matrix and $\boldsymbol{R_q}(\tau)$ is the CF matrix of modal coordinate.

Re-writing this expression in frequency domain applying the Fourier transform it obtains the SD matrix (2.3-3)

$$\boldsymbol{G}_y(f) = \boldsymbol{A}\,\boldsymbol{G}_q(f)\,\boldsymbol{A}^T \tag{2.3-3}$$

Where $\boldsymbol{G_q}(f)$ is the SD matrix of modal coordinates. This matrix, under the assumption that the modal coordinates are uncorrelated, that is, the off-diagonal elements of the CF matrix of modal coordinates is zero, is both diagonal and positive valued.

Performing a singular value decomposition (SVD) of the SD matrix (2.3-4) it is possible to find a matrix $\boldsymbol{R_q}(\boldsymbol{\tau})$ where the diagonal value, i.e. the singular values, can be interpreted as the auto-spectral densities of the modal coordinates and the singular vectors that is the columns of the matrix $\boldsymbol{U}$

$$\boldsymbol{G}_y(f) = \boldsymbol{A}\,\boldsymbol{G}_q(f)\,\boldsymbol{A}^T \tag{2.3-4}$$

2.4 The acquisition system and its parameters

The acquisition system can be decomposed in two parts, the hardware, and the software component.

For what concerns the hardware, the principal elements are the acquisition modules (Figure 32) whose role is to convert the signal from analogue to digital. The main properties that should be considered are the resolution of the module, the measure range, the gain, and the frequency of acquisition. Regarding this last parameter, the manufacturer provides a range of possible sampling frequencies for each acquisition module.

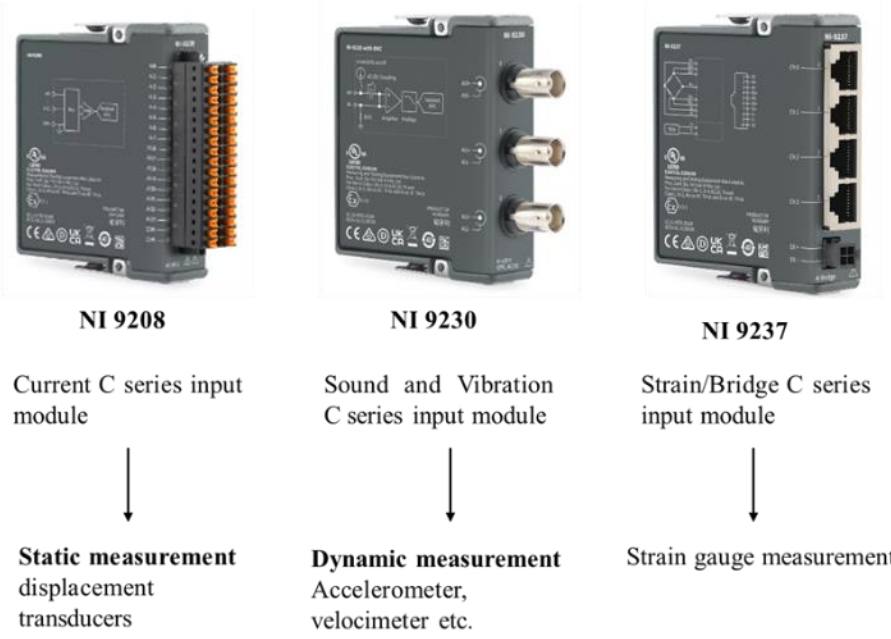

Figure 32: some types of acquisition modules by National Instruments enterprise

The resolution of the module, expressed in number of bits, gives information on the quality, or rather the number of digital signal points after its AD conversion. There are different types of modules, 8 bit (256 points), 12 bit (4096 points) and 24 bit ($16.8 \cdot 10^6$ points).

The measure range defines the maximum and minimum tension values that the module can acquire. Its knowledge permits to adapt the acquisition range of the module to the signal range leading, consequently, to measure the signal with the maximum resolution. For example, let is consider an accelerometer sensor with measurement range of +/- 0.5 g and sensitivity of 10 V/g, the measurement range of the acquisition module should be preferably +/- 5 V rather than +/- 10 V. This last value, indeed, does not fully exploit the resolution of the module, while a signal amplifier is needed. The operation of amplifying the raw signal before its digital conversion is defined as the gain, and it leads to exploit the resolution of the acquisition module as much as possible.

Finally, it is necessary to define the acquisition parameters that are the sampling frequency and the type of sample. This latter can be continuous or discrete, and it can be defined by choosing a specific number of samples, even though recently the type of sampling is always continuous.

The sampling frequency is chosen according to the **Nyquist-Shannon sampling theorem** as the maximum frequency to be measured.

$$f_M \rightarrow \text{maximum frequency to be measured} \tag{2.4-1}$$

$$f_N \rightarrow \text{Nyquist frequency} \tag{2.4-2}$$

this theorem should be applied so that the sampling of a given continuous signal is made without overlapping the infinite replicates of the Fourier transform, and avoiding signal distortion in which the higher frequencies components of the signal are confuse with the lower ones.

Basically, by knowing the maximum frequency of the signal to measure f_M, the Nyquist frequency that represents an upper bound about the f_M, is equal to $f_N = 2f_M$ and then the sampling frequency is equal to (2.4-3)

$$f_S = 2 \cdot f_N \rightarrow \text{sampling frequency} \tag{2.4-3}$$

2.5 Programming the software for the measurement chain

Finally, this section shows the software components of the acquisition system, which are in turn organized by a code that manages the acquisition procedure making it possible every operation within the measurement chain.

This thesis dissertation presents an acquisition code that has been properly developed to continuously acquire and store data and to transferring them to a cloud server for subsequent analyses, with reference to the case studies that will be introduced and further discussed in chapter 4.

The overmentioned code has been developed in LabVIEW suite, a National Instrument enterprise software. LabVIEW stands for Laboratory Virtual Engineering Workbench, and it is a graphical "G" programming environment that can be used to quickly create applications with professional user interface. It is an event-driven and object-oriented and a high-level programming language.

Even though LabVIEW has many features in common with typical programming languages, it has two unique aspects that makes it different from almost any other language: a graphical programming interface and a dataflow programming paradigm. The first one is obvious; LabVIEW is not text-based but is characterized by both a front panel viewable by the user and by a block diagram viewable by the developer. The block diagram contains functions, icons and terminals connected by wires. The function icons have input and output terminals, indicating points where data enter or exit the functions.

The second feature, the dataflow paradigm, is the novel aspect of LabVIEW. The flow of data from one function to the next dictates the order of execution of the functions on the block diagram. In many text-based languages, the order of execution depends on the order of the text in the program while in LabVIEW the data travel along wires in parallel. Functions are executed as soon as all their input data are available, while those that have no dataflow dependence are automatically executed in parallel with each other.

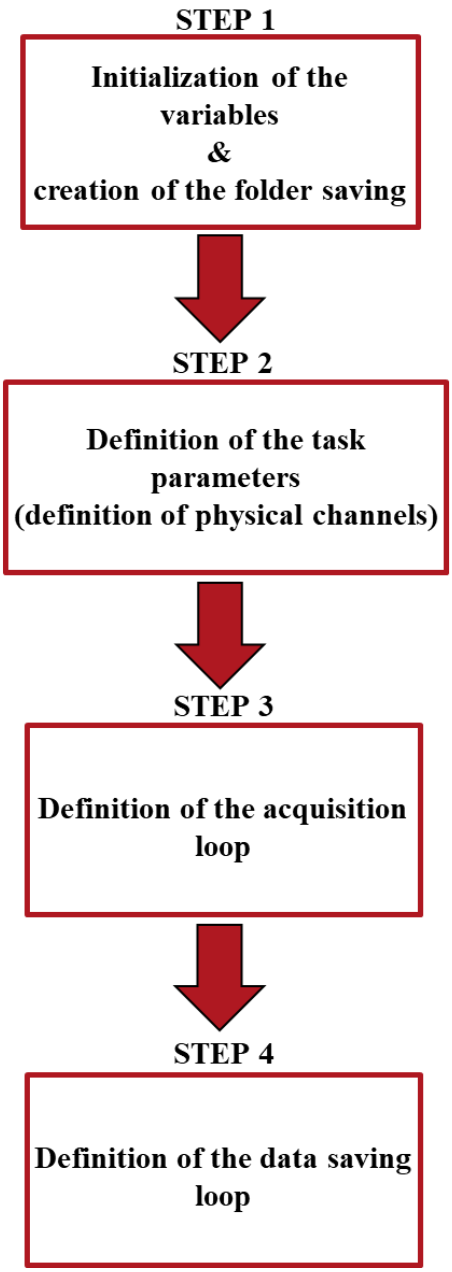

Figure 33: acquisition cycle steps

The developed acquisition process can be divided into four steps, how shown in Figure 33. This process in order to guarantee an embedded monitoring system are directly upload in the internal memory of the acquisition unit without having a host PC for the acquisition loop control.

The First step Figure 34 regards the initialization and the definition of all typologies of variables that will be utilized in the subsequent loop. In detail has been defined two types of variables, a single process shared variables and a real time global shared variable. The first ones are variables that in the data transfer between two loops not maintaining the determinism but can accept a light jitter between the inter-loop communication. These variables are Boolean variables for the execution control, String variable that contains the information about the identification of the data acquired (e.g., name of

saving file) and Time stamp variable that defines the start of the saving loop. Instead, the second ones are variables that should connect deterministic cycles with non-deterministic ones. This variable is a Real Time first-in-first-out (RT FIFO) variables that can be seen how buffers memory and has been used to transfer the acquired signal between a time critical thread, the acquisition loop and a lower priority threads the storage loop. It has been used a multi-element RT FIFO characterized by $\boldsymbol{m} \times \boldsymbol{n}$ matrix where $\boldsymbol{m}$ is the number of waveforms and $\boldsymbol{n}$ is scalar parameter fixed by the programmer and defines the number of repetitions in every loop of the acquired data package, i.e., Step 3.

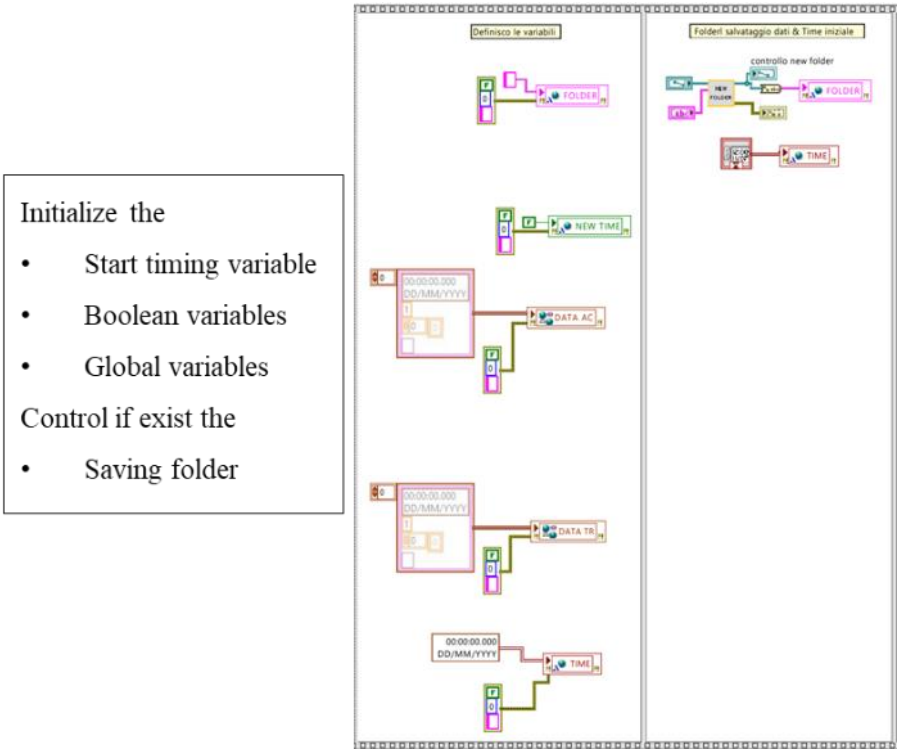

Figure 34: VI block diagram – Initialization of variables.

The second step Figure 35 regards the definition of the physical channels that characterized the acquisition task. In this stage, to not lack the synchronization of the different physical quantities that being in the measure chain, have been initialized a single loop to create the physical channel where are define the acquisition parameters such as the sensor sensitivity, sensor and acquisition module measure range, the sampling frequency, and the type of sampling (e.g., discrete sampling or continuous sampling). It is good to point out that this operation is done for each typology of sensor, that is dynamic or static sensor.

Channel definition

- Sensitivity
- Measure range
- Sampling frequency
- Type of sampling

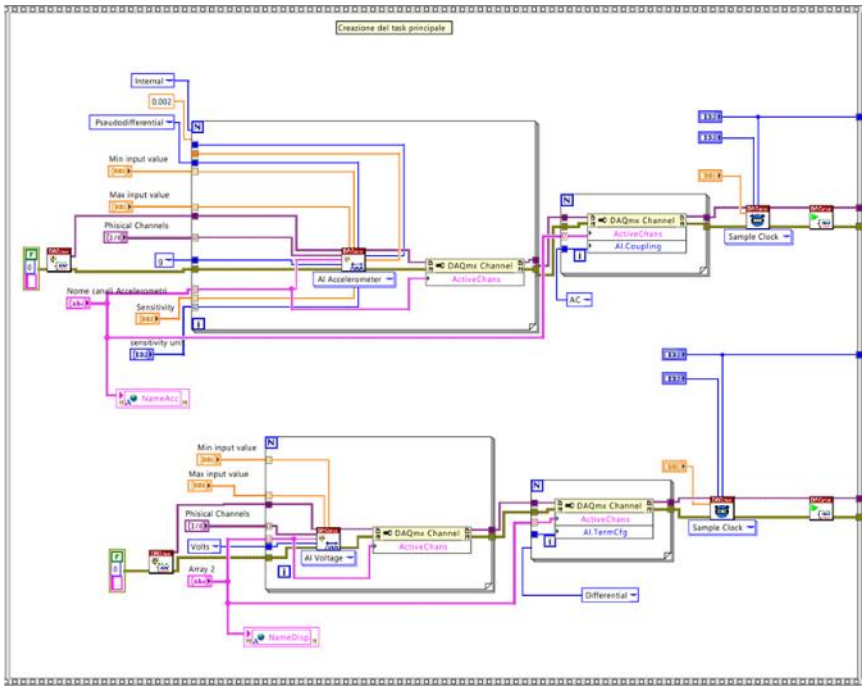

Figure 35: VI block diagram – Definition of the task parameters.

The third step Figure 36 regards the definition of the acquisition loop. Following the framework established in the previous step, for guarantee the determinism without jitter on the acquisition loop, that represent a time critical node in the acquisition process, has been initialized such reading block for each task (related to sensors family in the measure chain). The reading block is driven by the sampling frequency, and it has how result data acquired array. This array is sent in the RT global variable initialized in the step 1.

In addiction in this step there is a standby Boolean variable that operate in the real-time plotting of the acquired signal in order to make a visual inspection of the signal's qualities.

The fourth and last step Figure 37 regards the data saving loop. Here when the condition established by the Time stamp variable is verified each RT FIFO global variable are merged in a matrix array $\boldsymbol{m} \times \boldsymbol{n}$ where $\boldsymbol{m}$ are equal to number of samples and $\boldsymbol{n}$ the number of channels and saved in a TDMS file format.

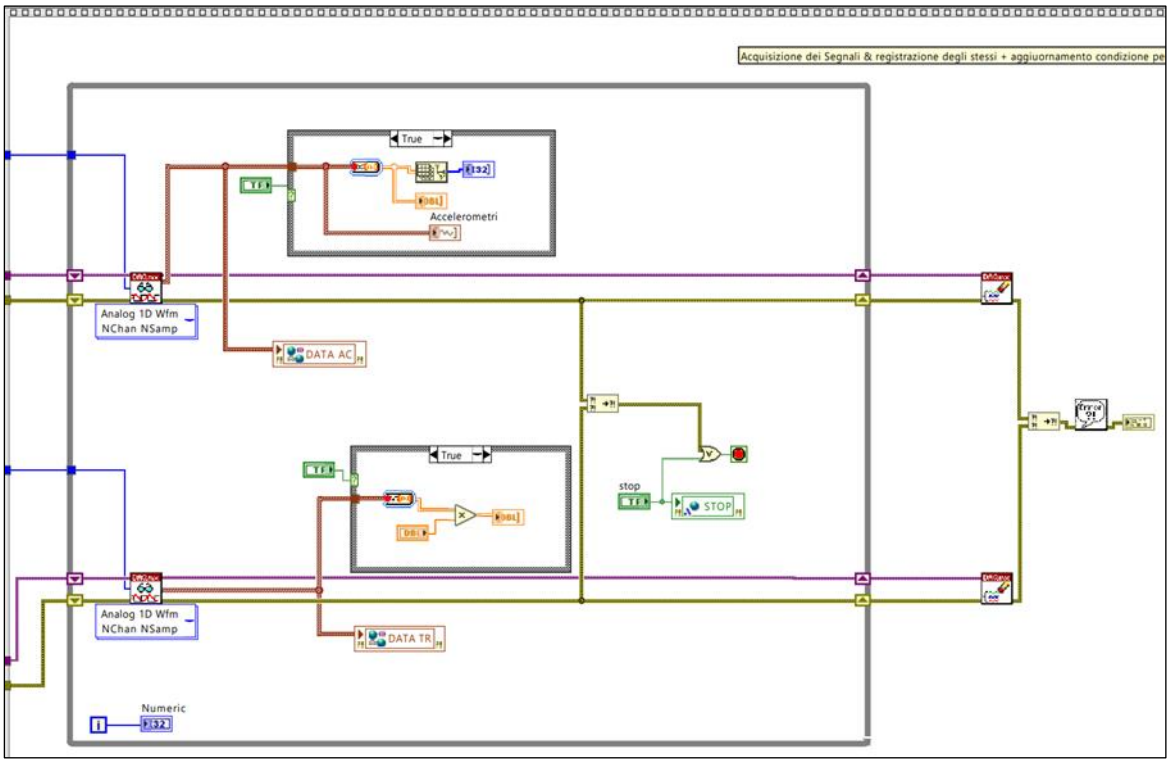

Figure 36: VI block diagram – Acquisition loop.

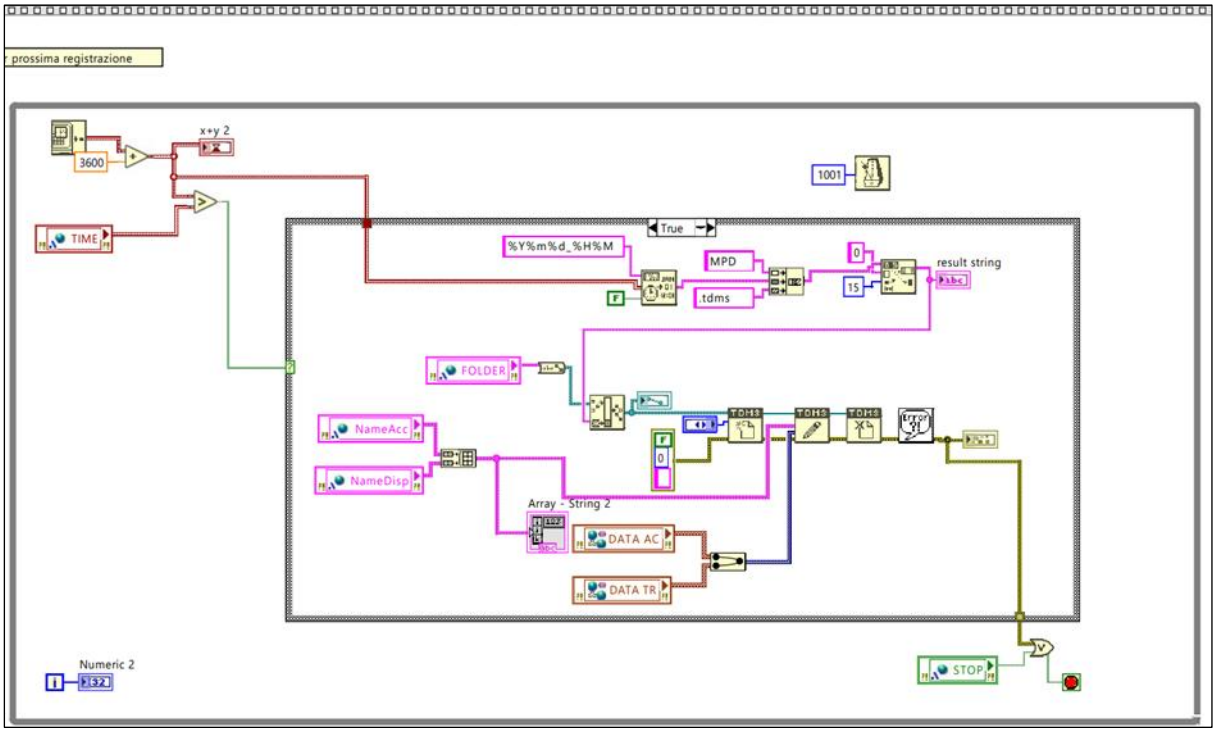

Figure 37: VI block diagram – Data saving loop.

3 Autonomous Procedure for the managing, post-processing and tracking of the modal properties from acquired data.

This chapter deals with the detailed description of an autonomous procedure, whose development has been the core of the present PhD Thesis. Such procedure, indeed, aims to manage and to post-process all the data that have been acquired and stored in a cloud server, from long-term monitoring as shown in Figure 38. The proposed procedure is also able to track over time the modal properties of the monitored structures that undergo excitations due to environmental actions.

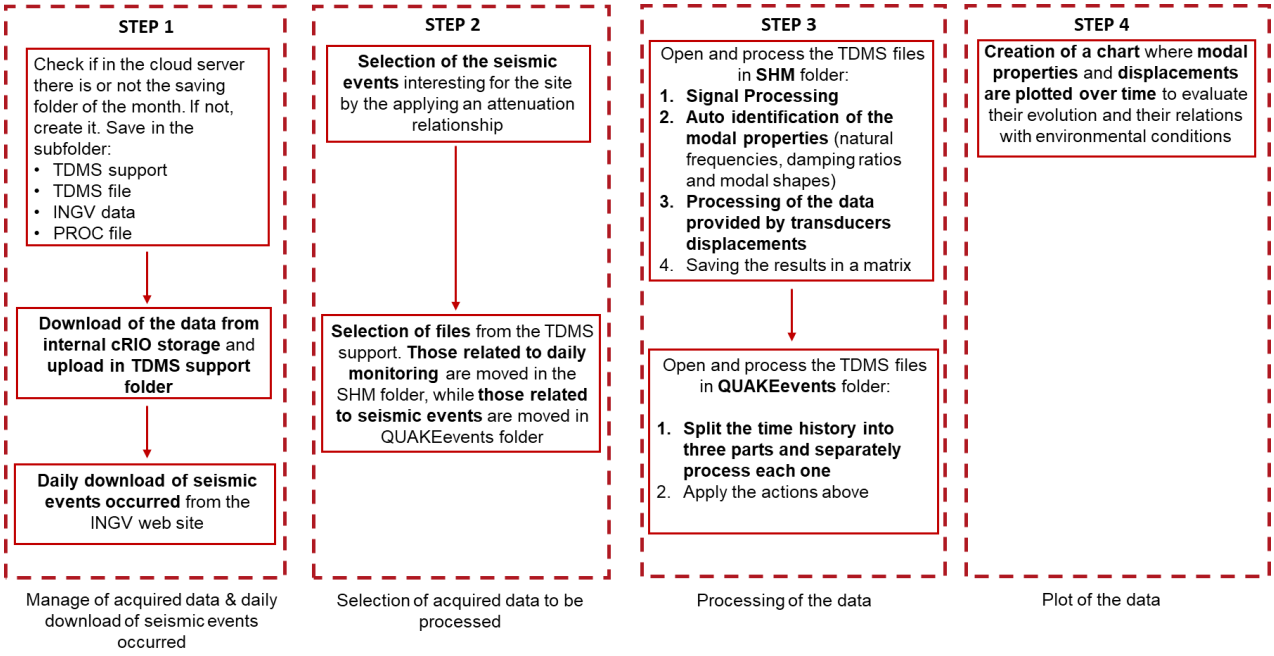

Figure 38: Autonomous procedure steps

The procedure is applied to the “Portico da Varano” that is an architectonical element characterizing the Ducal Palace of the city of Camerino.

The dynamic response over time of the monitored structure to environmental actions, as well as to extreme events, is collected in a time chart step 4 Figure 38. This way it is possible to observe and to detect the eventual variations of both natural frequencies, and modal shapes over time. Moreover, it is also important to observe if there is a correlation between the variation of the modal properties and the trend, over time, of the internal and external temperatures.

As a preliminary operation, the developed code menages the data acquired during monitoring. More in detail, the code moves the data from their physical storage that is the on-board memory of NI Compact Rio, to a specific folder of the cloud server that is named as current month and year, e.g.,

Decembre-2022. Successively, the data are going to be sorted in specific folders to divide data related to environmental actions, from those related to extreme events, i.e., seismic events.

A novel approach has been introduced, within the proposed procedure, step 2 of Figure 38, aiming to relate the data acquired during monitoring to a seismic event, which can occur near the site, and to detect possible changes in the dynamic behaviour of the monitored structure. More in detail, it is possible to check if there is any variation of the modal properties (i.e., natural frequencies and modal shapes) of the structure caused by a seismic event that can be significant in terms of magnitude and/or geographical proximity, by comparing the behaviour of the structure before and after the occurrence of the event. This issue falls within the field of the Characterization of the Seismic response of the Structures.

3.1 Characterization of the Seismic response of Structures.

In this section is described the novelty approach proposed to characterize and analysed the structural response when it is subjected to seismic input.

In the SHM, characterized by both dynamic and static sensors placed in strategical points, the acquired and analysed data related to a seismic event, together the data related to operational conditions, give a detailed chart of the structural behaviour in time.

In common practice, for the structural characterization from a defined input signal, it is followed the triggering approach, where a threshold value is assigned at the input signal to be acquired. More precisely, the acquisition system records the data only if the input signal is higher the threshold value, otherwise the data are disregarded.

This type of approach in continuous monitoring has some restrictions:

- we have discreet monitoring; the system acquires data in a certain daily time slot and is in stand-by outside of this. It is therefore not possible to draw a graph tracing the variations of the structural parameters over time and, if the extreme event occurred during a programmed daily time slot, when the system is in operation, the event is not detected by the system and does not we have information about the event.
- lack correlation about the signal source types; that is, we do not know if the signal is related to an environmental action (e.g., traffic, human activity, wind) or to an earthquake.
- the approach is Operator-dependent. Indeed, the threshold value is established by the operator who programs the acquisition system; thus, the sensitivity and the goodness of the threshold value (i.e., trigger), is related to the sensibility of the operator.

To overcome these restrictions, a novelty approach has been developed that relates acquired data to a seismic event by inferring the expected the Pick Ground Acceleration (PGA) from that event. This value is evaluated by applying the Ground Motion Prediction Equation (GMPE) which is a model that describes the movement of the ground on site. Therefore, we have both a continuously monitoring of the dynamic properties of the structure and of the events happened and underline if there is any changes after any events and also characterize the structural response known the event time history by the National Institute of Geophysics and Volcanology (INGV).

The stages followed to define this approach are:

i. a preliminary hazard analysis to calibrate an attenuation law, the GMPE, that provides the expected value of the PGA for each seismic event happened near the site.
ii. a daily database of the evens occurred, las section of step 1 Figure 38.
iii. selection of the events and the respectively data acquired files, step 2 Figure 38

Unlike the first point (i), the last two points, (ii) and (iii) are in the automatic procedure and are repeated every day.

3.1.1 Calibration of the Sabetta and Pugliese Ground Motion Prediction Equation

To obtain a better evaluation of the expected PGA in the site of interest, a preliminary calibration of the predictor parameters that drive the response of the attenuation law is performed. From the available hazard models in literature, the Sabetta and Pugliese model [Sabetta and Pugliese – 1996] [49] has been chosen to predict the PGAs.

This Hazard model is described by the following mathematical expression (3.1-1) where there are five predictor parameters that describe the ground motion intensity; an example of the resulting curves for each considered magnitude is shown in Figure 39.

$$\log(\mathrm{IM}) = \mathrm{a} + \mathrm{b} + \mathrm{c}\log(\mathrm{R}^2 + \mathrm{h}^2)^{1/2} + \mathrm{e}_1\mathrm{S}_1 + \mathrm{e}_2\mathrm{S}_2 \pm \sigma \qquad (3.1\text{-}1)$$

Where: i) IM is the intensity measure, the value of PGA; ii) a, b and c are three scalar parameters that influence the curve; iii) M is the magnitude value of the event; iv) R is the epicentral distance; v) S1 and S2, are two parameters that consider the soil type (these ones are further multiplied by two scalar parameters, e_1 and e_2); vi) h is a fictitious depth that incorporate all the factors that tend to limit the motion near the source and vii) σ is the standard deviation that take into account the uncertainty of the problem

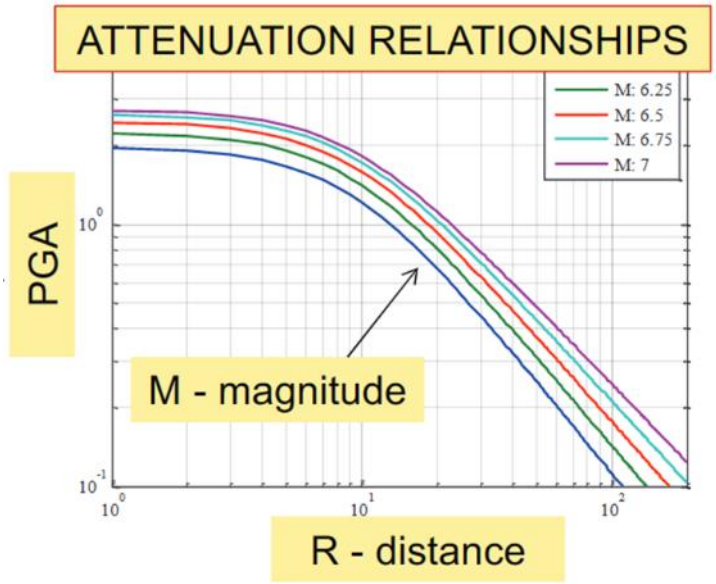

Figure 39: Example of the Intensity Measure (PGA) description by an Attenuation Relationship

Regarding the calibration procedure, a statistical approach, the Maximum Likelihood Estimation (MLE) method, has been used to find the most efficient and unbiased estimators of the variables that describe the PGA evolution with epicentral distance R and magnitude M of the event.

By defining a variable ϑ that groups all the predictor parameters, $\vartheta(a, b, c, h, e_1, e_2, S_1, S_2)$, of the Sabetta and Pugliese attenuation law (3.1-1), such GMPE can be rewritten in a general and functional form (3.1-2)

$$ln(IM) = lnIM(M, R, \vartheta) + \sigma(M, R, \vartheta) \cdot \varepsilon \quad (3.1\text{-}2)$$

where M and R , are respectively the magnitude and the epicentral distance of the event measured from the seismic station whereas, the variable ϑ collects the predictor parameters to be calibrated.

Aiming to simplify the problem some hypotheses have been done during the preliminary calibration of the parameters. The standard deviation σ of the probability distribution has been considered invariant with respect to the predictor parameters and its value has been assumed according to the value proposed by the authors [49]. Furthermore, the two parameters that provide information regarding the soil type (S_1 and S_2) are assumed equal to one, value that describes, according to the Authors of the GMPE, shallow and deep alluvium sites.

Due to the lack of recording stations in the city of Camerino, all the information related to the database of the recorded earthquakes refer to the seismic station located in Mount d'Aria, which is the closest one to the city of Camerino (Figure 40).

The mount d'Aria seismic station is located at 43.1927 latitude and 13.1427 longitude on a soil type category A, whereas the Ducal Palace, structure under investigation located in the city of Camerino, has the following geographical coordinates 43.1354 latitude and 13.0686 longitude.

The earthquake events considered for the preliminary calibration of the parameters of the GMPE, are those recorded from August 2016 to May 2021 for a total amount of 561 events, with magnitude ranging between 3.5 and 6.5, as shown in Figure 41.

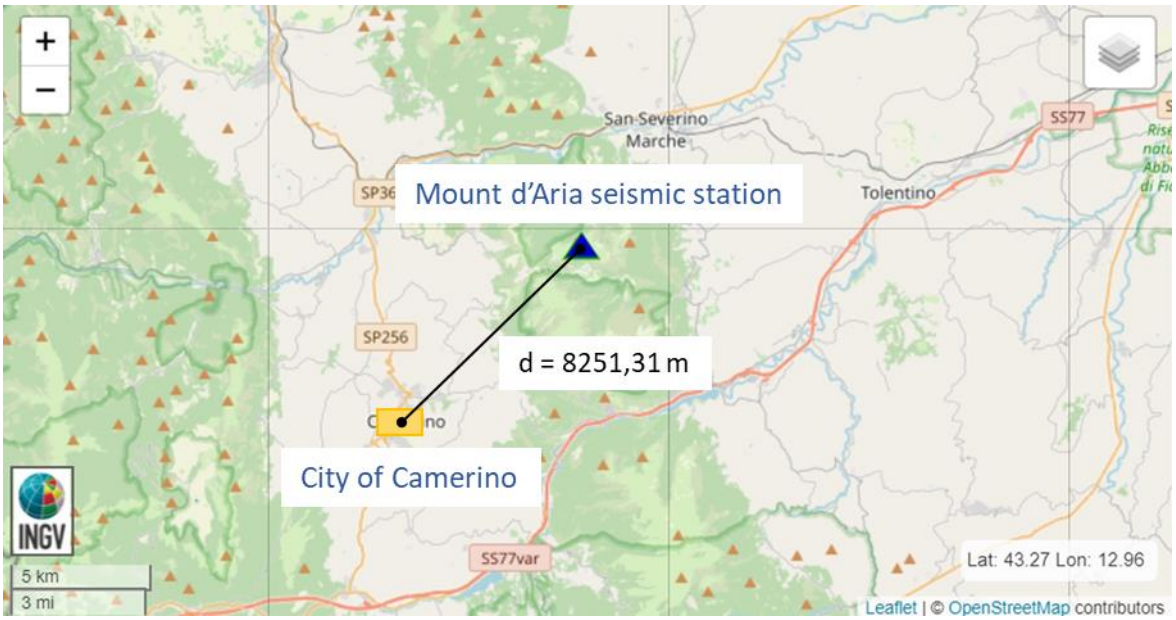

Figure 40: map with the location of the Mount d'Aria seismic station and the city of Camerino

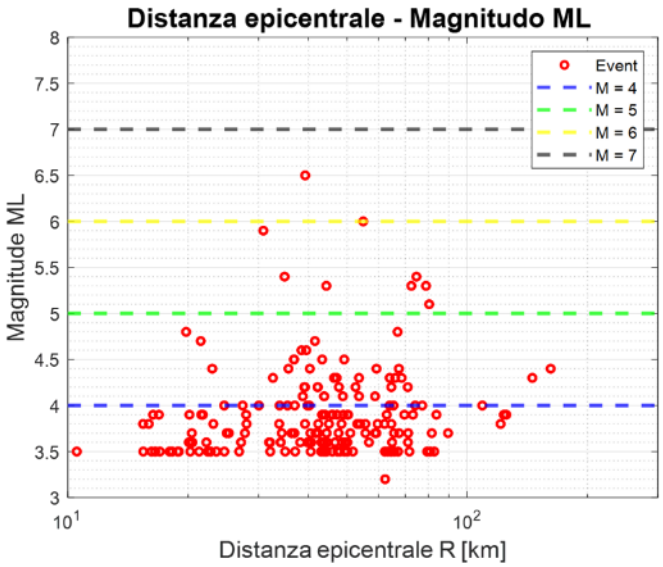

Figure 41: recorded events from August 2016 to May 2021 in mount d'Aria seismic station

The peak ground acceleration is known for each event as a function of magnitude M and of the epicentral distance R. From a literature review in the field of probabilistic seismic hazard analysis

[Baker 2013] [48], each PGA value has its own normal distribution Probability Density Function PDF (3.1-3). The GMPE provides a PGA that is the median value of the distribution.

$$PDF_{ln(IM)}|M,R,\vartheta = \mathcal{N}(f(M,R,\vartheta),\sigma(M,R,\vartheta)) \quad (3.1\text{-}3)$$

The optimization procedure has been carried out considering three different models characterized by increasing complexity, which means an increased number of variables governing the problem to be optimized. Therefore, as shown in Table 1, in each model there are some variables involved in the optimization procedure, while the others are assumed according to the GMPE as proposed by Sabetta and Pugliese 1996 [49] and their values are shown in Figure 42.

	Parameters optimized	Parameters from literature [49]
1st Model	a, b, c	c, e_1, e_2, h, S_1, S_2, σ
2nd Model	a, b, c, e_1, e_2	h, S_1, S_2, σ
3rd Model	a, b, c, e_1, e_2, h	S_1, S_2, σ

Table 1: Description of the optimization models

Freq. (Hz)	Const. Term a	Mag. Coeff. b	Dist. Coeff. c	Site Coeff. c_1	Site Coeff. c_2	h	σ
PGA (g)	−1.562	0.306	−1	0.169	0.	5.8	0.173
PGV (cm/sec)	−0.710	0.455	−1	0.133	0.133	3.6	0.215

Figure 42: parameters defined by Sabetta and Pugliese 1996 [49]

As previously stated, the parameters of the model have been determined through inference techniques, more in detail by means of the MLE method. Such method is the most efficient estimator of the unbiased vector of the parameters ϑ as reported in (3.1-4) [47]

$$\hat{\vartheta}_{\mathrm{MLE}}(\mathrm{x}) = \operatorname{argmax} \mathrm{L}_{\mathrm{x}}(\vartheta) \quad (3.1\text{-}4)$$

The likelihood (3.1-5) is the probability of the hypothesis ϑ for given data x (where x in this case represent values of PGA), and if each component of the observations x follows the same PDF the likelihood becomes the product of all the PDF (3.1-6). Such approach has been followed since each recorded Intensity Measure (IM) is the median value of a log-normal distribution function [48].

$$L_x(\vartheta) = P(x|\vartheta) \tag{3.1-5}$$

$$L_x(\vartheta) = \prod_{i=1}^{n} f(x_i;\vartheta) \text{ where } f(x_i;\vartheta) \text{ is the PDF} \tag{3.1-6}$$

expression (3.1-6) of the likelihood may generate numerical problem for rare observations, consequently, it is useful to work with the logarithms of the likelihood, as reported in (3.1-7) [47].

$$L_x(\vartheta) = \prod_{i=1}^{n} f(x_i;\vartheta) = \sum \log(f(x_i;\vartheta)) \tag{3.1-7}$$

The evaluation of the MLE is an iterative procedure developed in MATLAB where the initial values of the parameters (ϑ_0) are those defined by the authors (Sabetta and Pugliese). Figure 43a)-c) show the results of the parameters estimation for the three considered models. Each plot reports the recorded events in terms of epicentral distance R and intensity measure IM, while the points are related to different magnitude ranges ($2.5 \leq M \leq 3.5$ red points, $3.5 < M \leq 4.5$ yellow points, $4.5 < M \leq 5.5$ violet points, $5.5 < M \leq 6.5$ green points, and $6.5 < M \leq 7.5$ cyan points).

With the aim of choosing which of the proposed approximations is the one that provides the best costs/benefits ratio, the Akaike Information Criterion (AIC) [46] (3.1-8) is applied. The model that shows the smallest AIC value does not represent the best approximation, rather the one that provides the best compromise between the parameters to be determined (PGA) and the accuracy of the result (benefits).

$$AIC = 2k - 2\ln L(\vartheta) \tag{3.1-8}$$

where $2\ln L(\vartheta)$ is goodness of fit term and $2k$ is the penalty term.

Comparing the MLE values to the AIC index results, as shown in Table 2, the three models have similar MLE value and different AIC values. Therefore, since the first model is the one that has the lowest AIC index value, it is considered the one that provides the best parameter estimation to describe the attenuation relationship model of Sabetta & Pugliese.

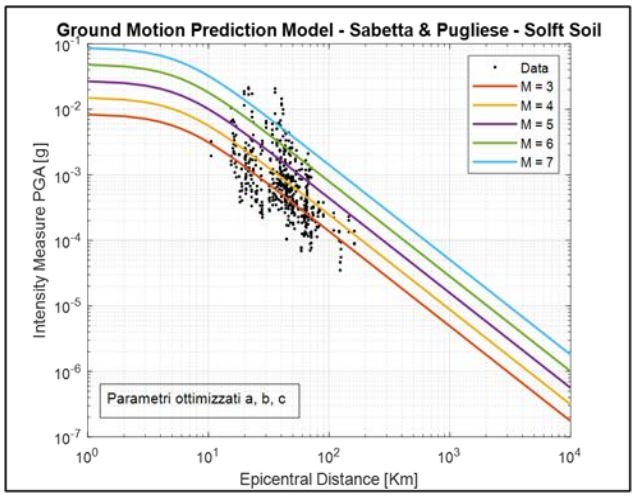

a) 1st Model

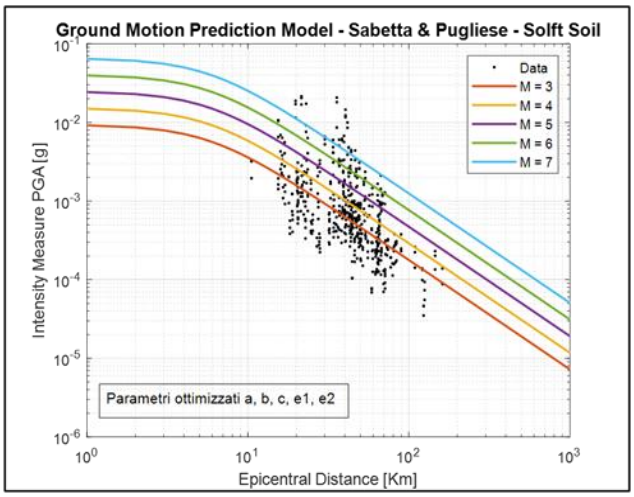

b) 2nd Model

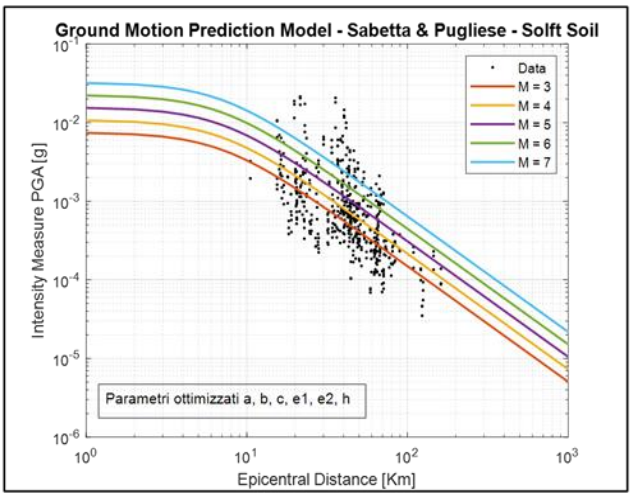

b) 3rd Model

Figure 43: results of the calibration for the three proposed models

Model	Maximum Likelihood MLE	Akaike criterion AIC
1st	289.83	-5.34
2nd	337.64	-1.64
3rd	337.64	0.35

Table 2: result in terms of MLE and AIC of the models

3.1.2 Daily database of seismic events occurred near the site of interest.

Among all the data acquired through monitoring it is necessary to identify those related to a seismic event happened near the site, through a daily download of a database of the events occurred. The database, indeed, can be realized from the daily data supplied by the Italian National Institute of Geophysics and Vulcanology (INGV) web site through a Web Services based on the International Federation of Digital Seismograph Networks (FDSN) specs.

In this phase we do not consider which events are significant for the structure under investigation, rather it is only a daily list of all extreme events, as shown in Table 3.

EventID	Time	Latitude	Longitude	DepthKm	Author	Catalog	Contributor	ContributorID	MagType	Magnitude	MagnitudeID	EventLocationName
33789411	2023-01-02T13:57:36.980000	43.9948	13.3383	5.9	'SURVEY-INGV'				'ML'	2	'--'	'Costa Marchigiana Pesarese (Pesaro-Urbino)'
33789031	2023-01-02T13:24:13.530000	43.9945	13.2127	30.1	'SURVEY-INGV'				'ML'	1.7	'--'	'Costa Marchigiana Pesarese (Pesaro-Urbino)'
33788901	2023-01-02T13:12:48.660000	44.2415	11.6403	9.1	'SURVEY-INGV'				'ML'	1.8	'--'	'2 km NE Casola Valsenio (RA)'
33788691	2023-01-02T12:44:09.550000	42.6812	13.2402	11.1	'SURVEY-INGV'				'ML'	1	'--'	'2 km SW Accumoli (RI)'
33788611	2023-01-02T12:35:07.760000	42.7863	13.1553	10.8	'SURVEY-INGV'				'ML'	0.6	'--'	'5 km E Norcia (PG)'
33788441	2023-01-02T12:12:52.790000	43.3808	12.5147	7.6	'SURVEY-INGV'				'ML'	0.6	'--'	'6 km W Gubbio (PG)'
33787251	2023-01-02T09:29:16.470000	36.4872	15.3325	27.8	'SURVEY-INGV'				'ML'	2.6	'--'	'Costa Siracusana (Siracusa)'
33787091	2023-01-02T08:54:43.830000	43.1348	12.8237	10.7	'SURVEY-INGV'				'ML'	0.9	'--'	'4 km NE Nocera Umbra (PG)'
33786761	2023-01-02T08:12:30.417000	35.4164	25.7959	19.5	'SURVEY-INGV-A'				'mb'	4.5	'--'	'Crete, Greece [Sea: Greece]'
33786271	2023-01-02T07:00:01.640000	40.82	14.426	0	'SURVEY-INGV-OV#SiSmi'				'Md'	1	'--'	'Vesuvio'
33786191	2023-01-02T06:45:46.430000	41.4897	14.6697	9.2	'SURVEY-INGV'				'ML'	1.3	'--'	'3 km S Mirabello Sannitico (CB)'
33785671	2023-01-02T05:28:08.996000	36.4957	21.7222	34.8	'SURVEY-INGV-A'				'mb'	4.7	'--'	'Costa Occidentale Peloponneso (GRECIA)'
33785391	2023-01-02T04:08:47.710000	43.2217	13.1242	10.1	'SURVEY-INGV'				'ML'	0.6	'--'	'4 km W San Severino Marche (MC)'
33785311	2023-01-02T04:01:37.460000	38.5777	16.7672	10	'SURVEY-INGV'				'ML'	1.5	'--'	'Costa Ionica Catanzarese (Catanzaro)'
33785201	2023-01-02T03:41:32.450000	41.6452	16.226	9.6	'SURVEY-INGV'				'ML'	1.8	'--'	'Golfo di Manfredonia (Foggia)'
33785151	2023-01-02T03:35:25.260000	38.3537	15.4297	119.6	'SURVEY-INGV'				'ML'	2.2	'--'	'Costa Siciliana nord-orientale (Messina)'
33785081	2023-01-02T03:20:29.460000	43.2312	12.6303	11.2	'SURVEY-INGV'				'ML'	1	'--'	'8 km N Valfabbrica (PG)'
33785031	2023-01-02T03:02:23.340000	41.2083	14.8682	15.6	'SURVEY-INGV'				'ML'	1.2	'--'	'2 km NE Pietrelcina (BN)'
33785011	2023-01-02T02:57:53.060000	42.3668	13.0172	9.6	'SURVEY-INGV'				'ML'	1.3	'--'	'3 km SW Castel Sant'Angelo (RI)'
33784971	2023-01-02T02:55:02.580000	38.8912	15.3823	230.8	'SURVEY-INGV'				'ML'	2	'--'	'Isole Eolie (Messina)'
33784801	2023-01-02T01:54:08.830000	45.7962	9.9923	11.8	'SURVEY-INGV'				'ML'	1.5	'--'	'1 km E Endine Gaiano (BG)'
33784661	2023-01-02T01:31:00.200000	42.7387	12.922	10.2	'SURVEY-INGV'				'ML'	1	'--'	'3 km NW Poggiodomo (PG)'
33784641	2023-01-02T01:05:49.280000	42.9188	13.0137	10.3	'SURVEY-INGV'				'ML'	1.5	'--'	'5 km NW Preci (PG)'
33784591	2023-01-02T00:42:11.010000	42.918	13.0103	10.5	'SURVEY-INGV'				'ML'	0.9	'--'	'5 km NW Preci (PG)'
33784491	2023-01-02T00:22:06.150000	42.919	13.0192	10.9	'SURVEY-INGV'				'ML'	0.9	'--'	'5 km NW Preci (PG)'

Table 3: Example of daily extreme events occurred in Italy from the INGV web site.

3.1.3 Selection of the data files related with the seismic events.

The selection of the events that can induce a significant structural response, from the daily collection of all the events occurred, is done by the application the calibrated Sabetta & Pugliese attenuation relationship.

Therefore, starting from the daily list of occurred earthquakes, as the one showed in Table 3, the following information are extrapolated:

1 the magnitude M of the events.

2 the geographic location in terms of Latitude and Longitude of the events.

By knowing the geographic location, in terms of Latitude and Longitude of the site where the structure interested by the SHM is located, it is possible to evaluate the distance between the site where the seismic event occurs and the site where the structure stands. Moreover, a lower bound threshold value for the peak ground acceleration is established (PGA threshold = 0.01 g) to select only the events that can produce a significant structural response.

Finally, it is necessary to clarify that among the parameters involved, the magnitude M is assumed as the one corrected with the Scordilis relation [50].

3.2 Post-processing of the data

All the data collected from the Structural Heath Monitoring (SHM) in order to make a daily monitoring of the dynamical properties of the structure under environmental actions (i.e., vibrations from traffic, anthropological activity etc.) that are significant to detect the operational conditions of the structure, and the data recorded during a seismic event occurred near the site of interest, selected as previously shown, will be processed as follow:

i. Figure 38 step 3, signal processing of the data to remove the unnecessary harmonic components from the signal, the unexpected trends, and to decrease the sampling order to have a signal lighter than the raw signal without losing the frequency contents of the signal.
ii. Figure 38 step 3, evaluation of the dynamic properties (i.e., natural frequencies, damping ratio and modal shapes) of the structure with a well-known procedure, the Stochastic Subspace Identification (SSI/Cov) (Section 1.2.3) algorithm where the results are driven by the covariance of the response. The output of this step consists in a stabilization diagram (Figure 4).
iii. Figure 38 step 3, analysis of the stabilization diagram by means of a machine learning tool that provides the hierarchical clustering of the stable poles (Section 1.2.4) for the automatic identification of the main vertical lines that stand for the principal vibration modes of the structure.
iv. Figure 38 step 4, mapping the vibration modes in terms of natural frequency to evaluate their trend over time by highlighting the vibration modes associated to the SHM with respect to those associated to extreme events,
v. Figure 38 step 4, mapping also the response of LVDTs over time.

Regarding the first step (i), the removal of unnecessary harmonic components from the signal, it has been done by a signal filtering operation. Among the different types of filters available in literature, a bandpass filter with cut of frequencies of 0.5 Hz as lower limit and 30 Hz as higher limit, has been used for the monitored case study in this study. For what concerns the frequency limits the lower and upper bounds have been defined according to the expected frequencies of the monitored case study. The fundamental vibration modes of the structure under investigation (Portico Varano of the Ducal Palace of the city of Camerino), indeed, are higher than 0.5Hz. On the other hand, the higher expected vibration mode has a natural frequency lower than 30 Hz. Such estimations have been done after an

experimental campaign performed with the purpose to evaluate the dynamical behaviour of the structure thanks to a preliminary Operational Modal Analysis test (OMA).

Subsequently, the signal has been resampled through a decimation to decrease the sampling order. Generally, natural frequency higher than 30 Hz are not expected for civil structures. Being the sampling frequency Fs equal to 2048 Hz, a decimation factor of 20 has been chosen in order to decrease the sampling frequency to 102.4 Hz. This value of frequency can detect every harmonic component of interest because the Nyquist frequency (from the theorem of sampling) is equal to 51.2 Hz. This last value represents the maximum signal to be sampled with the overmentioned sampling frequency, Fs, and it is also higher than the lower bound of frequencies (30 Hz).

Finally, the resampled signals have been also subtracted with polynomial expressions of order n=0 to remove eventual offsets of the signals from the zero and to evaluate if there is any loss in the frequency contents between the raw signals and the resampled ones, the Power Spectral Density (PSD) of the signals is performed (Figure 48(c)).

For what concerns data related to seismic events, the signals have been windowed before their processing procedure previously explained. The windowing has been done to obtain two different time histories over time, one before the event and the other after the event. This latter is done also to avoid considering the transient part of the signals in the subsequent analyses.

Regarding the second step (ii), that is the evaluation of the modal properties of the structure (i.e., natural frequencies, damping ratios and modal shapes) from the selected and resampled data, it is done thanks to the well-known identification procedure based on the SSI/Cov algorithm. The given input parameters (number of sensors and time lag values, those last values are evaluated following the rule described in the literature review) and the response matrix of the data we assess the output covariance matrix, known how the Toeplitz matrix, and evaluate the state matrix A of the dynamic system. From this one it is possible to assess by solving the eigenvalue problem the dynamics modal properties of the structure (Section 1.2.3).

Such procedure is iterative, and the number of iterations is assigned by a scalar variable that describes the system order. This latter is fixed and assumed equal to 100 to obtain a 50x50 submatrix of the state matrix A that contains the dynamic information of the system and a higher number of poles in the stabilization diagram as to obtain a good resolution in the vertical alignment of these ones.

Regarding the stabilization diagram, the threshold values to establish if a pole is stable or not, are:

- for a stable pole in frequency $\Delta f = 1\%$
- for a stable pole in damping ratio $\Delta \xi = 5\%$

- for a stable pole in modal shape $1 - MAC = 2\%$

Generally, the operation of selecting the vertical lines that identify the stable poles, which means the structural modes of the structure under investigation, is made manually by the operator. Such procedure is done within a continuously structural health monitoring, and it requires a high effort, consequently, it is preferable to exploit a Machine Learning tool, to identify the hierarchical clusters.

Each cluster represents, indeed, the vertical line of the stable pole and the rule to establish if a cluster can be representative of a vertical line is the count of the number of poles within the cluster itself. In the developed application the minimum number of poles has been assumed equal to 25.

For what concerns the rule used to establish if a pole can be part of a cluster or not, as explained in Section 1.2.4, the expression provided by [Magalhaes et all. 2009] [27] is employed, even though 0.5 has been assumed as the upper bound value of the distance.

The outcome of this procedure, summarized in fourth (iv) and fifth (v) steps, is a chart where the identified frequencies are grouped. It is worth to remember that the frequencies are detected thanks to the dynamic identification procedure and the static measurements provided by the linear voltage displacement transducers located across the existing cracks of the vaults on the Varano of the Ducal Palace. The trend over time of the natural frequencies has been monitored to evaluate if there is any correlation with the environmental condition (i.e., action of the temperature, which is another monitored parameter). Moreover, the chart is also able to provide information regarding the modal properties identified through SHM and the changes due to the occurrence of extreme events, thanks to the use of different flags in the chart.

4 Case-studies

The SHM algorithm developed within this Thesis has been applied together with other suitable monitoring techniques for the study of two case-studies that are the Portico da Varano of the Ducal Palace of Camerino, and the Santa Maria in Via Church. Both the case-studies belong to the cultural heritage and were damaged during the2016 Central Italy seismic sequence.

Either the SHM of Ducal Palace, and of Santa Maria in Via are part of the ARCH project "Advancing resilience of historic areas against climate-related and other hazards" funded by the European Union's Framework Programme for Research and Innovation (Horizon 2020) under grant agreement No 820999.

4.1 Portico da Varano of the Ducal Palace of Camerino

4.1.1 Description of historical evolution of the palace

The Ducal Palace [Cipriani et al. – 2022] [51] depicted in Figure 44 is a renaissance building of Camerino, a city located in Central Italy in the inner Apennine area of the Marche Region, about 65 km from the Adriatic Coast, 70 km from the city of Perugia and 190 km from Rome.

Figure 44 : Ducal Palace in Camerino, Italy: (a) aerial view from the North-West side (b) aerial view from South-East; (c) aerial view from South-West; (d) view of the inner courtyard from the North corner of the Portico da Varano

The Palace is also defined as “part of the city” thanks to their continuous interaction over-time that led to architectural and urban spaces mutually conditioned. Ducal Palace hosted the headquarters of the University of Camerino until the last seismic sequence of 2016 that made it unusable in safe conditions.

The nucleus of Ducal Palace has ancient origins, it was remodelled at the end of the XIV century and completed in the second half of the XV century under Giulio Cesare da Varano. Over the centuries, the layout of the Palace underwent many modifications thanks to acquisitions that led to the incorporation of other surrounding buildings, which caused a structural reorganizations and maintenance works, thus resulting in a complex structural system characterized by a significant irregularity either in plane, and in elevation (Figure 45). In detail, the structural system is characterized of sandstone masonry with variable textures, slab systems in wood, reinforced concrete, and vaulted ceilings, and weak connections between the masonry walls and the ceilings.

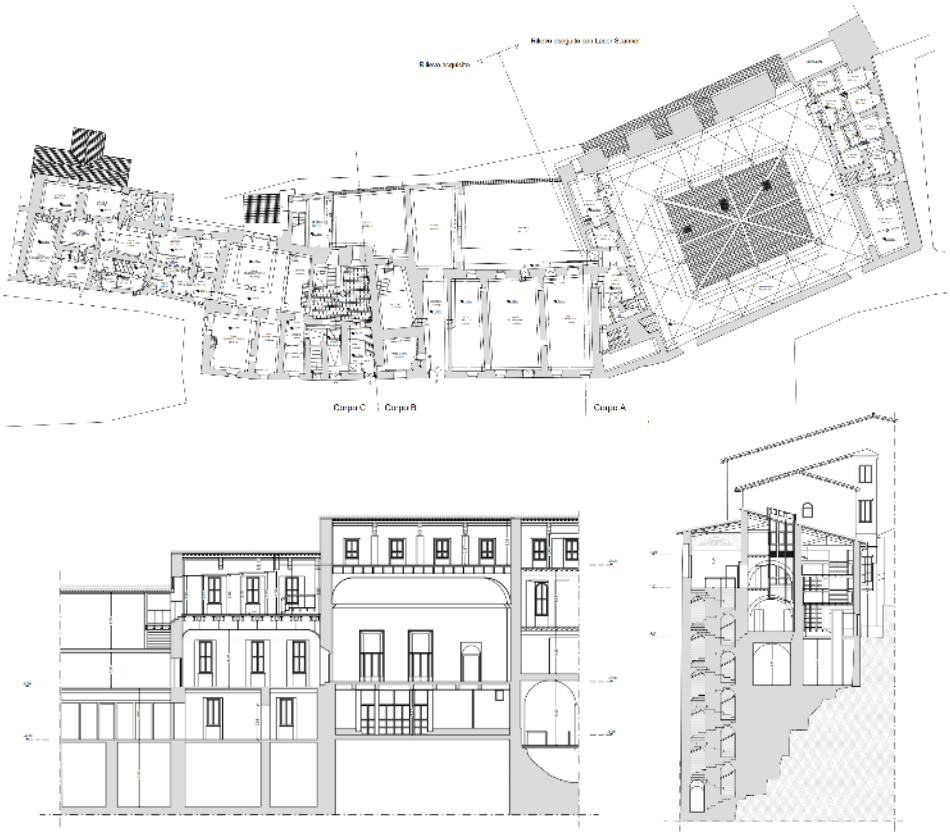

.

Figure 45 : Ducal Palace in Camerino, Italy: (a) plan view Q = + 0.00. (b) section views

After the seismic sequence that struck central Italy from August 2016 to January 2017, the structural vulnerabilities of the Ducal Palace strongly emerged, with damages observed both in the elevation structures and at the floor levels (Figure 46).

Given the complexity of the Palace, a specific area, the Portico da Varano or Sottocorte, an architectural symbol for the city probably designed by the great military architect Baccio Pontelli (Figure 47) has been identified. The damages suffered by the vault of the quadriporticus, and by the perimeter walls have interdicted the public access to the Palace and have required safety securing measures. Important damages concerning non-structural elements were also detected, with detachments of internal plaster and cracks located in the “camorcanna” ceilings, some of them decorated with fresco paintings. The Portico da Varano is characterized by a trapezoidal shape in plan with sandstone masonry, n. 14 circular sandstone columns, vaulted ceilings, reinforced concrete slabs and steel floor slabs with arches.

Figure 46 : damages after 2016 central Italy earthquake

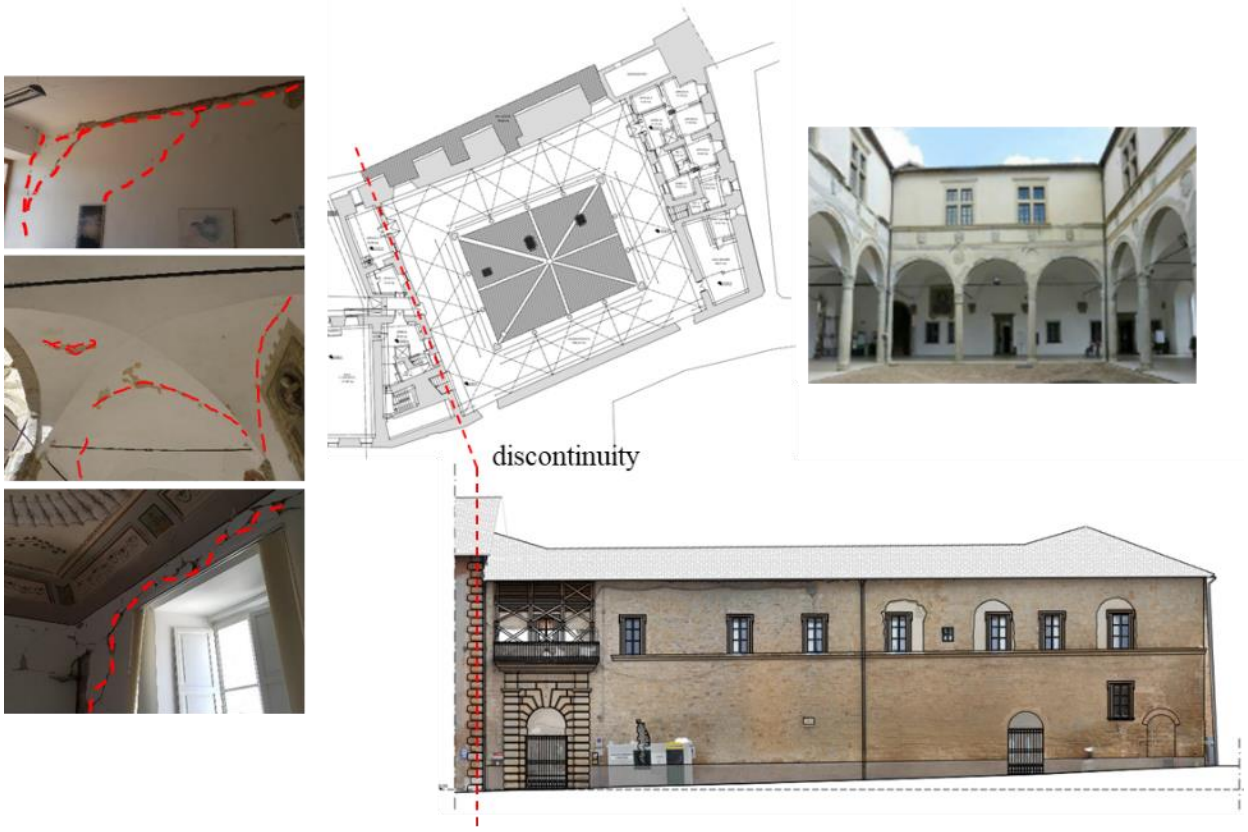

Figure 47 : Portico da Varano: (a) damages after 2016 central Italy earthquake (b) plan view Q = + 0.00; (c) Nord-West view from Cavour square; (d) internal view

Aiming at achieving a better and real comprehension of the structure and at track the variations of the properties that defines the safety of the structure, a static and dynamic monitoring system has been installed.

4.1.2 Dynamical Identification

4.1.2.1 Operational Modal Analysis (OMA) of Portico da Varano

Ambient vibration tests have been performed with the OMA technique to obtain a first evaluation of the dynamic behaviour of the structure in terms of natural frequencies, damping ratios, and modal shapes of the main global vibration modes. Since now on such values will be considered as control values for the monitoring.

The test setup is characterized by *i*) n. 12 uniaxial high sensitivity piezoelectric accelerometers (PCB 393B31); *ii*) n. 3 acquisition modules NI 9234 of the National Instrument (NI) enterprise; *iii*) a NI Compaq DAQ chassis (cDAQ-9178) for the channels synchronization; *iv*) a wireless thermometer (Elitech RC-51H) to measure the environmental conditions during the test. The signal acquisition has been controlled through the NI Signal Express software with a Dell Precision 7450 laptop.

Three configurations of sensors have been used to achieve a complete representation of the dynamic behaviour of the structure in its horizontal direction, characterized either by reference and moving sensors. Such configurations are necessary given that the first-floor level, which is safely accessible despite the damages due to earthquake, cannot be realistically modelled as a rigid diaphragm due to its geometric and material features.

Data acquisition has been performed at a sampling frequency of 2048 Hz for about 30 minutes. This duration corresponds to more than 4000 times the fundamental period of the building, as suggested in [Kita et all. – 2019] [37] Afterwards, the signals have been pre-processed to remove the linear trend by subtracting the logged signal with a zero-degree polynomial, by filtering them with a band-pass filter with a cut-off frequency between 1 and 30 Hz, and finally resampled at a frequency of 100 Hz to reduce the amount of data and to make subsequent analyses faster.

Figure 48, Figure 49 and Figure 50, shows the three configuration of sensors and the Power Spectral Density (PSD) of both raw and resampled data.

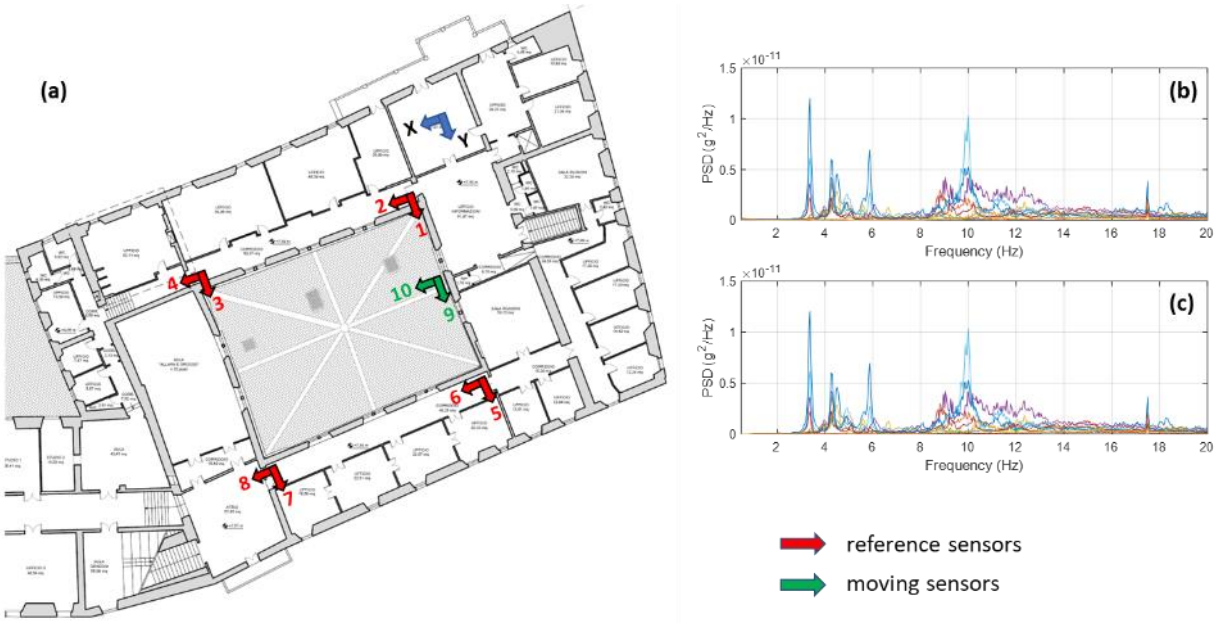

Figure 48 : Configuration n.1: (a) reference and moving accelerometer sensors, (b) Power Spectral Density of raw data, (c) Power Spectral Density of resampled data.

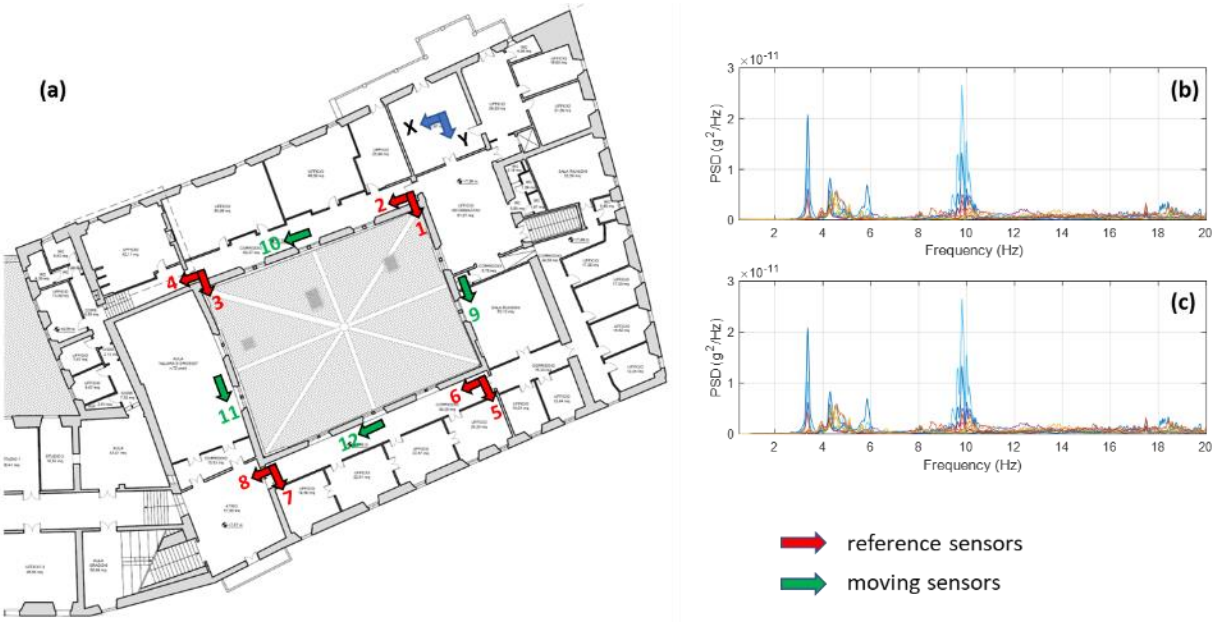

Figure 49 : Configuration n.2: (a) reference and moving accelerometer sensors, (b) Power Spectral Density of raw data, (c) Power Spectral Density of resampled data.

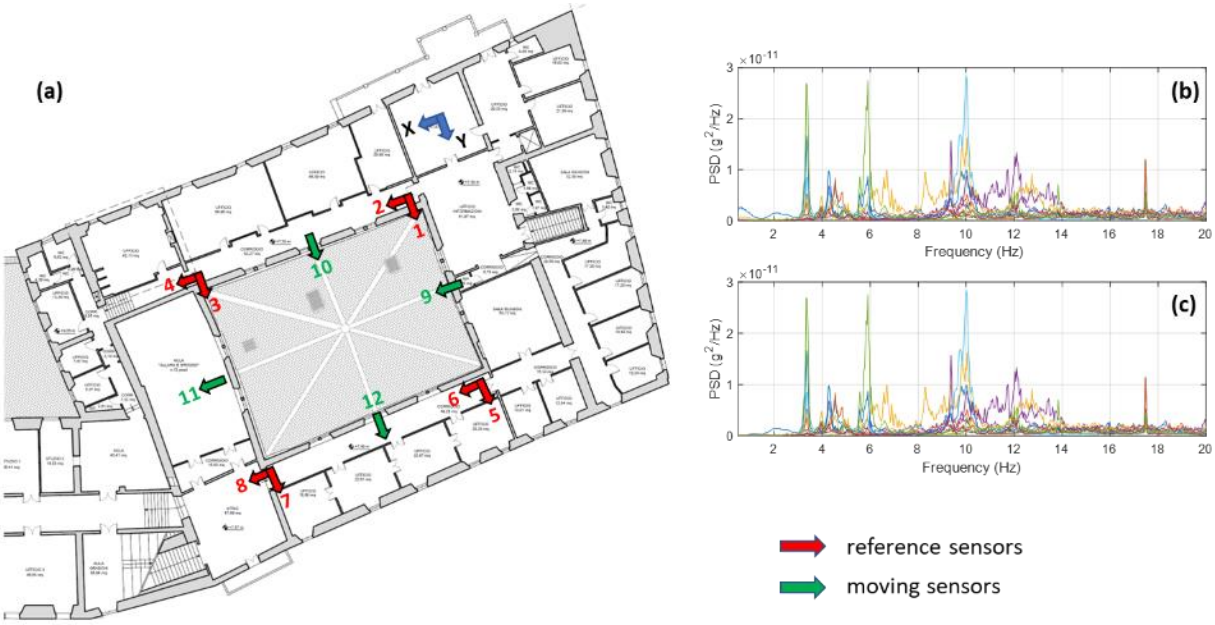

Figure 50 : Configuration n.3: (a) reference and moving accelerometer sensors, (b) Power Spectral Density of raw data, (c) Power Spectral Density of resampled data.

To approach the identification of the modal parameters (i.e., natural frequencies, damping ratios, and modal shapes) the Post Separate Estimation Re-scaling (PoSER) merging strategy [Dohler et all – 2010] [52] and [Reynders at all – 2009] [53] has been used. Such strategy is based on the evaluation of the modal parameters for each measurement configuration and on the grouping of all the configurations in equivalent one. More in detail, for each configuration of sensors, the modal

parameters identification has been done with the Stochastic Subspace Identification algorithm where the results are driven by the output covariance (SSI/Cov), by the assessment for each setup of the modal shape scale factor of (4.1-1) [Magalhaes - 2010] [24], and finally by the re-scaled Mode Shapes matrix. Figure 51 shows the flow-chart of the merging strategy used.

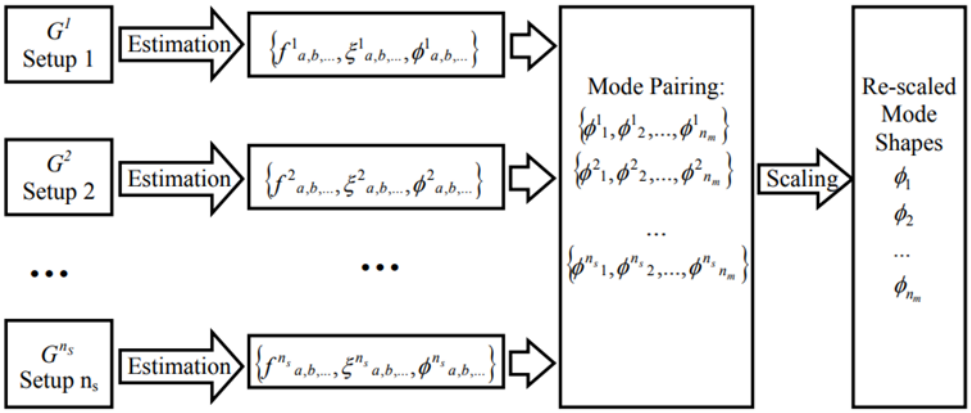

Figure 51 : Classical merging strategy (PoSER) from [Filipe Magalhaes – Phd Thesis]

$$\alpha_i^{j\to k} = \frac{\left(\phi_i^{j,ref}\right)^H \cdot \left(\phi_i^{k,ref}\right)}{\left(\phi_i^{j,ref}\right)^H \cdot \left(\phi_i^{j,ref}\right)} \tag{4.1-1}$$

where:

- $\phi_i^{j,ref}$ contains the mode shape components of mode i at reference output evaluated in setup j.
- $\phi_i^{k,ref}$ contains the mode shape components of mode i at reference output evaluated in reference setup k.

The stabilization diagrams for each measurement configuration are shown in Figure 52. Table 4 summarizes, instead, the results of the merging strategy and the mode shapes identified, for a total of four modes whose deformed shapes are shown in Figure 53 together with the AutoMAC matrix and the Modal Complexity Factor (MCF) index. This takes values between 0 (real mode) and 1 (complex mode). The rules for determining if a pole is stable are: *i*) $\Delta f \leq 1\%$; *ii*) $\Delta\xi \leq 5\%$ and *iii*) $MAC \leq 98\%$.

(a)

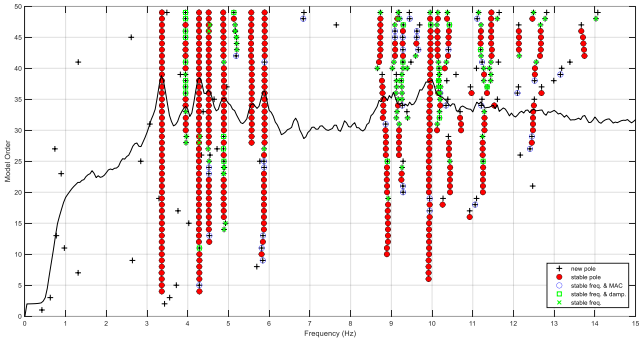

(b)

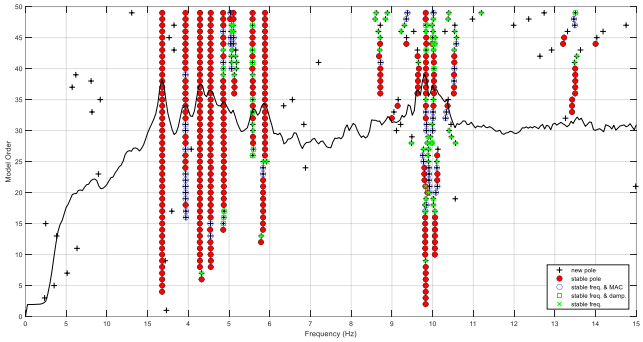

(c)

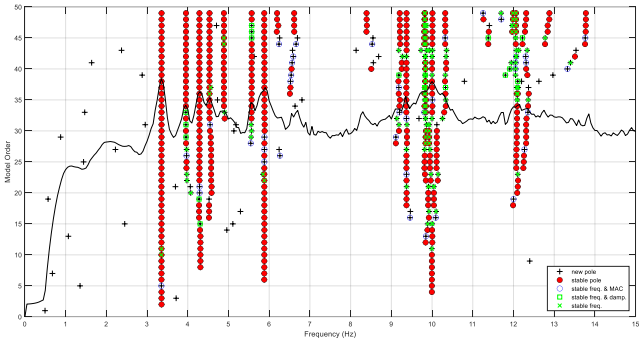

Figure 52 : Stabilization Diagram: (a) test setup n.1, (b) test setup n.2, (c) test setup n.3

Mode	**Frequency [Hz]**	**Damping ratio [%]**	**MCF**
1st Mode	3.36	1.56	0.02
2nd Mode	4.28	1.53	0.06
3rd Mode	4.53	3.48	0.11
4th Mode	5.88	1.50	0.03

Table 4 : Results of Ambient Vibration Test (AVT)

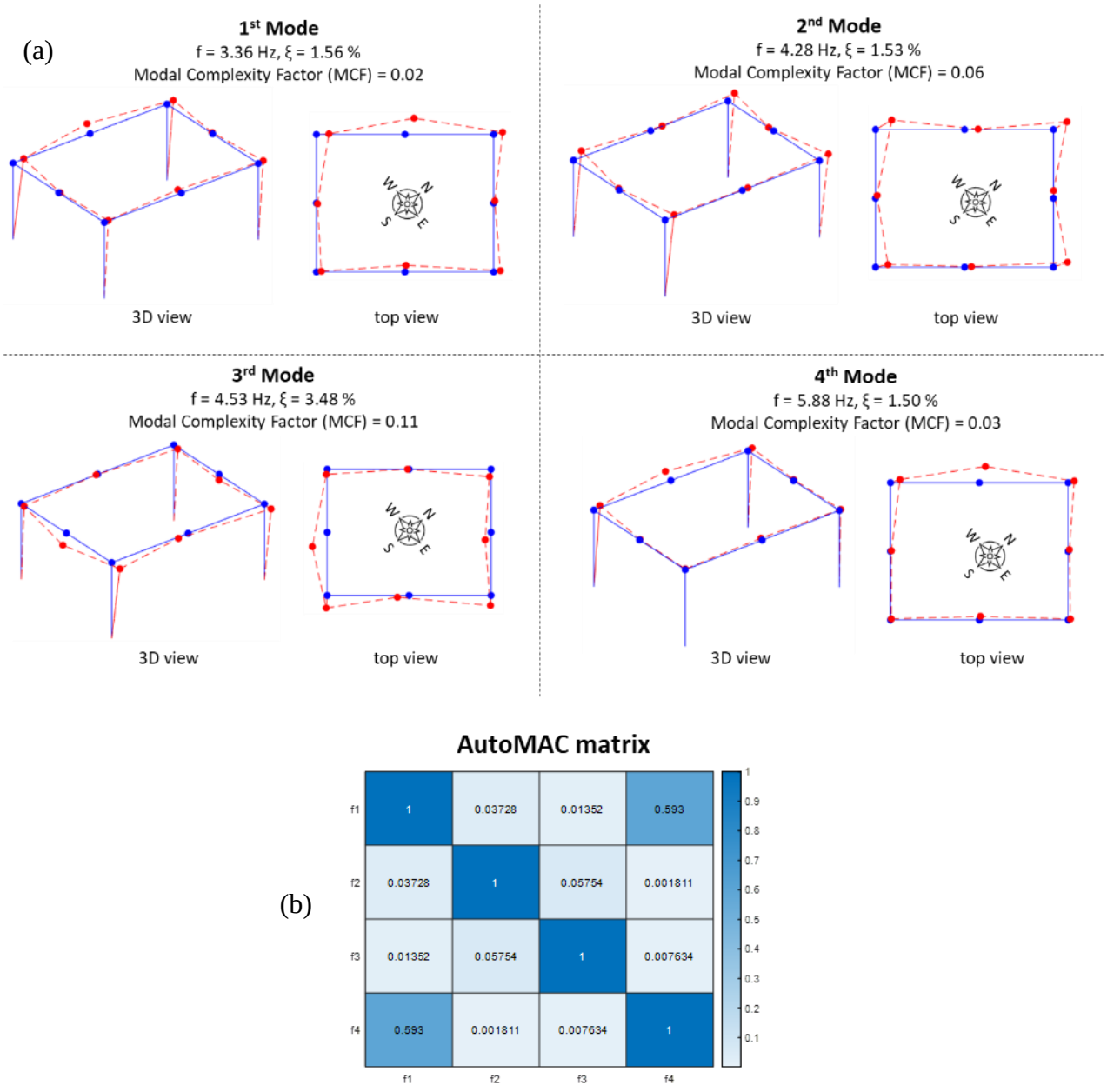

Figure 53 : (a) mode shapes identified and (b) the AutoMAC matrix.

From the observation of the modal shapes results the following comments can be drawn: *i*) the behaviour of the structure shows that the ceiling does not behave as a rigid diaphragm; *ii*) the modal shapes in the horizontal directions, X and Y, are strongly influenced by the displacement of midpoints of each side of the building; *iii*) the direction of major displacement is focused in the area where the damages on the vaulted ceilings (North direction) are located.

4.1.2.2 Hammer test of tie-rods

To provide a global view of the dynamic behaviour of the structure, Experimental Modal Analysis (EMA) have been performed in addition to Operational Modal Analysis (OMA). EMA tests have been carried out with an impact hammer on the Portico da Varano tie-rods, which play a crucial role

in the stability of both masonry arches, and vaults under either static (gravity) loads, and dynamic actions (e.g., those induced by seismic events [Resta et all. 2020] [59], [Gentile et all. 2017] [56], [Duvnjak et all. 2020] [55], [Gentilini et all. 2013] [57]).

Experimental modal analysis with impact hammer represents a widely used typology of structural dynamic characterization tests [Ewins D. J. 2000] [8] being a non-invasive and non-destructive way to acquire the principal resonant frequencies of the system, based on a known external input. Such technique is largely used to evaluate the dynamic properties of ancient metal tie-rods. The acquired information can also be used to estimate the tensile force of the rods by using mathematical expressions to link the first modal shape frequency with the tensile force (see [Kim and Park 2007] [58] and [Bokaiant A. 1990] [54]).

The dynamic identification tests have been carried out following the Single Input Multiple Output (SIMO) test procedure, where the structural response due to an impulsive force has been measured with n.3 accelerometers sensors, placed as shown in Figure 54(a). More in detail, for each tie-rod tested (Figure 55), the experimental campaign has been done by giving n. 3 impulsive forces in the A2 point and by evaluating the response in the A1, A2 and A3 points. Each recording has a length of 20 sec with a sampling frequency of 2048 Hz.

Figure 54(b)-Figure 54(e) show the instrumentation used to perform the tests and that encompasses: *i*) n.3 piezoelectric accelerometers PCB 393A03, sensitivity 102 mV/g, measurement range +/- 5 g and frequency range from 0.5 to 2000 Hz; *ii*) impulse force test hammer PCB 086D20, sensitivity 0.23 mV/N, measurement range +/- 22240 N pk and mass of 1.1 Kg; *iii*) a coaxial cable, *iv*) acquisition module NI 9234 with n.4 analog channel, 51.2 kS/s for each channel, measurement input +/- 5 V, 24 bit resolution and anti-aliasing filters; *v*) a Compaq DAQ chassis, cDAQ 9171; and *vi*) a workstation DELL to acquire data with the NI Signal Express software.

The outcomes of the experimental modal analysis are assessed through the Frequencies Response Functions (FRFs) that represent the response or "Output" of the system due to the external excitation, or "Input". The FRFs are evaluated with the well-known analytical expression (4.1-2) called "Inertance" as described in [Ewins - 2000] [8], where A is the accelerometer measurement (Output), and F is the hammer measurement (Input).

$$A(\omega) = \frac{Output}{Input} = \frac{A}{F} \tag{4.1-2}$$

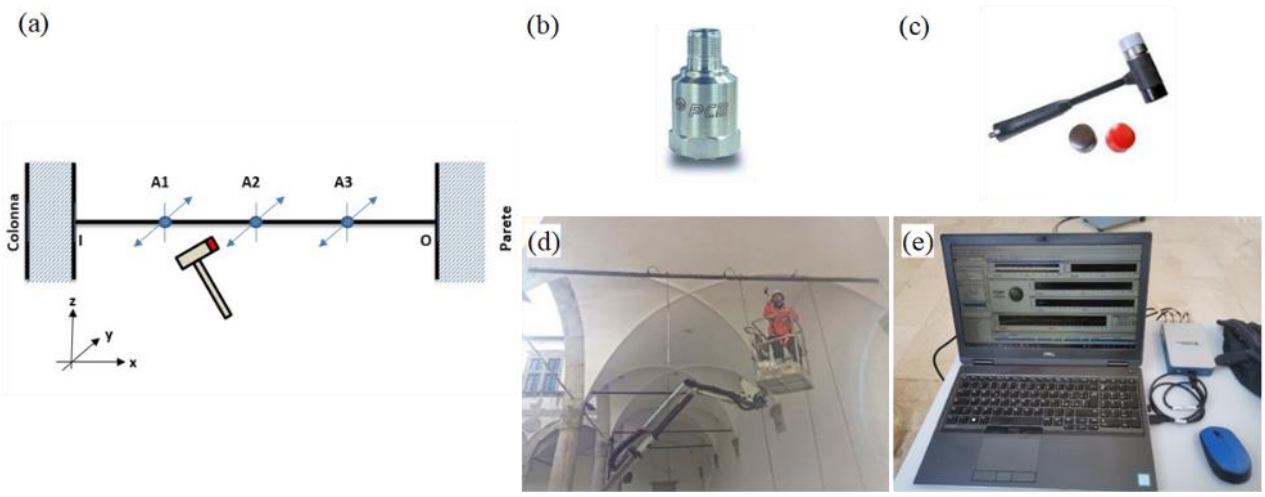

Figure 54 : Impact Hammer Test: (a) sensors configuration, (b) accelerometer PCB 393A03, (c) hammer PCB 086D20, (d) execution step of the test and (e) acquisition system.

Figure 55 : location of tie-rods tested.

The extraction of the dynamic modal properties (e.g., natural frequencies, damping ratios, and modal shapes) from the FRF, has been done through the peak-picking method [Ewins D. J. 2000]. Such technique has been chosen since, by observing the FRFs, the resonant peaks of each vibration mode of the system are well separate.

In Figure 56, Figure 57, and Figure 58, are presented the results achieved for the tie-rods C01, C16, and C18 assumed to be representative of the response of the structure with the used monitoring system. Table 5 compares the results obtained with a previously dynamic identification performed by the University of Parma on the 12th of January 2012.

Tie-rod	Section [mm^2]	Natural Frequencies [Hz]		
		1st	2nd	3rd
1	35x25	2.80 (5.30)	6.60 (11.10)	11.80 (17.10)
2	54x32	8.30 (8.30)	17.44 (17.50)	28.39 (28.50)
3	56x33	5.55 (5.00)	12.30 (11.60)	21.49 (20.80)
11	55x35	8.10 (7.80)	17.55 (17.00)	29.59 (28.90)
12	54x35	8.75 (9.10)	18.90 (19.50)	31.80 (32.80)
13	57x35	7.60 (6.80)	16.95 (15.70)	28.90 (27.40)
14	56x35	11.95 (11.70)	25.65 (25.30)	42.45 (41.90)
15	55x35	11.04 (11.10)	23.40 (23.80)	38.90 (39.10)
16	56x35	11.00 (11.20)	23.54 (24.10)	38.90 (39.80)
17	55x33	11.40 (11.20)	24.30 (23.80)	40.50 (39.60)
18	59x33	12.45 (12.20)	26.45 (25.40)	42.75 (43.00)
frequencies evaluated by the University of Padova				

Table 5 : Results from EMA analysis

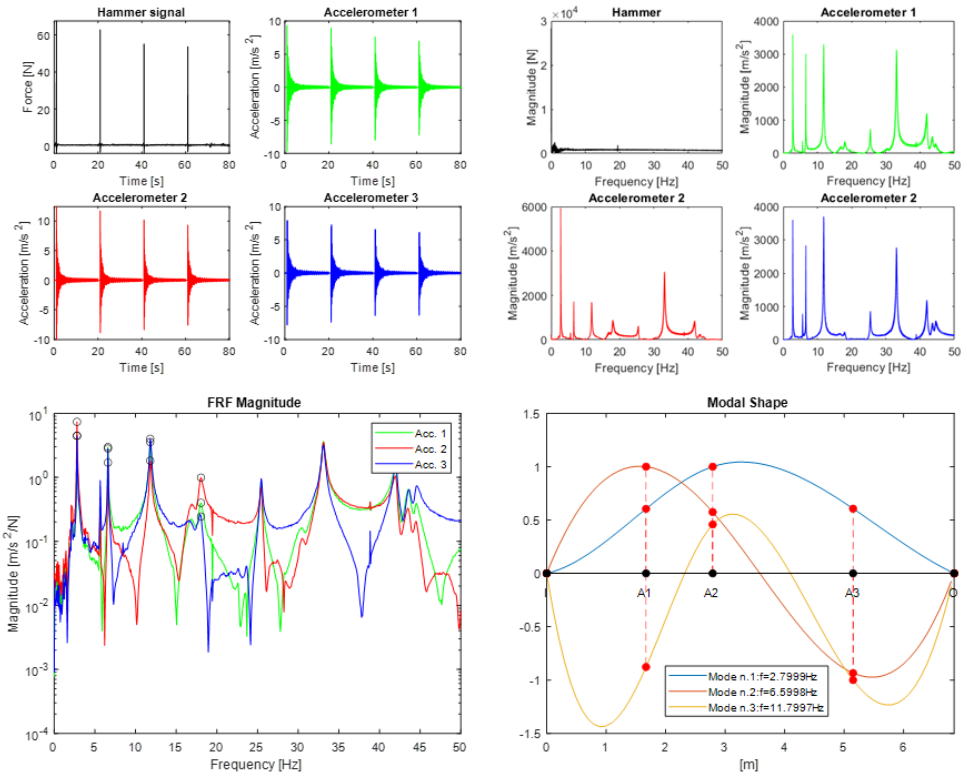

Figure 56 : C01 tie-road: (a) Accelerometers and Hammer time histories, (b) Accelerometers and Hammer Fourier Transform, (c) Frequency Response Function (FRF) and (d) modal shapes

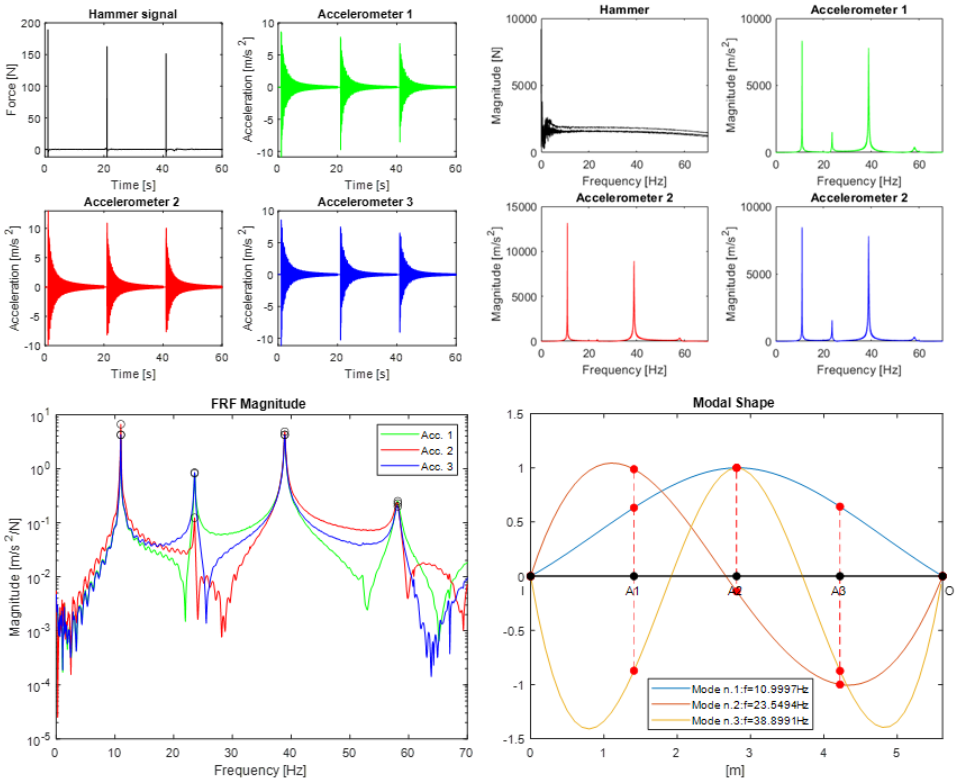

Figure 57 : C16 tie-road: (a) Accelerometers and Hammer time histories, (b) Accelerometers and Hammer Fourier Transform, (c) Frequency Response Function (FRF) and (d) modal shapes

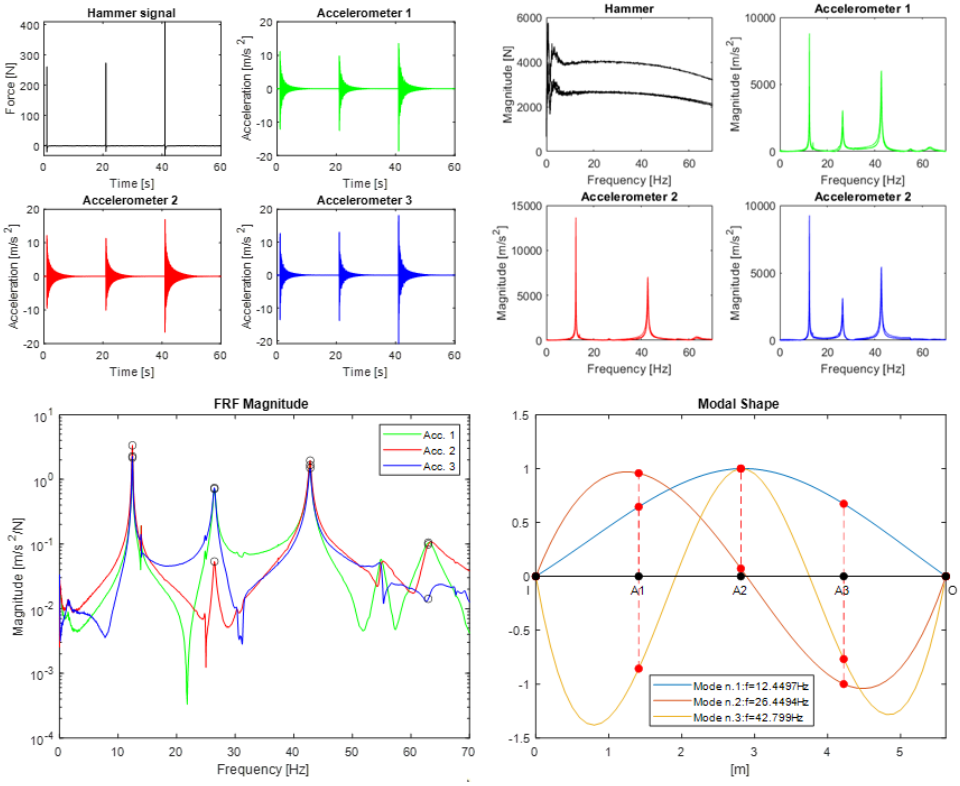

Figure 58 : C18 tie-road: (a) Accelerometers and Hammer time histories, (b) Accelerometers and Hammer Fourier Transform, (c) Frequency Response Function (FRF) and (d) modal shapes

Finally, aiming at evaluating the current stress state of the tie-rods, the experimental modal analysis results have been analysed using the analytical expression (4.1-3), which is known from the theory of flexure. Such expression provides a value of the tensile force for each k-th measured frequency related to the modal shape of the mechanical system.

$$F = \frac{M \cdot L^2 \cdot (2f_k)^2}{k^2} - \frac{EJ}{L^2} \cdot (k\pi^2) \qquad (4.1\text{-}3)$$

where M is the mass of the element, L is the length of the element, E is the elastic modulus of the material, J is the moment of inertia of the section, and k is the mode number. The results of the mean axial force estimated as the mean of the axial force evaluated for each frequency and for each tie-rod are summarized in Table 6. The Coefficient of Variation (CV) describe the variation on the axial force evaluated for each frequency. It has been estimated as the ratio between the standard deviation σ and the mean value of the axial force.

Tie-rod	B [mm]	H [mm]	A [mm2]	J [mm4]	M Kg/m	L m	F_{medio} [kN]	CV [%]	F_{medio} [kN]	CV [%]
1	35	25	875	4.56E+04	6.88	6.85	3	-	27	24%
2	54	32	1728	1.47E+05	13.58	6.99	180	2%	181	2%
3	56	33	1848	1.68E+05	14.53	7.13	90	8%	77	11%
11	55	35	1925	1.97E+05	15.13	6.37	151	2%	139	1%
12	54	35	1890	1.93E+05	14.86	6.33	177	3%	192	3%
13	57	35	1995	2.04E+05	15.68	6.23	129	1%	104	2%
14	56	35	1960	2.00E+05	15.41	5.56	262	1%	248	1%
15	55	35	1925	1.97E+05	15.13	5.8	236	2%	238	1%
16	56	35	1960	2.00E+05	15.41	5.76	233	1%	244	1%
17	55	33	1815	1.65E+05	14.27	5.6	225	2%	214	2%
18	59	33	1947	1.77E+05	15.30	5.62	290	1%	286	6%

red text – axial force evaluated from University of Padova

Table 6 : Results of tie-rods axial force

The comparison between the experimental results achieved and those obtained by the University of Parma, shows that there is a variation in the first three frequencies identified, especially for the tie-rod C01. This variability of the frequency values, detected in both experimental campaigns, can be related to the material ageing, but also to the evolution of a different damage scenario that can affect the building after an extreme event such as the earthquake.

4.1.3 Dynamic and static monitoring system

Aiming at shading further light to the evolution of the dynamic behaviour of the structure in terms of modal properties and crack patterns of the vaulted ceilings and to better describe their evolution over-time, both a dynamic and static monitoring system have been deployed on the Portico da Varano.

The dynamic monitoring system installed encompasses: *i*) n.4 piezoelectric accelerometers PCB 393 B31 at the first horizontal floor, with a sensitivity of 10 V/g, and a measurement range of +/- 0.5 g; *ii*) n.3 piezoelectric accelerometer PCB 393 A03 on the C01, C16 and C18 tie-rods, with a sensitivity of 1 V/g, and a measurement range of +/- 5 g. All the installed accelerometers are connected to a NI 9234 module for the A/D signal conversion.

In detail, Figure 59 (a) reports the simplified accelerometers configuration installed on the main (first) floor of the Portico da Varano. Such a configuration has been adopted to reduce the data to be stored and processed, since the objective of the monitoring system is to control the evolution of the local collapse mechanism involving the out-of-plane overturning of the four internal façades. This simplified configuration has been chosen after a comparison of the components of the midpoint's displacements (points A01, A02, A03, A04 in Figure 59 (a)) recorded in the X and Y directions, with those identified with the complete configurations (Figure 48, Figure 49 and Figure 50) previously shown. Table 7 reports the variation of the displacements between the complete configurations adopted in the dynamic identification and the reduced configuration; as observable the variations are close to zero for all the Modes, with the exception of Mode 2. The 2nd modal shape shows a high variation on the displacement component; however, this is result can be disregarded because that modal shape regards the in-plane behaviour (see Figure 53(a)).

Regarding the configuration of the monitored tie-rods (Figure 59(b), it has been chosen since the major crack patterns on the vaulted ceilings are localized in this area.

For what concerns the static and environmental monitoring system, instead, it consists of: *i*) n.2 triplets of displacement sensors (Figure 60(b), linear potentiometers (Gefran PZ67-A) with measurement range of +/- 50 mm; *ii*) n.2 wireless sensor Elitech RC-51H for internal temperature and relative humidity (Figure 59(a)); and *iii*) a weather station, WatchDog 2700 (Figure 59(a)), to measure temperature, relative humidity, wind speed and wind direction. Displacement sensors are connected to a NI 9209 module while the environmental sensors have an own internal data logger.

Point of measure	direction of measure	Mode 1	Mode 2	Mode 3	Mode 4
A01	X	{ }	{ }	{ }	{ }
	Y	0%	87%	0%	0%
A02	X	0%	98%	0%	0%
	Y	{ }	{ }	{ }	{ }
A03	X	{ }	{ }	{ }	{ }
	Y	0%	75%	0%	0%
A04	X	0%	91%	0%	0%
	Y	{ }	{ }	{ }	{ }
{ } point without measure component					

Table 7 : Variations of the midpoint displacement components recorded between the simplified configuration and the complete ones.

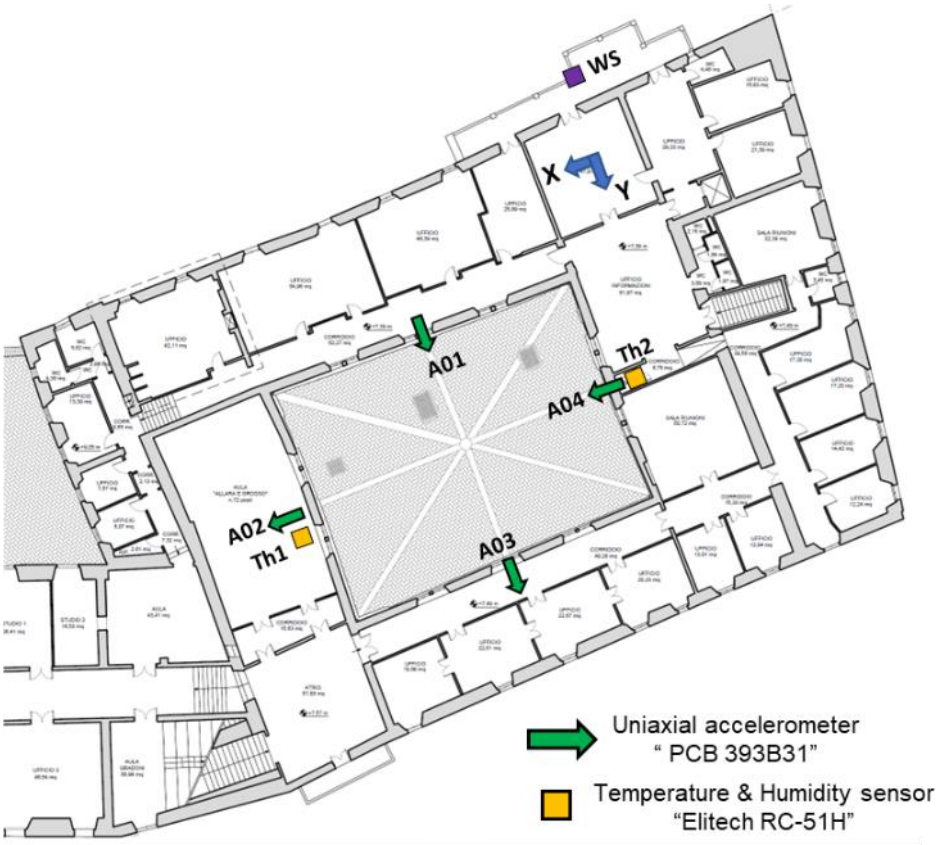

(a)

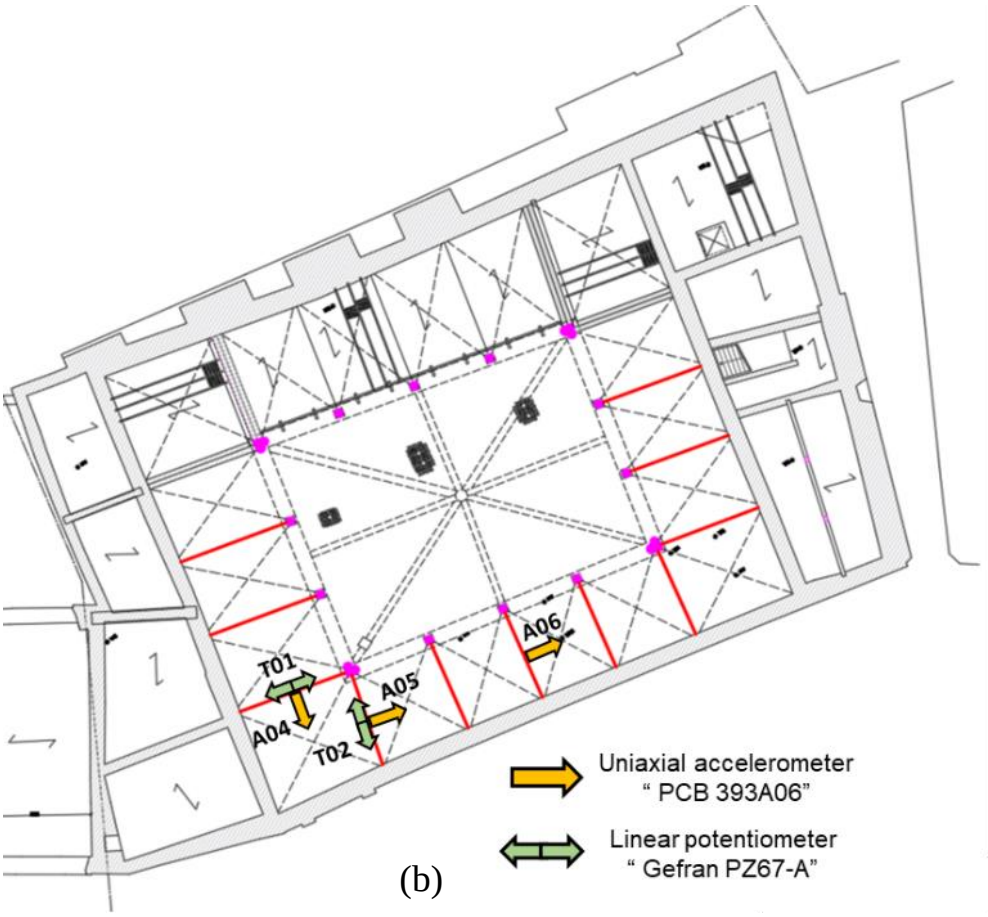

Figure 59 : Sensor's configuration installed as the (a) first floor and (b) on the tie-rods.

Figure 60(a) and (c), depicts the measurement configuration of the three linear variable displacement transducers (LVTDs), which can measure all the possible motions configuration of the crack, such as side scrolling or stretching and that may lead to a further opening of the crack itself. The third LVDT, provides a redundancy measure that allow to evaluate if there are coupled rotational movements.

Data acquisition, storage, and data transfer are controlled by a cRIO 9045 real-time connected to the network via router and remotely controlled. The acquisition software deployed on the cRIO, which has developed in Labview environment, acquires data continuously and in real time, by saving it in the internal storage of the controller. Thanks to a host pc connected in the same network these data are taken and stored in a cloud server. This approach, based on the continuous streaming of data and on the determinism guaranteed by the acquisition system, makes it possible to investigate eventual dependencies on environmental conditions in a short time, but also to record the response to seismic events without the risk of losing data samples. The data are stored in 10-minute-long files.

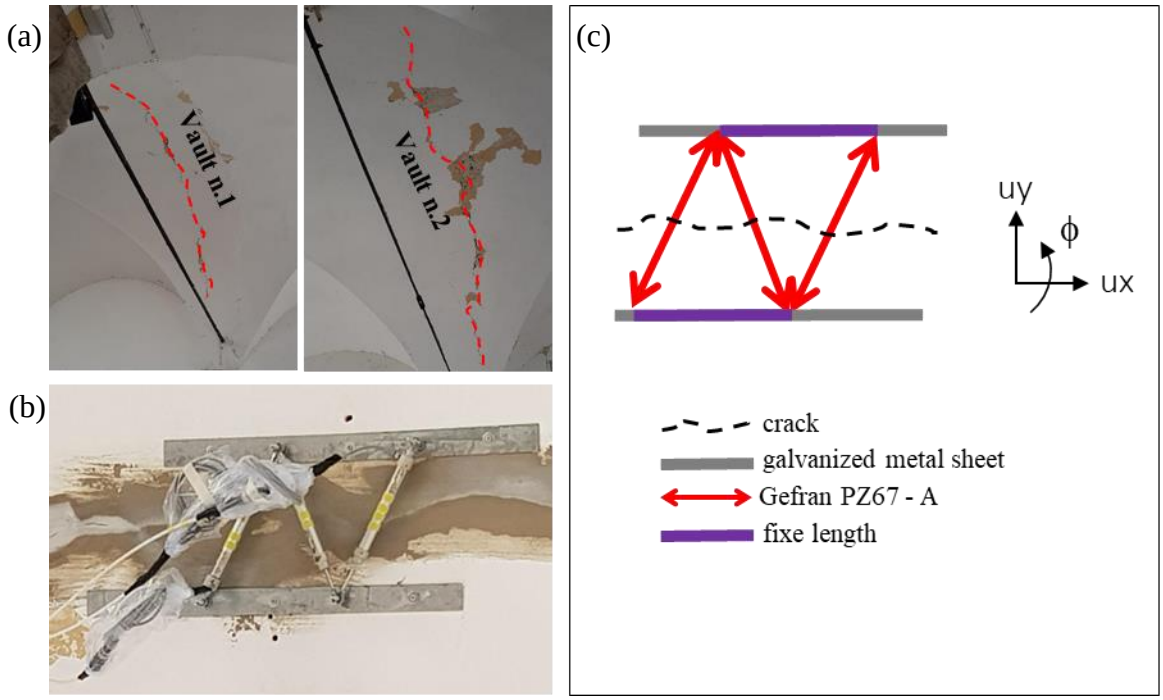

Figure 60: (a) crack pattern on the vaults of the Portico da Varano n.1 and n.2; (b) configuration of the linear transducers displacement installed across a crack; and (c) further details regarding the measurement of the crack evolution through the monitoring by LVDTs.

4.1.3.1 Overview of dynamic monitoring results

As previously introduced, the dynamic monitoring system designed for the Portico da Varano aims at monitoring the out of plane behaviour of the internal four sides together with the description of the variations of the modal properties over-time. The results shown in Figure 61, related to natural frequencies and environmental temperature recorded from November 2021 up to April 2023, highlights the ability of the simplified configuration of sensors to keep and to track the natural frequencies of the vibration modes that describe the over-turning mechanism.

By analysing Figure 61, it can be observed that the natural frequencies identified show a fluctuation over-time that can be related with the variation of environmental conditions through seasons (i.e., temperature). In detail, an increasing of the values of the natural frequency's values with the temperatures emerges, and it can be attributed to the thermal expansion that leads to the closure of cracks and to an increment of the interlocking between the elements composing the masonry.

For what concerns the identification of the natural frequencies of the first four modal shapes, previously identified in the preliminary OMA ambient vibration test (see Section 4.1.2.1), it is possible to observe that these values are confirmed and can be considered as are correctly identified thanks to the points concentration in the graph of Figure 61. Specifically, the first and the fourth natural frequencies are well bounded, while the second and the third ones have a major dispersion.

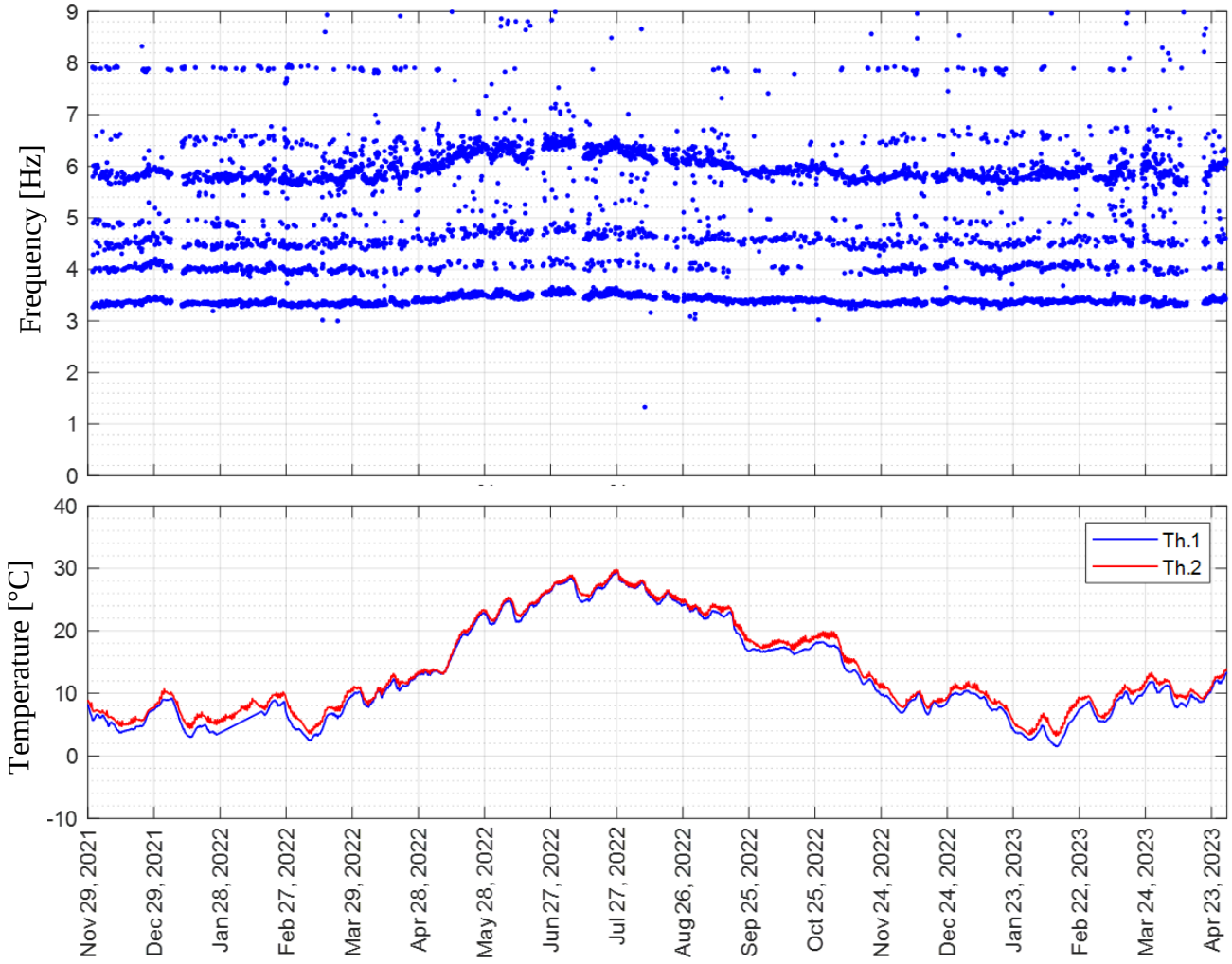

Figure 61: identified natural frequencies trend over-time of the Portico da Varano, (b) trend of the temperature's over-time.

In order to have also an idea of the variation of the modal shapes, and to check if the identified frequencies are related to the behaviour analysed in the preliminary OMA ambient vibration tests (see Section 4.1.2.1, Figure 53(a)), the modal assurance criterion (MAC) index has been evaluated for each identified frequency. The values of the modal shapes vectors assessed from the preliminary OMA ambient vibration tests have been taken as the zero (reference) condition. The results are shown in Figure 62, Figure 63, Figure 64 and Figure 65.

The results show that the first, third, and fourth natural frequency identified follow their own modal shapes that describe the out-of-plane mechanism of the structure, with a MAC index higher than 80% (black dots form Figure 62 to Figure 65).

There is a light coupling between the first frequency and the fourth one, since both of the modal shapes describe the same response direction.

The second frequency identified, instead, is related to the in-plane response of the structure, which is beyond the objective of the monitoring.

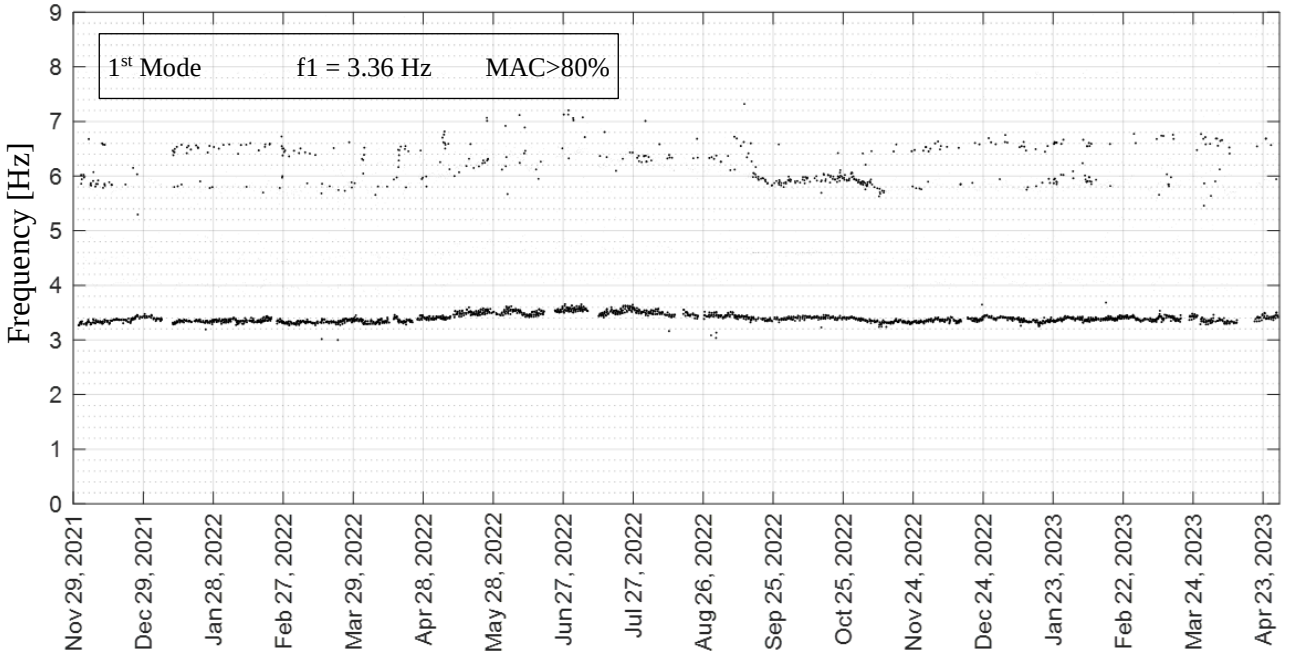

Figure 62 : first natural frequency - MAC index over-time

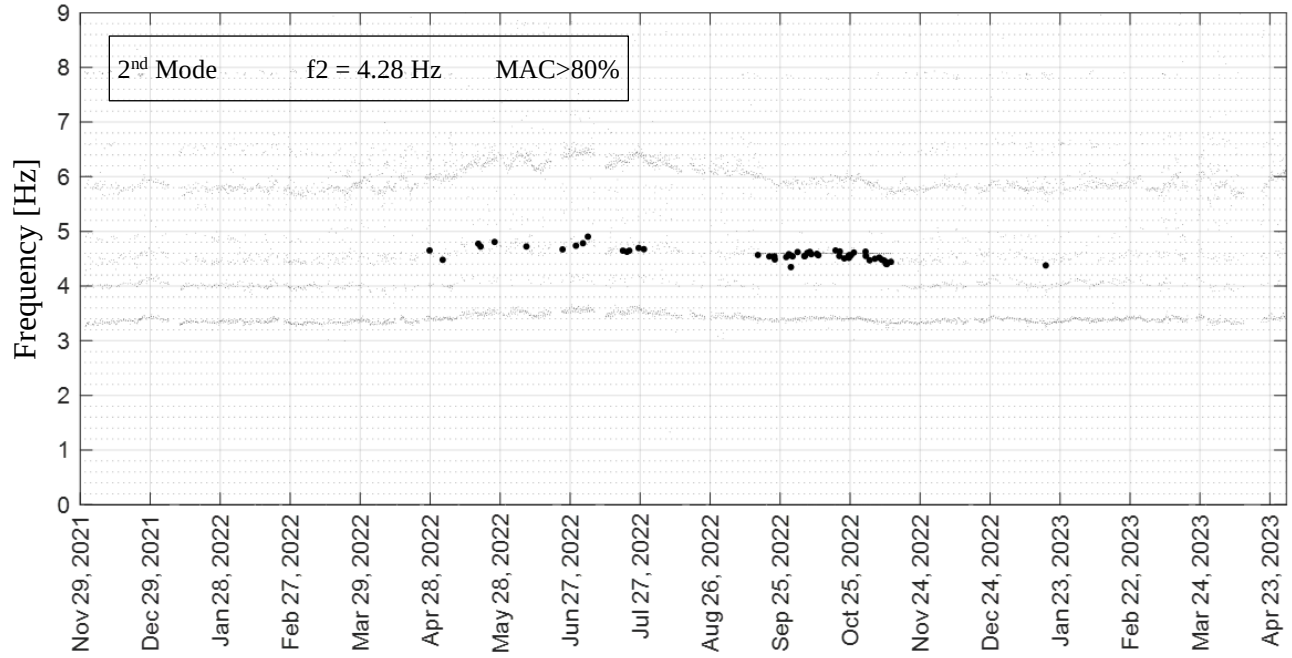

Figure 63 : second natural frequency - MAC index over-time

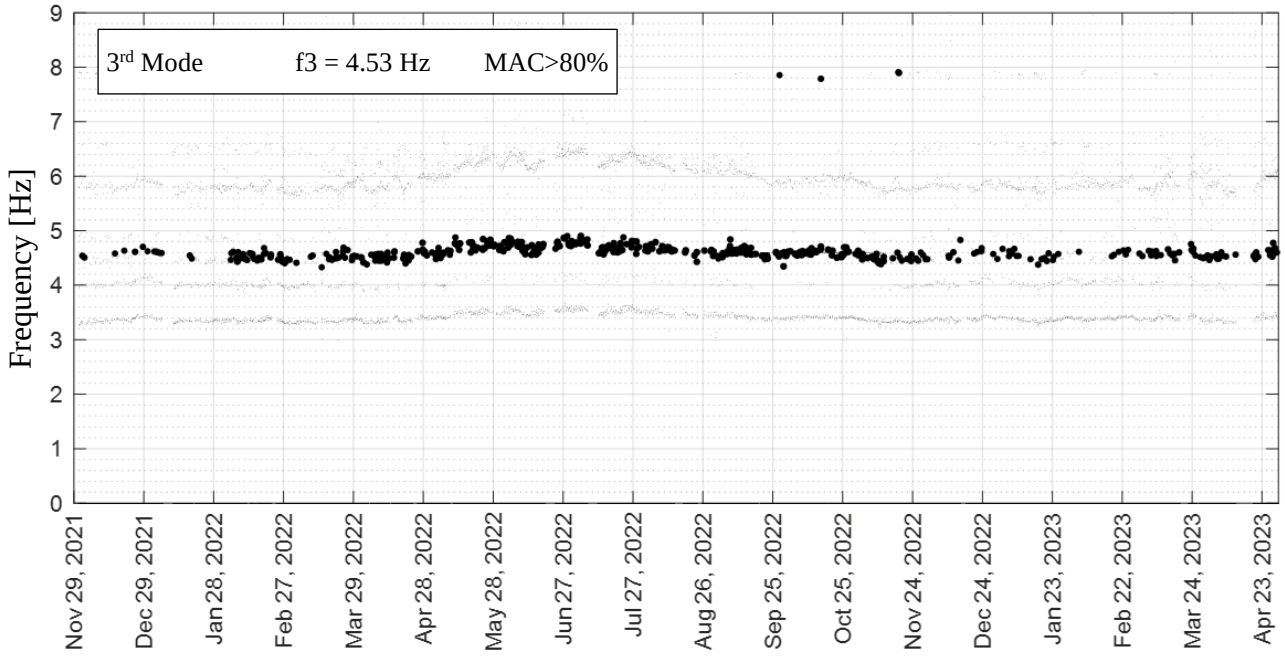

Figure 64 : third natural frequency - MAC index over-time

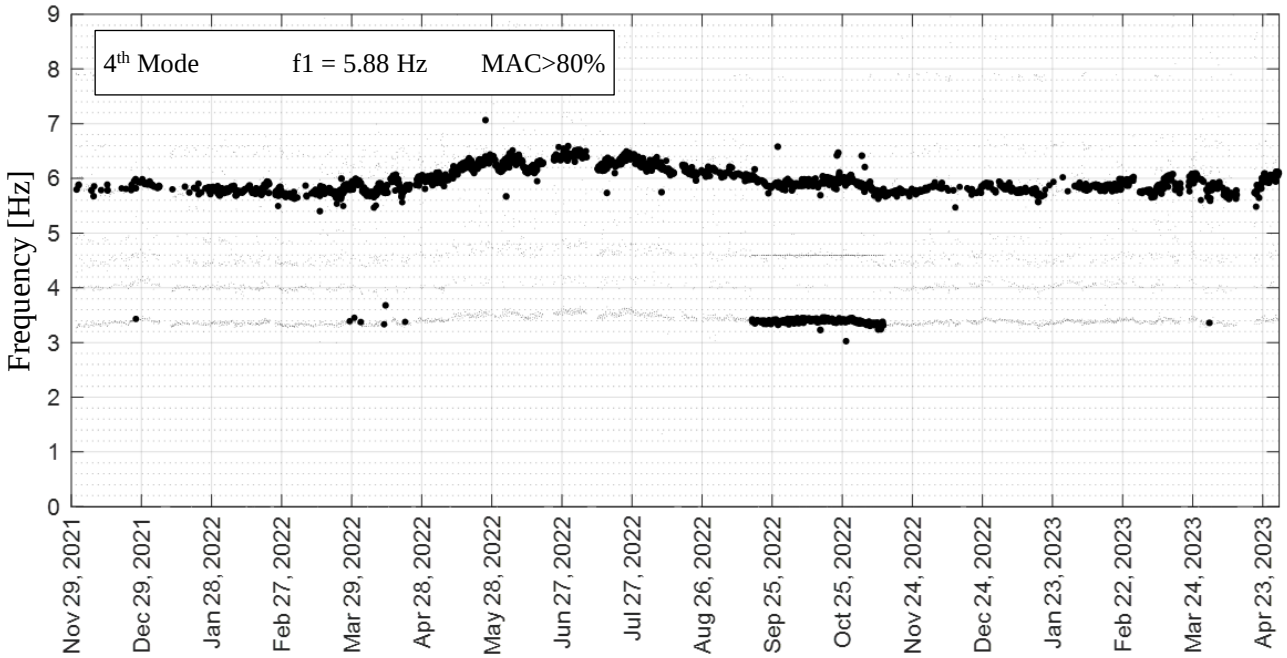

Figure 65 : fourth natural frequency - MAC index over-time

In addiction in Figure 66 the results of the monitoring of three tie-rods that are taken as reference (i.e., C01, C16 and C18) are shown to describe the evolution of their tensile force, physical quantity directly correlated with the first modes of vibration. The results show a slightly fluctuation of the first natural frequencies with the temperature, with a light decrease followed to an increase of temperatures and a light increase followed to a decrease of temperatures.

For what concerns the tie-rod C01, it is not possible to track the main natural frequency because the values of the identified frequencies are scattered. This can be related to a malfunction of the sensor.

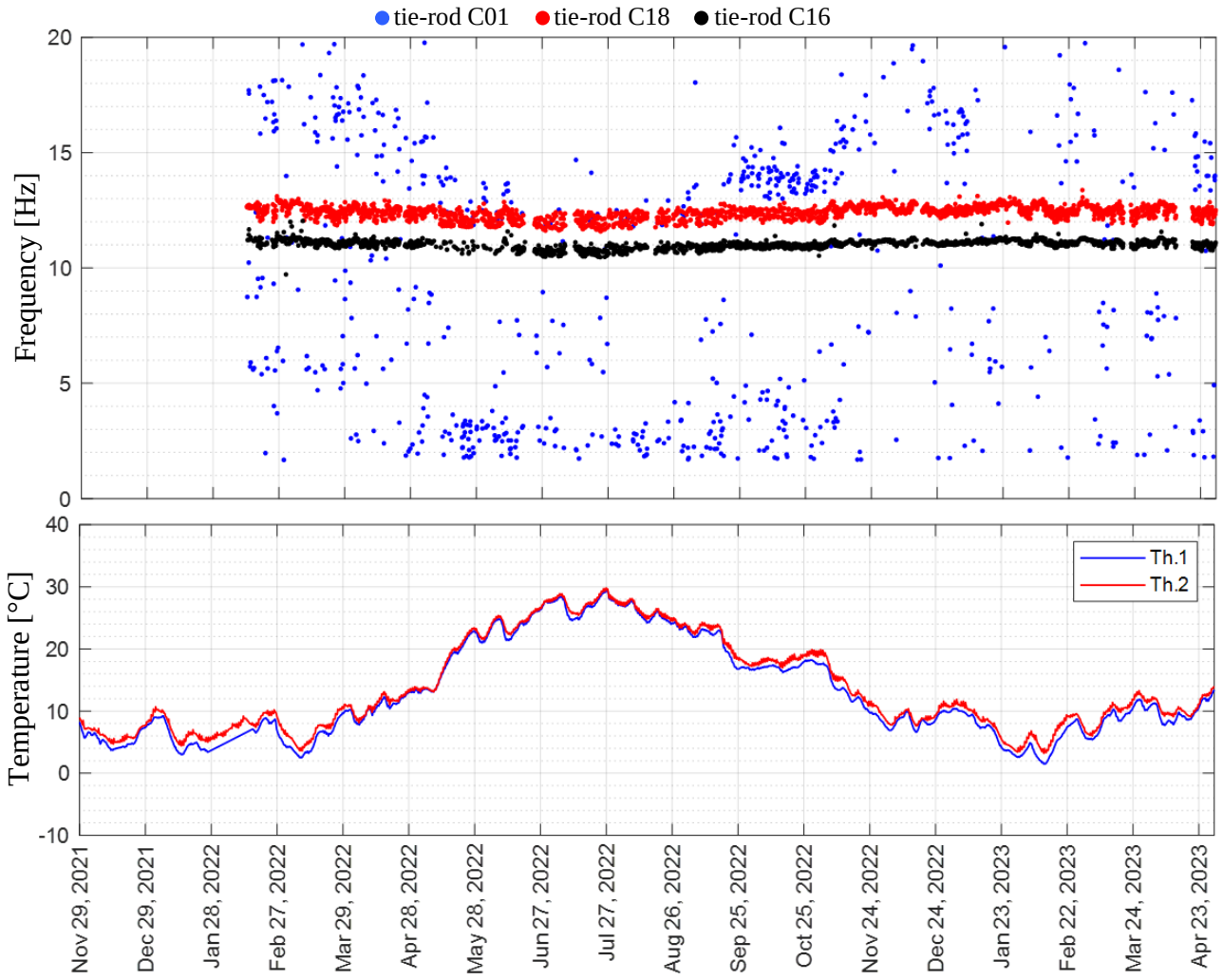

Figure 66: (a) C01, C16 and C18 natural frequencies trend over-time, (b) trend of the temperature's over-time.

4.1.3.1.1 Environmental effects – Frequency vs Temperature

How shown in Figure 61 and described in section 4.1.2.1, the identified natural frequencies along the monitoring are characterized by a fluctuation that can be related to the temperature effects. In Figure 67 are make in relation each frequency with a MAC index higher than 80% with the temperature values. The second frequency is discarded because how explain in section 4.1.1.1 it is related with a in plane response that is outside the monitoring target.

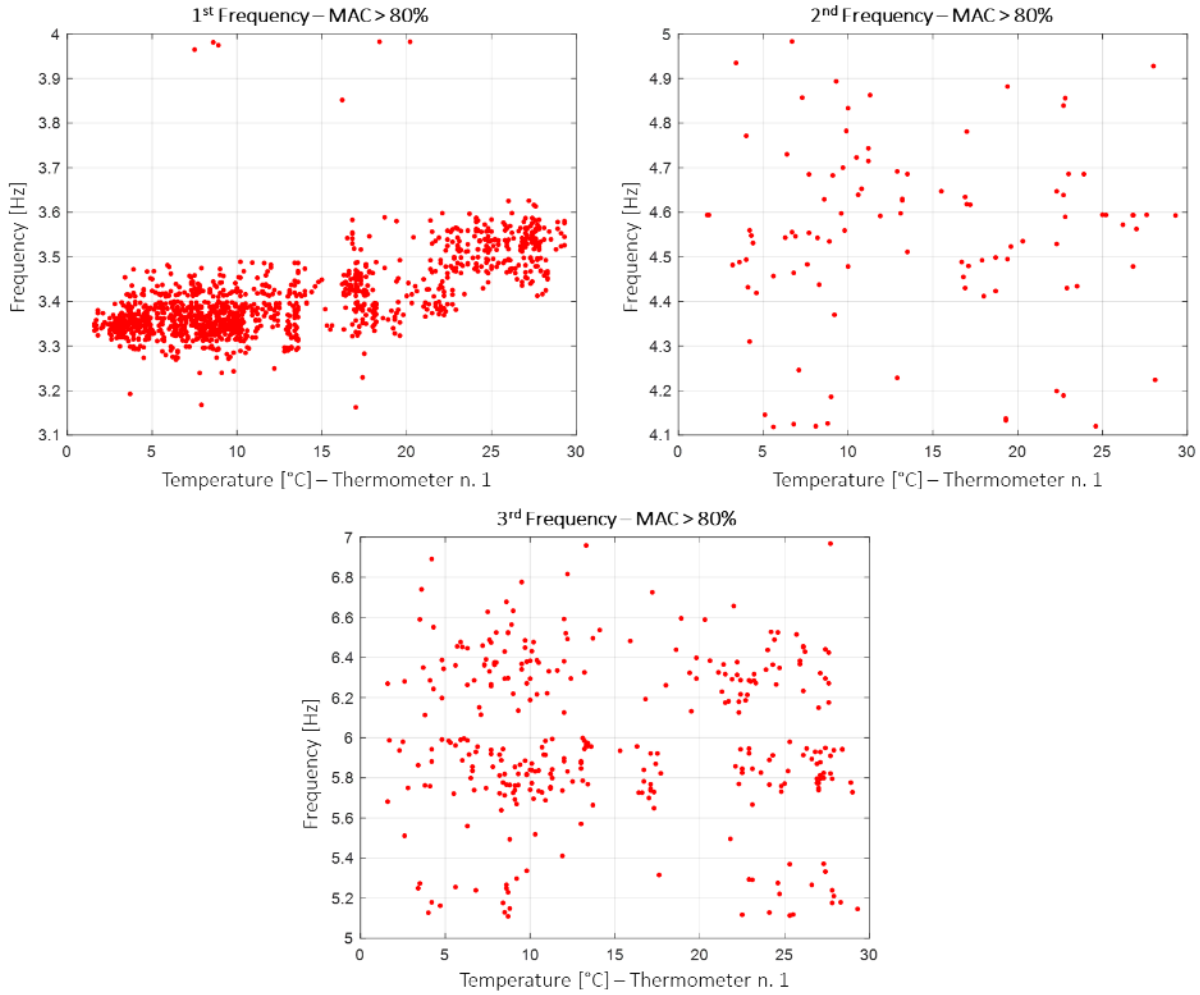

Figure 67: Frequencies vs Temperature plotting – taking frequencies values with index MAC > 80 % .

In Figure 67 it is observed that the first frequencies, characterized from a few observation of 1259 data, have a trend can be described with a linear regression model (LRM) while both the third and the fourth frequency, characterized from a smaller number of observations, have an hight dispersion and indeed it is difficult to identify a trend of the parameters.

The statistical model used to relate the response Y (i.e., the dependent variable) with an independent variable X is the linear regression, known as Linear Regression Model (LRM) [Benjamin and Cornell] [79]. More in detail, the idea is that the Y variable is affected in its mean in a linear manner by the X variable.

In this type of analysis, the objective is to assess the regression function (4.1-4) that minimize the Mean Squared Error (MSE) (4.1-5) that represent a pointwise measure of error.

$$\boldsymbol{m}(x) = E(\boldsymbol{Y}|\boldsymbol{X} = x) \qquad (4.1\text{-}4)$$

$$MSE\{\hat{f}(x)\} = b[\hat{f}(x)]^2 + Var[\hat{f}(x)] \quad (4.1\text{-}5)$$

In detail the linear model is described with the Equation (4.1-6)

$$\boldsymbol{y_i} = \boldsymbol{m}(\boldsymbol{x_i}) + \boldsymbol{\epsilon_i} = \beta_0 + \beta_1 x_{i1} + \ldots + \beta_d x_{di} + \boldsymbol{\epsilon_i} \quad (4.1\text{-}6)$$

where $\boldsymbol{\beta}$'s are the unknown coefficients to be fitted and ϵ_i is the error term.

The results are shown in Figure 68 and the principal statistical parameters of the model, the squared R, a parameter that represent the goodness of correlation, the Mean Squared Error (MSE) and the Root Mean Squared Error (RMSE) a coefficient that represent the standard deviation of the residuals are summarized in Table 8.

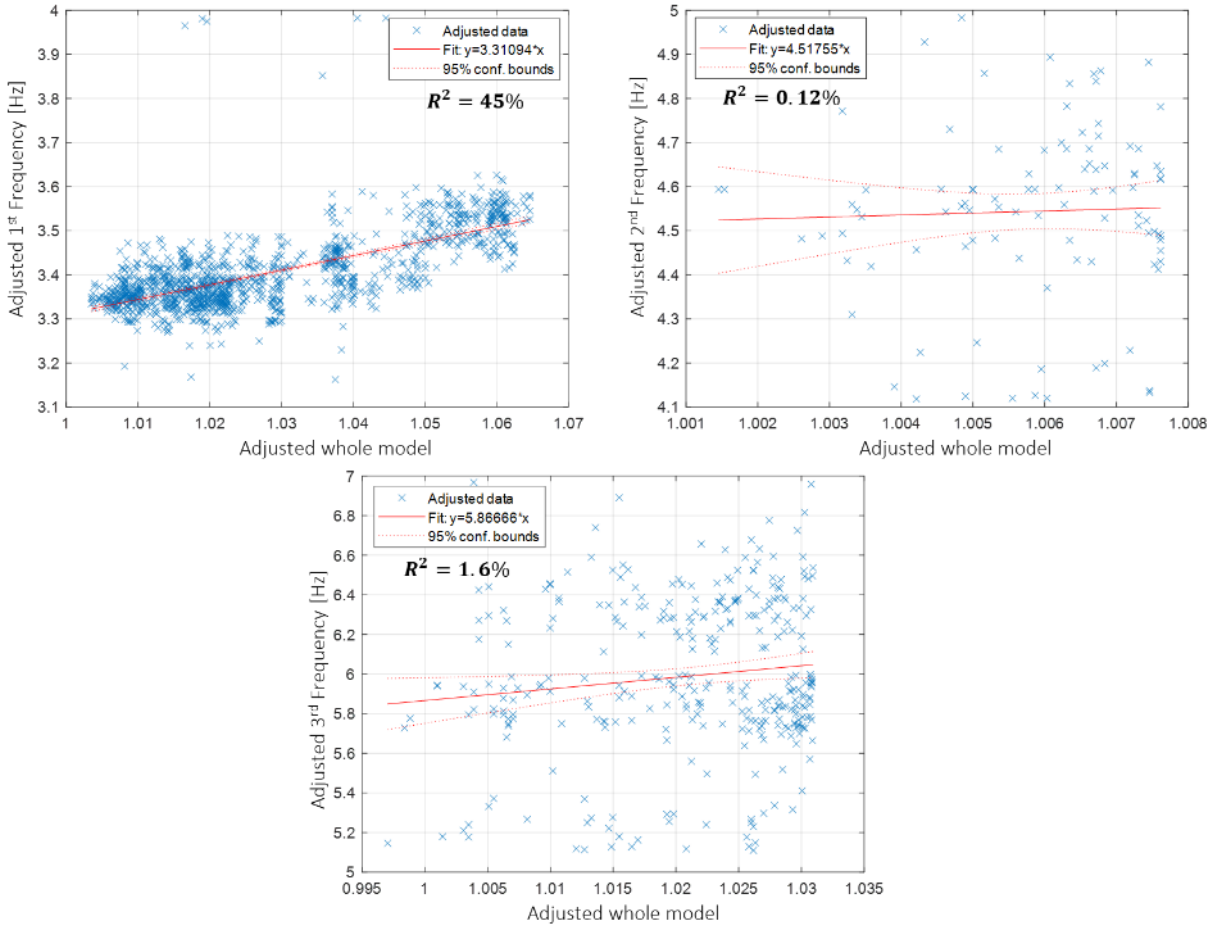

Figure 68: Results of Linear Regression Model (LRM) to relate the response with the temperature.

Model	R^2	MSE	RMSE
1st Frequency	0.45	0.004	0.063
2nd Frequency	0.0012	0.04	0.20
3rd Frequency	0.016	0.15	0.39

Table 8: Statistical parameters of the linear regression models.

These results shown that the LRM to relate the response of the Y variable, i.e., the identified frequencies with the X variable, i.e., the temperature values, give acceptable results only for the 1st Frequency, where $R^2 = 0.45$ and $MSE = 0.004$.

How future development it is necessary to develop a refined statistical model in order to relate the response Y with the independent variable X to describe and find a relation also for the higher frequencies.

4.1.3.2 Overview of static monitoring results.

The static monitoring system designed for the Portico da Varano aims at evaluating the evolution of the damage state detected after the seismic sequence that stoke Central Italy between August 2016 and October 2016.

The activities of monitoring have been focalized on the evaluation of the vaulted ceilings crack patterns, localized in Figure 60, with a configuration of the sensors, reported in Figure 69, which is able to reconstruct the time-history of displacements, that involve sliding, detachment and rotational movements of the cracks. The results, shown in Figure 70 and in Figure 71, highlight that the behaviour of the cracks follows the temperature trend with a contraction related to temperature decrease and a relaxation related to temperature increase.

In detail both the monitored vaults, show detachment movements close between 0.35 mm and - 0.14 mm for the first vault and between 0.02 mm and – 0.03 mm for the second vault, with light sliding movements without rotations.

Regarding the X and Y displacement components, they have been assessed by applying geometrical theorems (e.g., cosine theorem and Pythagoras' theorem) starting from the transducer's measurements. Figure 69 shows the quantities involved and how they have been defined.

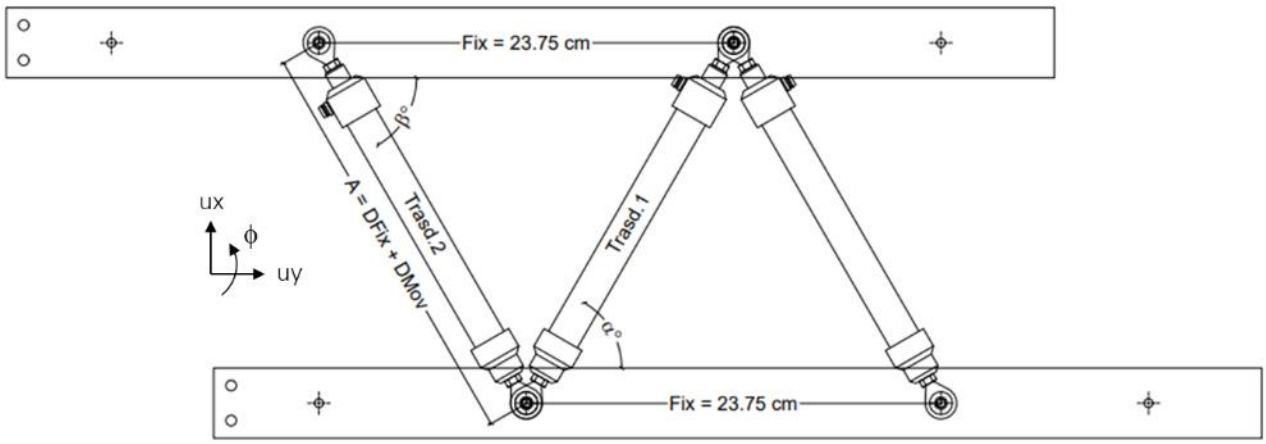

$A = DFix + DMov$ = transducer case + transducer measure

$Ux = A(Trasd.1)\sin(\alpha)$ $\quad$ $Ux = A(Trasd.2)\sin(\beta)$

$Uy = A(Trasd.1)\cos(\alpha)$

Figure 69: Configuration of the transducers displacement installed across the crack on the vaulted ceilings and displacement components described.

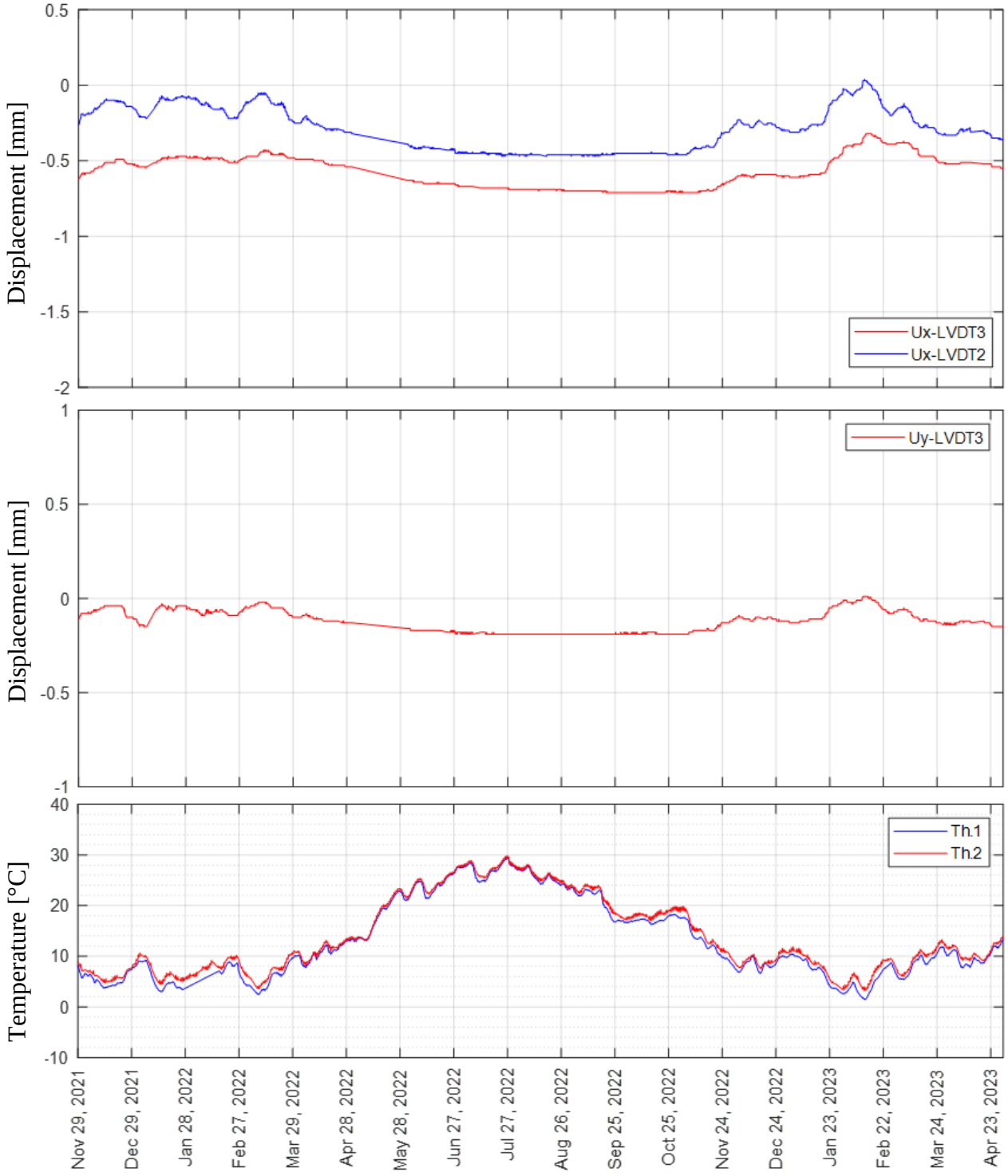

Figure 70 : Displacement components recorded for the cracks located in the Vault n.1 over-time (a) X direction, (b) Y direction, and (c) trend of the temperature over-time.

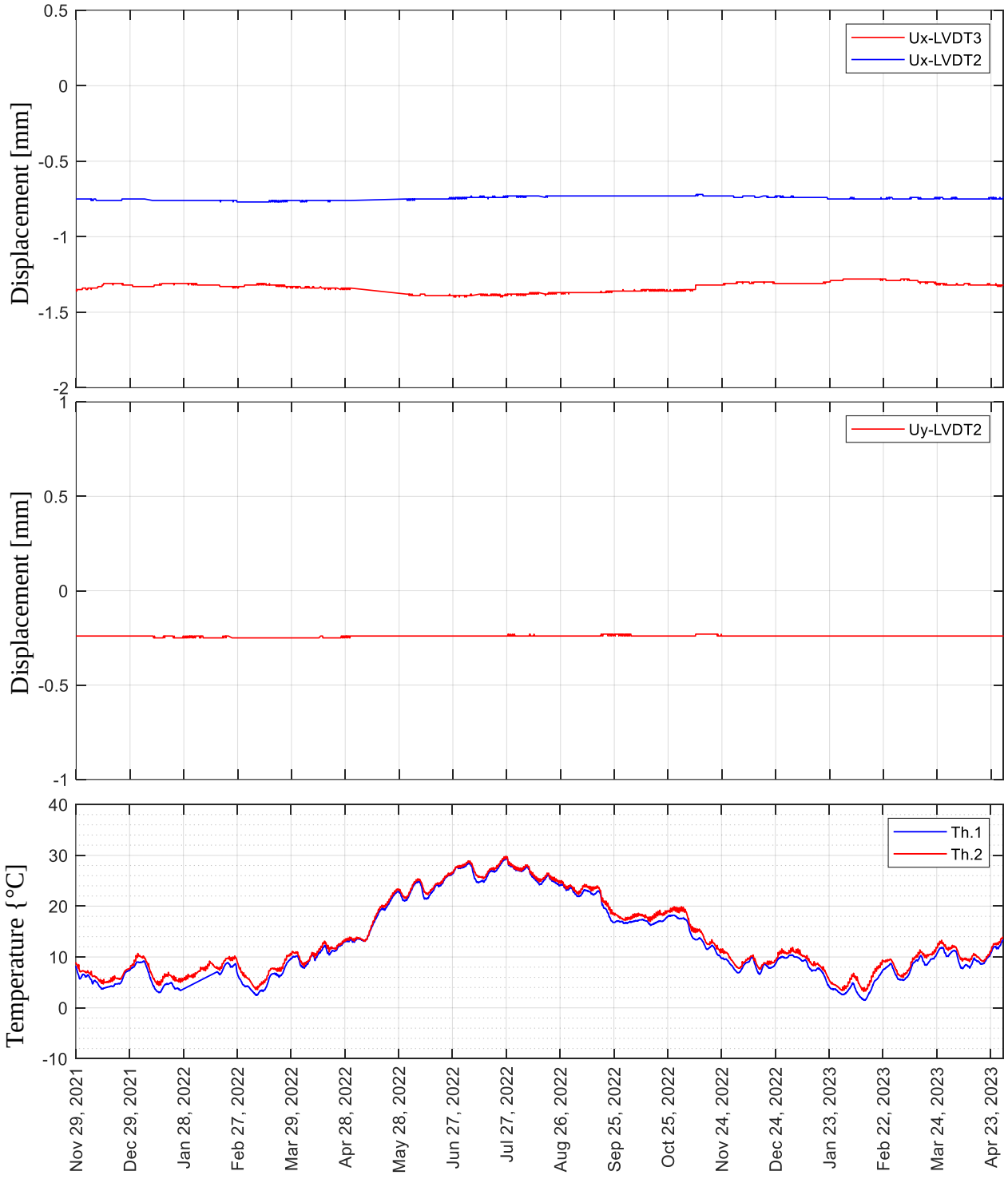

Figure 71 : Displacement components recorded for the cracks located in the Vault n.2-over-time (a) X direction, (b) Y direction, and (c) trend of the temperature over-time.

4.1.4 Structural response characterization from low energy earthquakes

As previously described in Section 3.1, an innovative tool has been developed concerning the approach to characterize the structural response of the Portico da Varano when subjected to low energy earthquakes with the observation of their effects on the monitored key parameters such as modal properties (i.e., natural frequencies and modal shapes) and on the measurement of displacements on the monitored elements. Unlike the standard approach that fixes a threshold limit on the input signal (i.e., the trigger) that defines the starting point of the acquisition system, this novel approach aims at relating the data acquired during monitoring to a seismic event, which can occur near the site, and at detecting possible changes in the response of the monitored structure by comparing the behaviour before and after the occurrence of the event.

The events identified during the monitoring period are shown in Figure 72, where the red dots sizes are related to the epicentral distance (i.e., the higher is the size, the higher is the distance from the monitored structure). Such graph also provides information regarding the Magnitude of the events occurred and some information concerning the seismicity of the area.

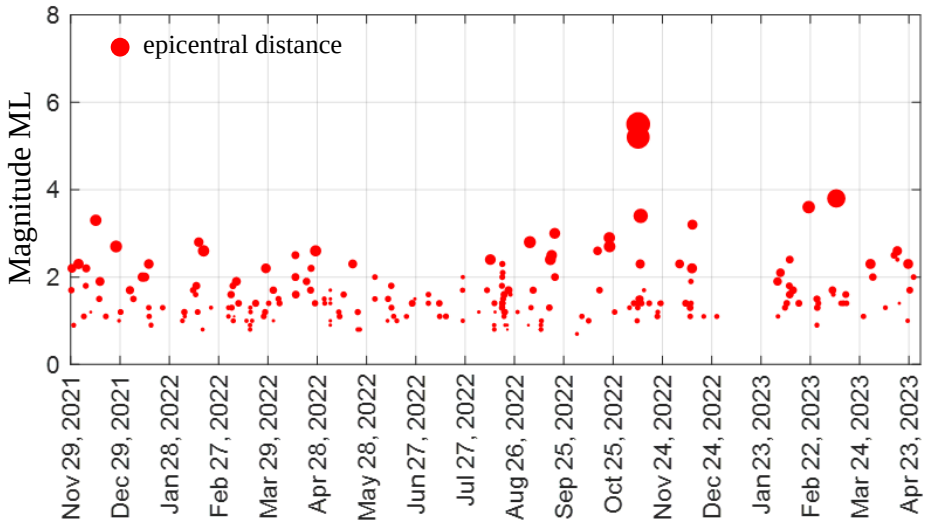

Figure 72 : : Magnitude and epicentral distance of the earthquakes occurred during the monitoring period.

As examples, the effects due to three differ events represented in Table 9 in term of magnitude ML, epicentral distance D and expected PGA assessed applied the GMPE model calibrated are shown.

Figure 73, Figure 74 and Figure 75, reports the time history acquired during the event by the four accelerometer sensors placed on the first floor of the Portico da Varano. In the graph it is possible to identify three regions that, in detail, define the occurrence of the event (Region n.1) and two more regions that are, respectively, before (Region n.2) and after the event (Region n.3).

Event	ML	D [km]	PGA [g]
Caldarola 14/02/2022 17:08 UTC	2.5	11.02	0.019
Pesaro 09/11/2022 06:07 UTC	5.5	96.52	0.015
Umbertide 09/03/2023 19:13 UTC	3.8	57.76	0.01

Table 9: Information of the analysed seismic events.

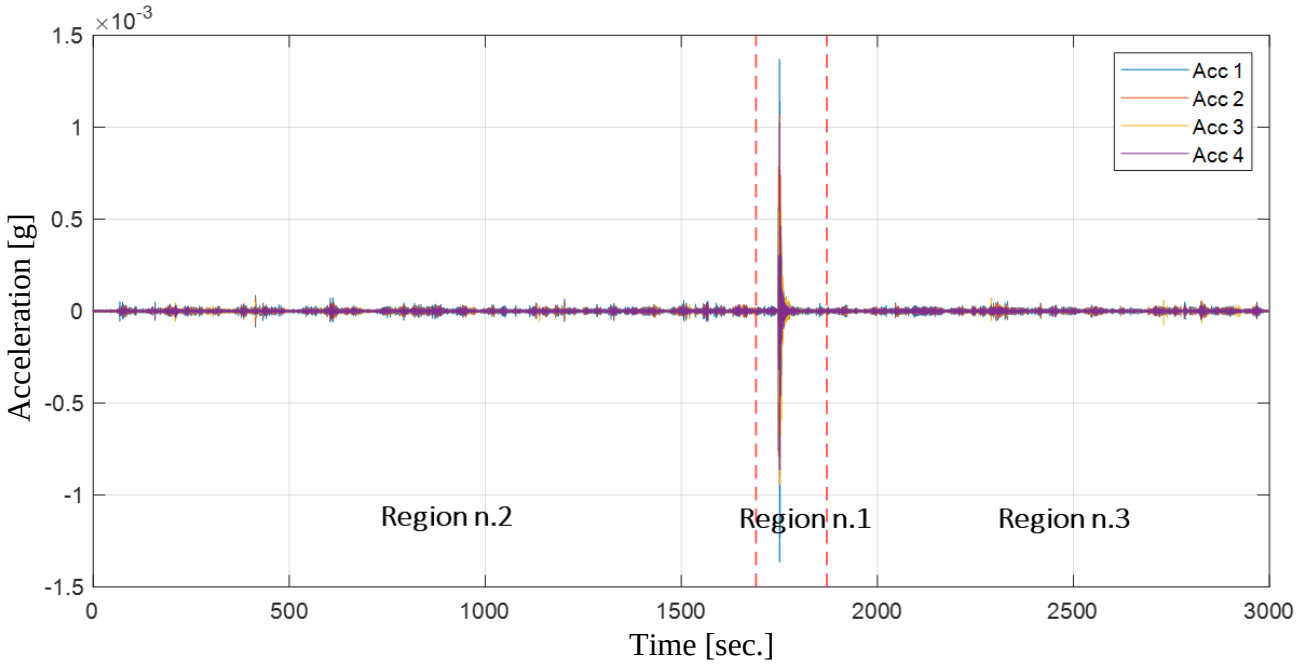

Figure 73 : Caldarola earthquake – Time history acquired by the accelerometers on the Portico da Varano first-floor.

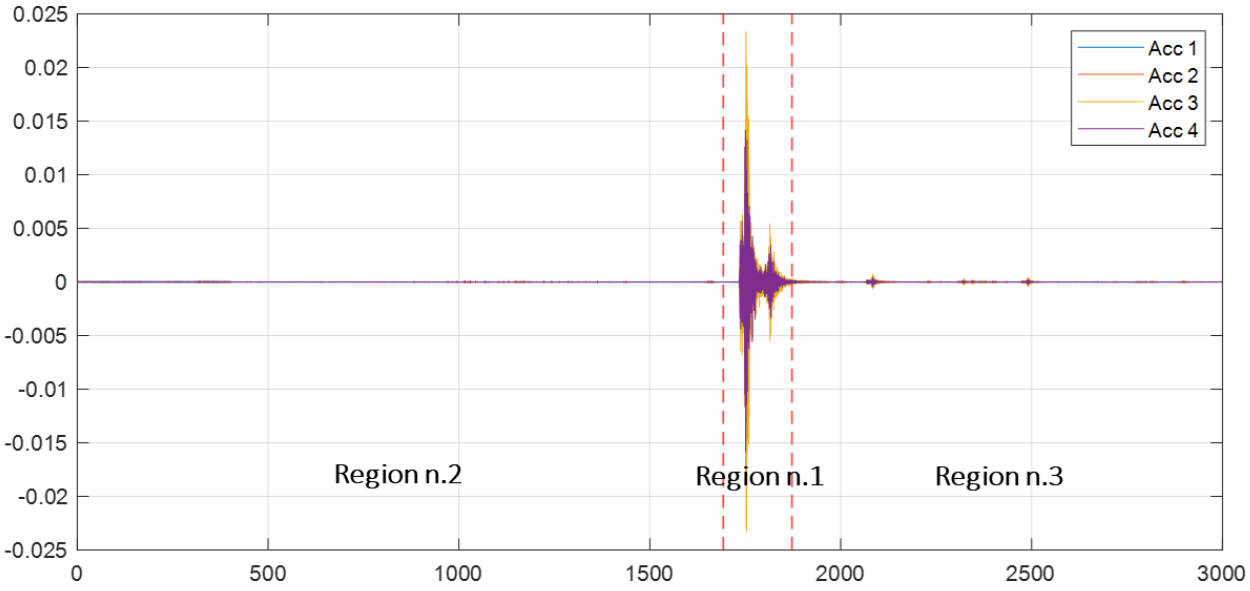

Figure 74 : Costa Marchigiana Pesarese earthquake – Time history acquired by the accelerometers on the Portico da Varano first-floor.

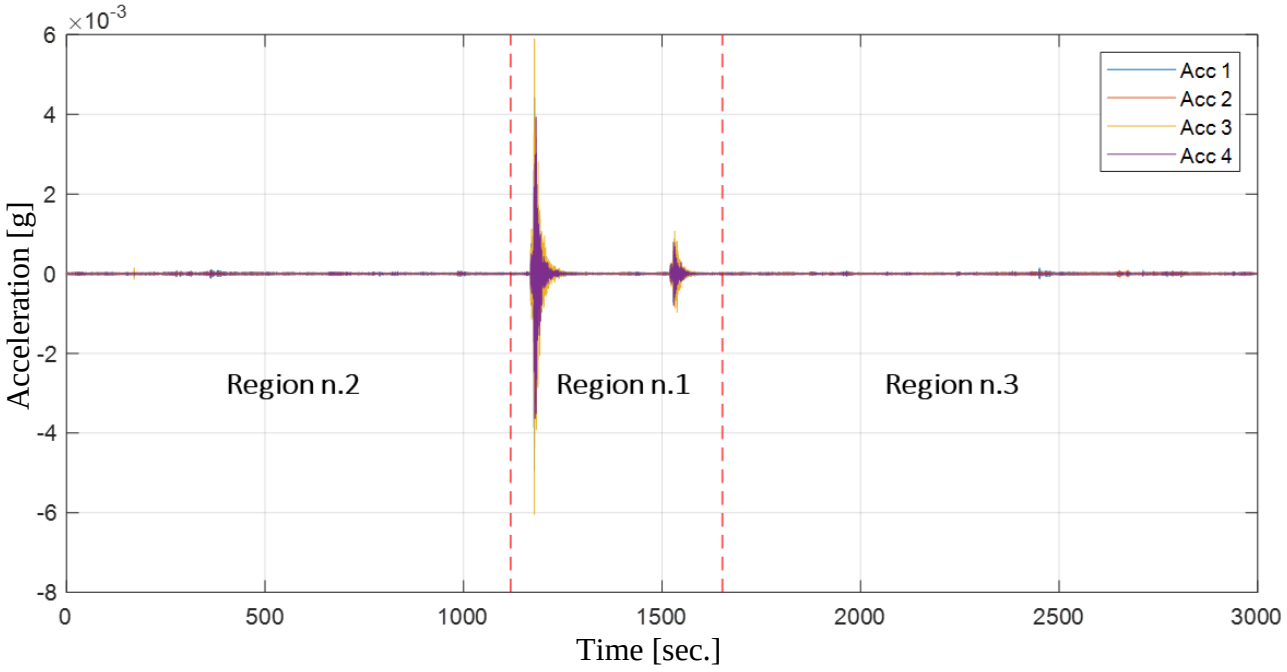

Figure 75 : Umbertite earthquake – Time history acquired by the accelerometers on the Portico da Varano first-floor.

The analysis regards the evaluation of the modal properties (i.e., natural frequencies and modal shapes) in Region n.2 and n.3, which means before and after the event, by means of operational modal analysis techniques. The SSI/Cov identification algorithm with cluster analysis has been performed and the variation of the response has been evaluated and compared with the modal properties evaluated during the monitoring period.

For each event, the results are shown both in a Table where the natural frequencies identified before and after the event are reported and, in a chart where is possible to observe both the daily trend and the effects of the events on the structural response. More in detail, Table 10 and Figure 76 reports the Caldarola event, Table 11 and Figure 77 reports the Costa Marchigiana Pesarese event and Table 12 and Figure 78 reports the Umbertide event.

Caldarola (MC) event – ML = 2.5, R = 11.02 km				
region	f1 [Hz]	f2 [Hz]	f3 [Hz]	f4 [Hz]
2 (Before the event)	3.42	{ }	{ }	5.96
3 (After the event)	3.40	{ }	{ }	5.91
{ } frequency not identified				

Table 10: Results of Caldarola earthquake on identified frequencies.

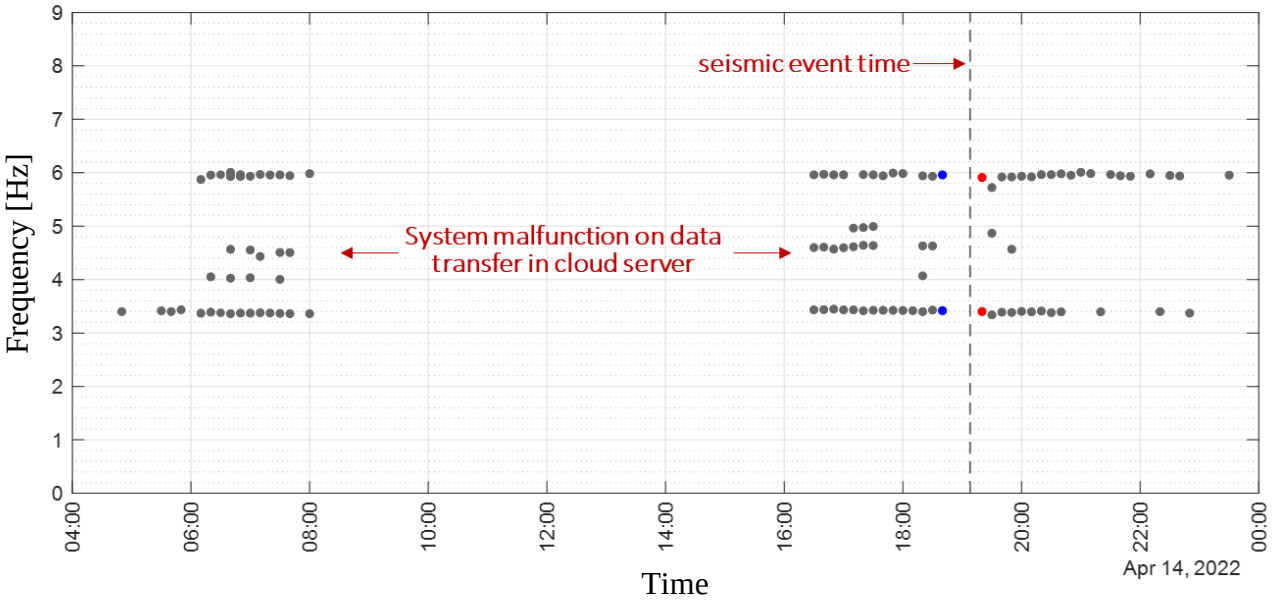

Figure 76 : Zoom of the identified frequencies trend across the occurrence of the Caldarola event.

It is observed that the event has not produced effects on the modal properties of the structure, in detail it is observed a slight drop on the identified frequencies of 0.6 % in the first frequency and of 0.84 % in the fourth frequency. This behaviour is inside the daily fluctuations of the modal parameters identified on monitoring period.

Costa Marchigiana Pesarese (PU) event – ML = 5.5, R = 96.52 km				
region	f1 [Hz]	f2 [Hz]	f3 [Hz]	f4 [Hz]
2 (Before the event)	3.36	{ }	4.59	5.81
3 (After the event)	3.13	{ }	{ }	5.21
{ } frequency not identified				

Table 11: Results of Costa Marchigiana Pesarese earthquake on identified frequencies.

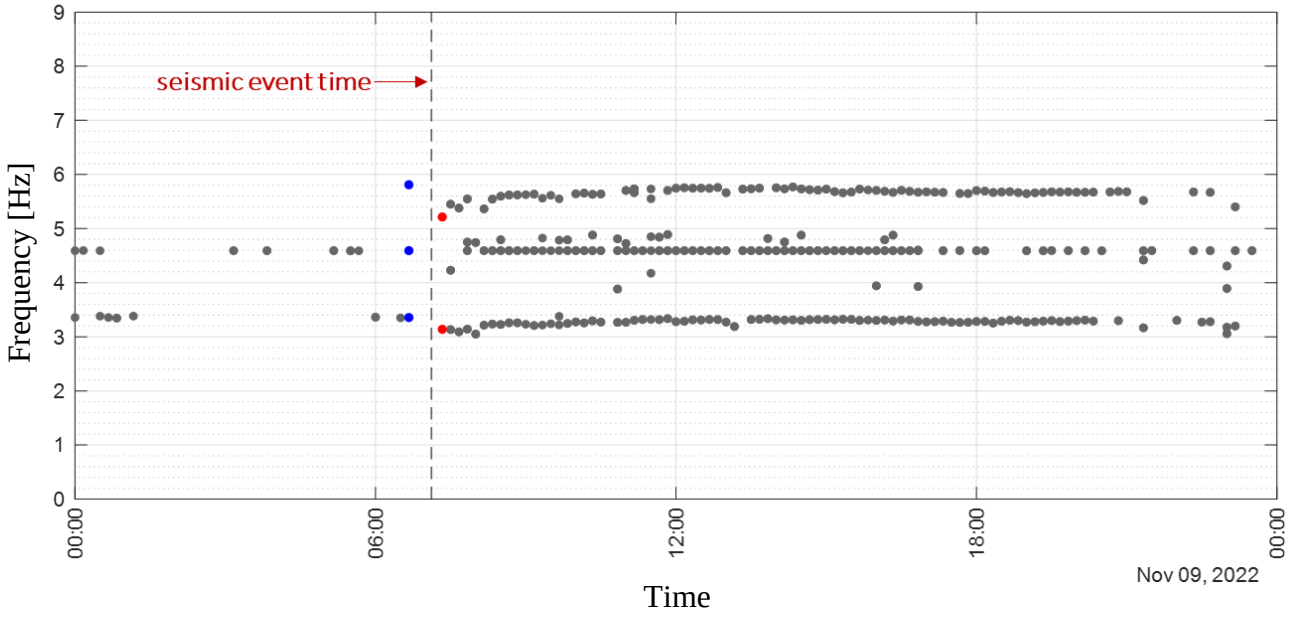

Figure 77 : Zoom of the identified frequencies trend across the occurrence of the Costa Marchigiana Pesarese event.

It is observed that the event has not produced effects on the modal properties of the structure, in detail it is observed a drop on the identified frequencies, of 6.84 % in the first frequency and of 10.33 % in the fourth frequency.

Umbertide (PG) event – ML = 3.8, R = 89.3 km				
region	f1 [Hz]	f2 [Hz]	f3 [Hz]	f4 [Hz]
2 (Before the event)	{ }	{ }	{ }	5.86
3 (After the event)	3.38	{ }	{ }	{ }
{ } frequency not identified				

Table 12 : Results of Umbertite earthquake on identified frequencies.

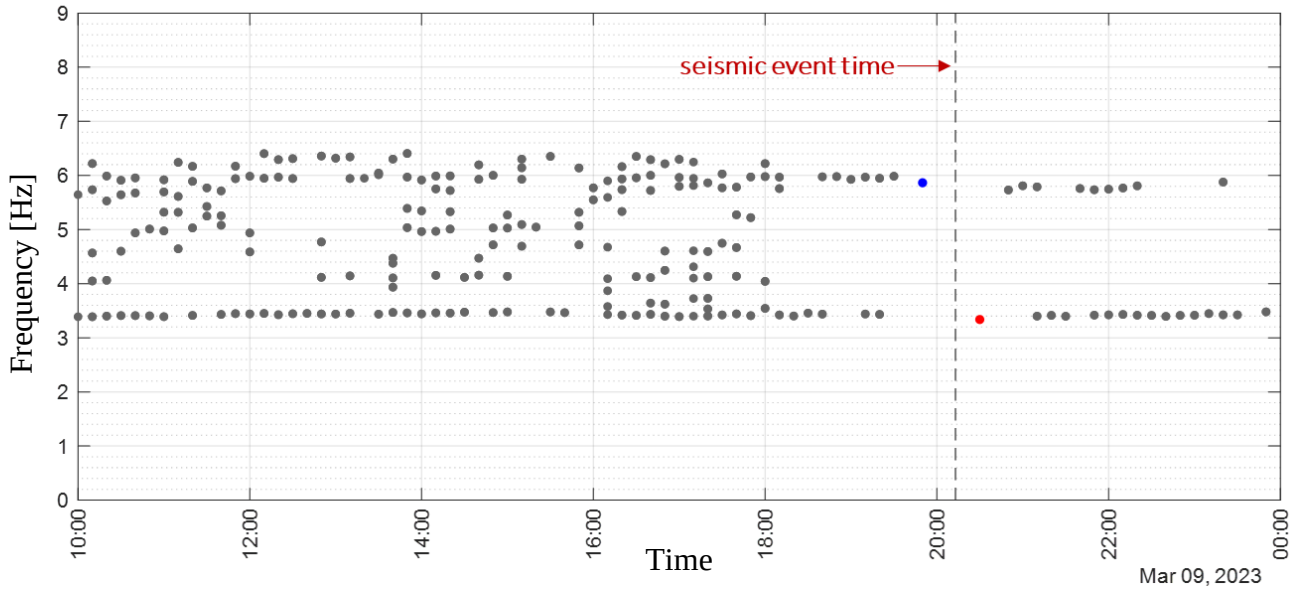

Figure 78 : Zoom of the identified frequencies trend across the occurrence of the Umbertide event (08-11 March 2023).

It is observed that the event has not produced effects on the modal properties of the structure, in detail it is observed that the structural response is related to environmental actions which traffic, human activity and so on. Therefore, the behaviour is inside the daily fluctuations of the modal parameters identified on monitoring period.

4.1.5 Results of structural monitoring.

In this section are summarized the main results obtained by the monitoring system configured. More in detail it is observed that:

- the adopted dynamic sensors configuration Figure 59 is able to control the progression over time of the identified local mechanisms during the preliminary AVTs.

- the automatic OMA process developed utilizing the SSI/Cov with the clustering analysis is a robust tool and permit to track the fluctuation of the parameters with the environmental conditions over time (Figure 61).
- the natural frequency identified are related with modal shapes with a MAC index higher that 80% with a lack significant coupling (from Figure 62 to Figure 65).
- the LVTD's configuration is able to get the displacements time history of the cracks.
- the approach to identify the seismic events with values of intensity that can be of interest for the site give an indication about the degree of seismicity of the area (Figure 72).
- the information about the fluctuation of modal properties between the structural response before and after an event increase the behaviour knowledge of the structure and can give a support to identify and justify if it is observed an hight variation on the identified frequencies (Figure 78).

Further detail to developed for improve the interpretation of the collected monitoring data are:

- to calibrate a finite element model (FEM) of the Portico da Varano with modal updating techniques.
- to impose a state of damages on the updated FEM model in order to fix threshold values at the monitored parameters to identify a state of damage.
- to remove the environmental (i.e., temperature) effects on the natural frequency's values identified thought a statistical model that infer the distribution of each frequency with changes of temperature values.
- to give a confidence level at the estimated parameters with Bayesian approaches

4.2 Santa Maria in Via Church in Camerino

4.2.1 Description of the structural system

The Santa Maria in Via church, as described in [Arezzo et all. 2021] [60], is located in the historical centre of Camerino, a small town in the Central Italy Apennines Mountains. Its construction dates back to the 13th century; historical documents demonstrate that the original church was smaller and very different with respect to its current aspect. In the 17th century, between 1639 and 1642, the church gains the actual baroque appearance after heavy rehashes, which consisted in merging and suitably modifying neighbouring buildings and in the erection of the towering anterior body that still today gives the monumental appearance to the façade of the church. In 1799 a strong earthquake strokes the town destroying many buildings including the cathedral; Santa Maria in Via church underwent impressive damage that consisted mainly in the failure of the elliptical masonry dome that was replaced with a fake dome richly decorated with gypsum stucco and frescoes.

The church, in its current configuration (Figure 79), underwent other strong earthquakes in 1873 and 1997 that also severely damaged the church. The church has a trapezoidal plan (Figure 80a) that incorporates a central elliptical hall, the octagonal sacristy, and other rooms. The hall major axis passes though the entrance and the opposite main altar located in a deep presbytery; on the minor axis, above two side entrances, there are two small chancels. Four radial chapels, characterized by hemicycle niches, open on the central hall. The plan of the church appears to be massive and strong. Parts around the central elliptical hall are characterized by three levels and constitute a confinement for the elliptical hall, which rises about 8 m higher with an octagonal tiburium, which approximates the elliptical shape of the hall. Four large windows are realised on the tiburium walls above the lateral chapels. At the outside, the tiburium is stiffened by buttresses in correspondence of corners. Another peculiar element of the church is the octagonal bell tower which rises at a corner of the plan above the last level served by a spiral staircase. The last element composing the church is the already mentioned anterior body of the façade. This part is placed against the building (Figure 80b) interacting, at the lower part, with the main body of the church and, at the upper part, with the tiburium for a maximum height of about 23 m. The plan of the façade body is trapezoidal with an average length of the bases of about 16 m (façade width) and depth of about 6 m. Inside, the body has three floors, the first at a level of 4.5 m from the ground floor, the second at the level of the first eaves and the third at the level of the clock that characterises the façade elevation. The plan is divided into three rooms, separated by two masonry orthogonal spine walls with communication openings. The upper block of the façade body is characterized by the presence of a system of steel ties in the two orthogonal horizontal directions, anchored to the masonry walls. To access to the chancel and the upper floor, a

spiral staircase is incorporated into the façade wall, on the left side, producing a significant discontinuity within the wall body of the façade.

The main body of the church appears to be constituted, at least at the exposed surface, by very regular and compact brick and lime mortar masonry. The body of the façade, on the contrary, is made of stone masonry covered by a thin curtain of brick. The tiburium is entirely realised with an irregular stone masonry constituted by roughly worked blocks, sometimes rubbles, without transverse connection elements and external lime plaster. Thus, the church is constituted by a very particular structural system characterized by different interacting bodies sometimes made of poor masonry. This gives the system a very high vulnerability already exhibited after the past strong earthquakes. Last restorations dates after 1997 earthquake when the church was reopened in 2006, an external and internal view of the church after restorations intervention followed the 1997 earthquake is shown in Figure 79.

Figure 79 : Santa Maria in Via church a) North-Est external view, b) internal view

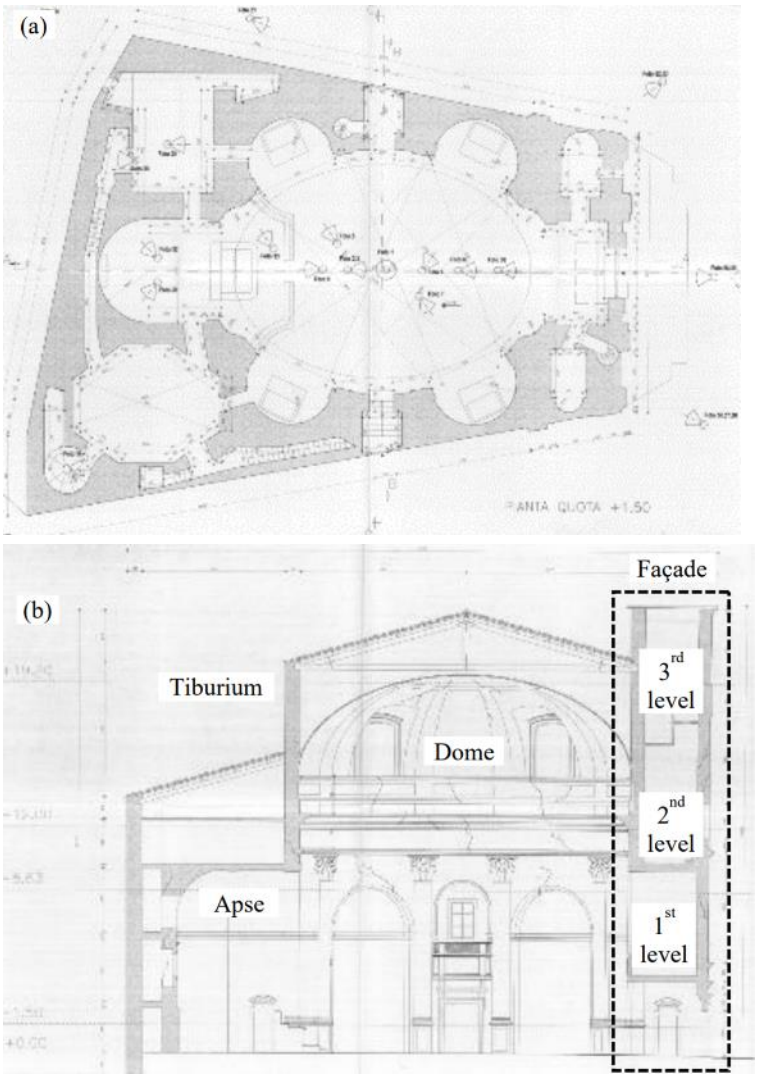

Figure 80 : Santa Maria in Via church a) planimetric scheme; b) longitudinal cross-section.

4.2.2 Damages and safety system after the 2016 Central Italy earthquake

The 2016 Central Italy Earthquake dramatically struck the city of Camerino, producing impressive damage all over its historical centre. In particular, the Santa Maria in Via church underwent progressive damage starting from the shock on August 24th that produced shear cracking patterns at the lower part of the façade body. Events on October 26th worsen the situation of the façade body, produced an impressive collapse of the bell tower and damaged the top level of the tiburium at the roof connection. Event on 18th January 2017, which was associated to a heavy snowfall, finally produced the collapse of the tiburium rear part, a portion of the roof and of the fake dome. Figure 81 depicts main collapses of the church. Basically, the strong base of the church overcame the earthquake without important effects. On the contrary, all peculiar elements towering over it have been badly hit. In particular, the most impressive mechanism is the one produced by the interaction between the anterior body and the tiburium. From a laser scanner survey, it is evident that the upper part of the anterior body is about 0.30 m out of the vertical line passing at the base of the below wall. The upper

part appears to be a rigid body that assumed the final position probably due to a cumulated damage after many historical earthquakes because cracking opening, surveyed after the last earthquake, are well below 0.30 m. The horizontal movement of the upper part of the anterior body explains formation of shear crack patterns (after August 24th) and of the subsequent masonry disaggregation at the lower part (after October 26th). Also collapse of the tiburium rear part occurred on 18th January 2017 can be a consequence of the anterior body translation as these were connected with two ties running under the roof. As for the bell-tower collapse, instead, an intrinsic weakness was probably the cause of the masonry disaggregation.

Figure 81 : Damages occurred in the Santa Maria in Via church after the 2016 seismic sequence (a) collapses of the roof of the tiburium and of the bell tower, (b) damages on the lateral part of the façade, and (c) detail of the collapse of the fake dome.

In order to ensure the safety of the structural system of the church for subsequently restores interventions, several safety structural interventions have been done. The main one, is the construction of an external retaining steel structure designed to prevent the anterior body collapse (Figure 82(a)). The mobilized mass of 1300 tons, the out-of-verticality of 0.30 m and the need of permitting the passage of trucks and other machinery necessary for the future city reconstruction, made typical buttress systems not suitable as securing system.

Thus, two lateral steel braces combined with four latticed beams were used to avoid the collapse of the body. The structure covers the front side and the two lateral sides of the anterior façade body for the whole height; masonries lacunas at the lateral sides are filled with steel latticed systems in order to restore gravitational loading paths. The contact with masonry is realized with timber elements in order to adapt the steel system to the deformed masonry; steel telescopic elements are also used for the gross adaptation of the system. To ensure the system stability in case of extreme events and to confine the base body of the church, 14 steel strand cables connected to the steel structure and surrounding the whole church, are used. The whole steel structure is founded on a stiff RC surface foundation. Other important securing systems are the provisional roof built to protect the internal part of the church against weather and the latticed structure built on both sides of the tiburium walls to prevent their out of plane collapse (Figure 82(b)). This latter system is also connected to the main system.

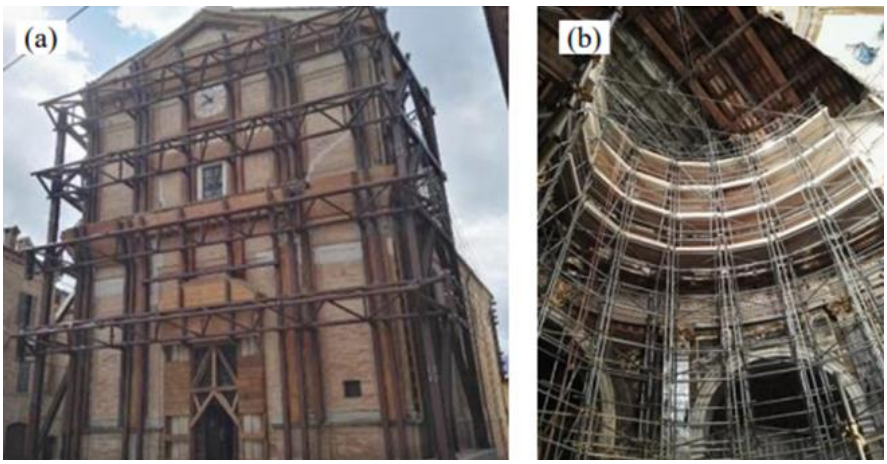

Figure 82 : Safety interventions realized in the Santa Maria in Via church after the 2016 seismic sequence (a) securing of the anterior façade, and (b) the provisional roof and internal latticed structure.

4.2.3 Dynamical Identification of the Church

The identification of the global dynamic of the church has been carried out through ambient vibration tests employing 16 accelerometers and two sensor configurations shown in Figure 83(a), and Figure 83(b).

To get information on the overall behaviour of the church, it was decided to monitor 8 points located around the ellipse of the tiburium, at two different heights from the ground level. At each point (from A to H) two uniaxial accelerometers were placed with measurement directions along the main axes of the church hall (called x and y directions). In detail, in the first configuration the accelerometers were positioned in 8 different points (from 1A to 1H) at 12 m from the ground, while in the second configuration two accelerometers were left in the same position (1B) to be used as references while

the others were moved at 19.7 m from the ground; positions 2C and 2H were excluded as inaccessible. The instrumentation installed involves, *i*) piezoelectric accelerometers PCB 393B31 with a sensitivity of 10V/g; *ii*) analog to digital conversion modules NI 9234 of National Instrument (NI) enterprise, each module is characterized by n.4 analog channel, 51.2 kS/s for each channel, measurement input +/- 5 V, 24-bit resolution and anti-aliasing filter, *iii*) a 9045 cRIO and three 9185 cDAQs.

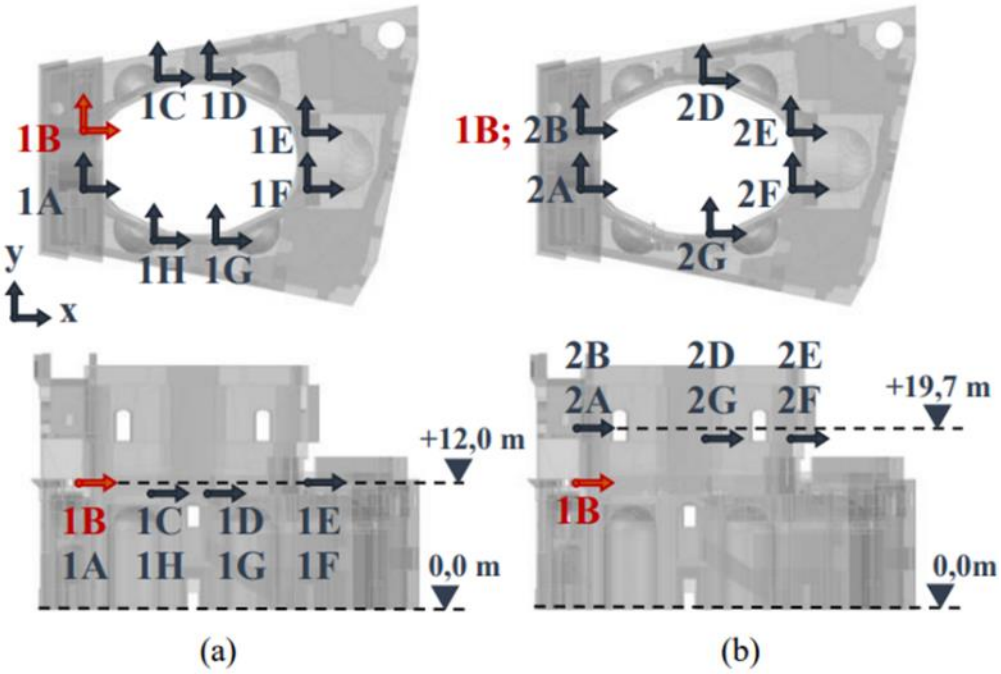

Figure 83 : Measurement configuration a) Conf.1 n.8 measuring stations (16 Accelerometers), b) Conf.2 n.6 measuring stations (12 Accelerometers) plus reference station 1B.

A distributed sensor network has been set up by placing one cRIO for the measurement station close to the reference point 1B and three mobile cDAQs near the remaining measuring points as shown in Figure 84. The channels synchronization has been achieved through Time Sensitive Technology (TSN) that provides distributed time synchronization and deterministic communication using standard Ethernet networks. Finally, for each data set a sampling frequency of 2048 Hz and a time logging of 1800 sec (30 min) have been set.

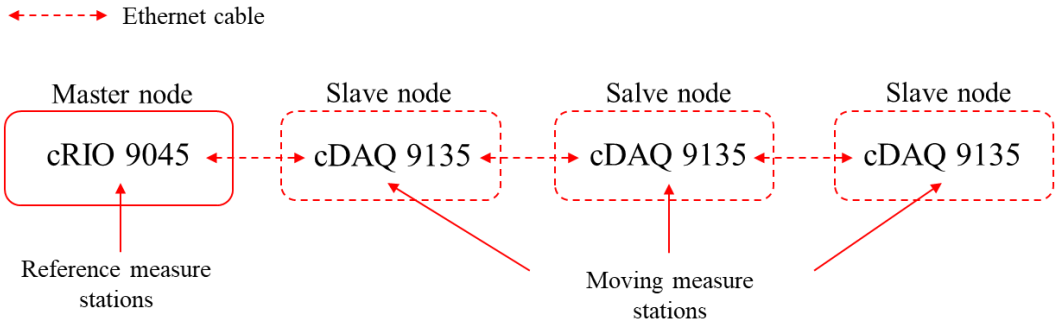

Figure 84 : Sensor network set up.

Before the identification of the dynamic parameters, the signals have been pre-processed by removing the baseline, by subtracting the contribution obtained by "fitting" the signal with a 3rd degree polynomial, by filtering with a low-pass filter with a cut-off frequency of 25 Hz, and by resampling at a frequency of 51.2 Hz to reduce the amount of data and to make subsequent analysis faster. The identification of the modal parameters has been carried out using the Principal Component - Subspace Stochastic Identification (SSI-PC) technique, that is a particular algorithm that extracts the state space model from input-output data where the output data is modelled as a low-dimensional subspace spanned by the principal components of the data matrix, and the input data is modelled using a regression model. The method uses an iterative technique to minimize the prediction error and to obtain the state-space model.

Since the acquisitions relevant to the two configurations are asynchronous, in order to obtain a correct mode shape, it has been necessary to proceed with a data merging operation; in this case the results obtained with the PoSER (Post Separate Estimation Re-scaling) technique are shown. Figure 85(a), and Figure 85(b) show the stabilization diagram obtained from the tests in Configuration 1 and Configuration 2, respectively. Here the stable modes in terms of frequency (difference less than 1%) and mode shape (MAC greater than 95%) are identified by a solid black circle. In the same figure, the frequency-damping diagrams are also shown, where the values of the damping ratios relative to the stable solutions can be appreciated. Figure 85(c) shows the selected modal parameters, such as natural frequencies, damping ratios, and mode shapes.

Globally, 6 modes of vibration have been identified. It is interesting to note that, despite the complex crack pattern, the dynamics of the structure, presents the first two translational and well decoupled modes and a third torsional mode, which could be expected for the undamaged system. This is also clear from the values of the autoMAC matrix shown in Figure 86. As for the higher modes, these need to be further investigated but they overall seem to involve the local dynamics of the tiburium and of the façade.

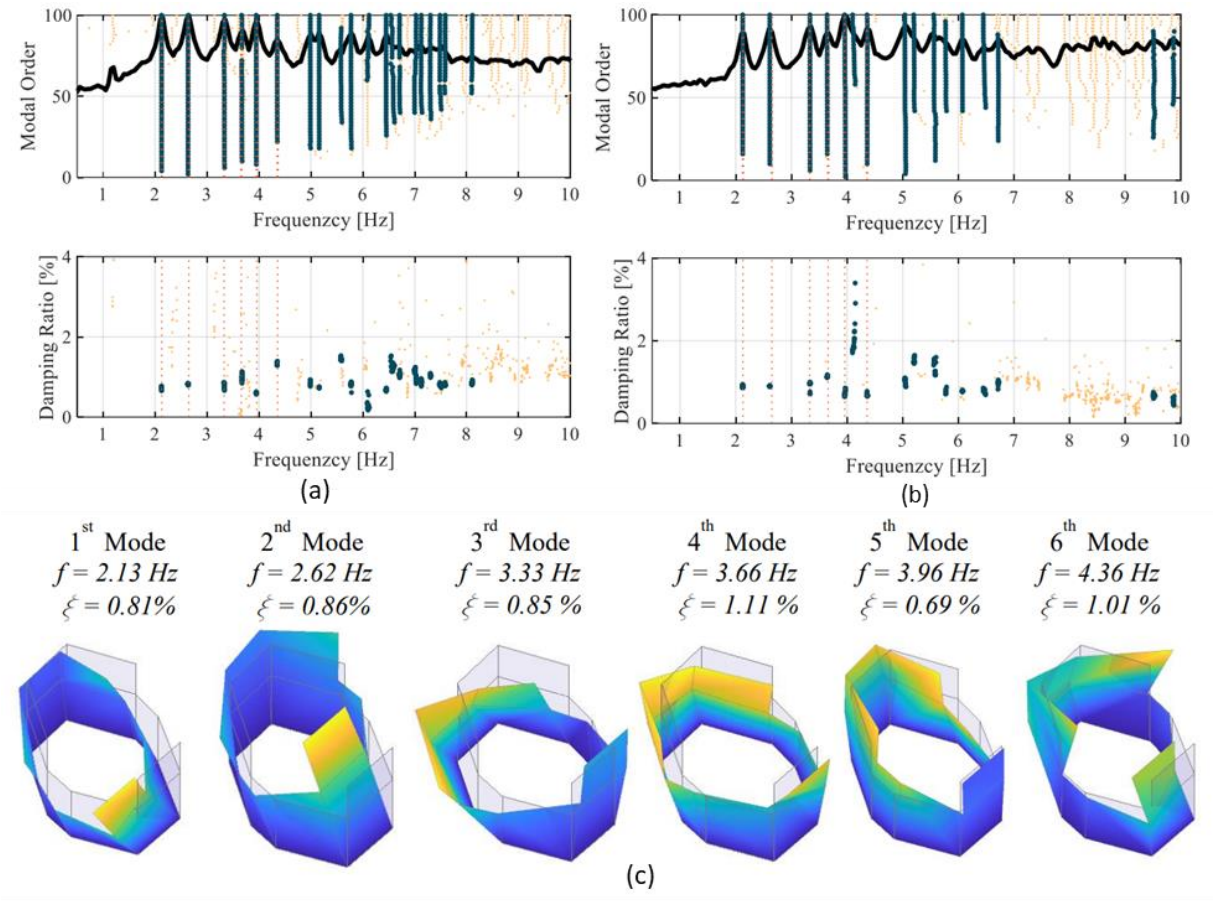

Figure 85 : Results of the dynamic identification: Stabilization diagram and Frequency Damping ratio plot of a) Conf.1 and b) Conf.2; c) identified modal parameters.

2.13	100	0.0	2.7	4.8	0.0	4.3
2.62	0.0	100	0.0	11.4	0.7	8.6
3.33	2.7	0.0	100	28.9	2.0	0.5
3.66	4.8	11.4	28.9	100	1.1	1.1
3.96	0.0	0.7	2.0	1.1	100	0.6
4.36	4.3	8.6	0.5	1.1	0.6	100
f [Hz]	*2.13*	*2.62*	*3.33*	*3.66*	*3.96*	*4.36*

Figure 86 : AutoMAC matrix obtained from the identified mode shapes.

4.2.4 Dynamic and static Monitoring system

The main purpose of the monitoring system of the church of Santa Maria in Via is to control the evolution of the façade over-turning mechanism activated by the 2016 seismic events. In this sense a permanent continuous static and dynamic monitoring system, remotely controlled, is designed.

Regarding the dynamic monitoring, the following instrumentation has been installed: *i*) n.4 piezoelectric accelerometers PCB 393 A03 at 12.6 m from the ground, with a sensitivity of 1 V/g and a measurement range of +/- 5 g; *ii*) n.1 piezoelectric accelerometer PCB 393 B31 at 12.6 m from the ground, with a sensitivity of 10 V/g and a measurement range of +/- 0.5 g; *iii*) n.1 triaxial MEMS accelerometer at the ground level to measure the base input signal; *iy*) n.2 capacitive tiltmeters SEIKA NB2 on the façade, with measurement range of +/- 10 degrees, a resolution minor that 0.002 degrees a linearity deviation of 0.2 % of measuring range. Accelerometers are connected to a NI 9234 module while the tiltmeters are connected to a NI 9230 module.

Regarding the static and environmental monitoring, the instrumentation installed encompasses: *i*) n.2 displacement sensors, rotative capacitive sensors TSF 100 with measurement range of +/- 50 mm, infinite resolution and a linearity minor that 0.25 % Full Scale (F.S.); *ii*) n.2 type T thermocouples with a plate terminal installed both on one element of the steel securing system and inside the church; and *iii*) n.1 wireless sensor Elitech RC-51H for internal temperature and relative humidity placed inside the church hall. Displacement sensors are connected to a NI 9230 module while the thermocouples are connected to a NI 9210 module. Figure 87 shows, respectively, the location and the type of sensors.

Data acquisition, storage and data transfer are controlled by a real-time cDAQ NI 9133 connected to the network via a router and remotely controlled. The acquisition software deployed on the cDAQ, which was developed in Labview environment, acquires data continuously, in real time, and sends it via ftp protocol to a server located at the Faculty of Engineering in Ancona. This approach, thanks to the continuous streaming of data and the determinism guaranteed by the acquisition system, makes it possible to investigate possible dependencies on environmental conditions in a short time, but also to record the response to seismic events without the risk of losing data samples. The data are stored in 20-minute-long files.

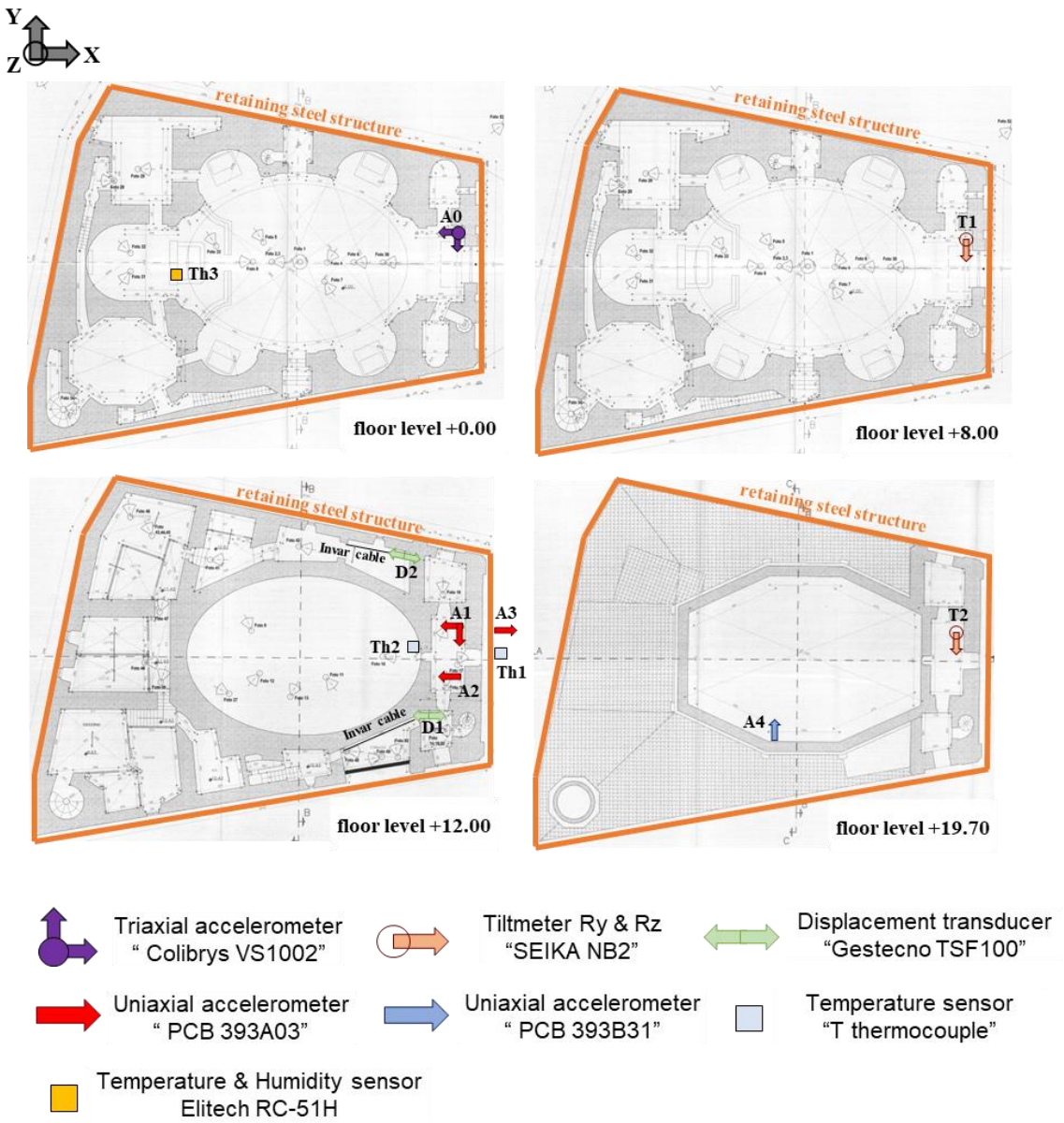

Figure 87 : Location and types of sensors.

1.1.1. Finite element model and Modal Updating

With the aim at identifying a reduced number of sensors used for the identification and for the monitoring of the Santa Maria in Via Church, better explained in the next chapter through the use of the Optimal Sensors Placement (OSP), a deep knowledge of the dynamic response of the structure is necessary. Consequently, a finite element model (FEM) of the structure has been developed.

More in detail, the geometrical model of the church has been elaborated after several geometrical surveys of the church, also considering the location and the extension of the damages following the 2016 central Italy seismic sequence. Regarding the typology of materials, being not available any in situ or laboratory mechanical test to evaluate the mechanical properties, visual inspections have been

done to classify and to group the typologies of masonry in macro elements, by assigning them mechanical properties available from literature.

Four different masonry types (M1, M2, M3 and M4) were recognised. M1 masonry consists of two unconnected outer layers of regular-textured bricks containing a rubble infill. This type of masonry is used to build the perimeter walls of the façade. M2 masonry is a multi-layered stone masonry with irregular courses, used to build the inner walls of the façade and few walls of the body of the church, especially those with a high thickness. M3 masonry is a double-layer masonry with rubble filling and, as M1, the connection between the different layers is almost absent. This typology is adopted for most of the walls and, consequently, presents various thicknesses. Finally, M4 masonry is composed of two layers: the inner layer consists of brickwork, while the outer layer consists of rough stone blocks with irregular courses. This type is used for the walls of the lantern. Figure 88(a) shows volumes and location of each masonry typology within the body of the church. The collapsed parts of the church (rear part of the lantern and lateral sides of the façade) were filled with steel lattice systems, indicated as the Braced-up regions in which are considered as additional material to those previously described.

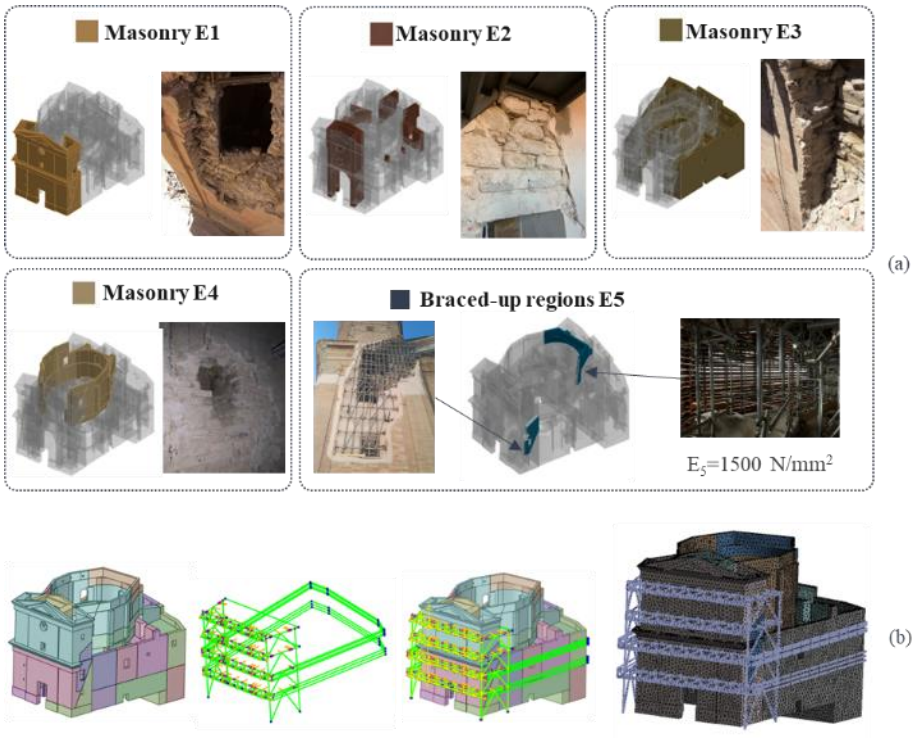

Figure 88 : Church model (a) recognized masonry typologies (b) FEM model.

The structure was modelled with solid elements (SOLID186 and 187) by means of the ANSYS software. Five different regions of homogeneous and isotropic material relating to each masonry type described in the previous section were modelled. Furthermore, the external steel system was included in the model because it can contribute to the whole structural dynamic response, being in contact with

the church façade; beam elements are used to model both the steel trusses and the steel cables surrounding the entire church. Figure 88(b) shows the geometric model and the FEM one.

Finally, with the aim at numerically reproduce the dynamic behaviour of structure experimentally identified through Operational Modal Analysis (OMA) techniques, it has been used the Particle Swarm Optimization (PSO) algorithm to calibrate model parameters [Arezzo et all. - 2022] [61]. This procedure is a stochastic optimization technique inspired by the social behaviour of a population of birds [Kennedy and Eberhart – 1995] [62], and some applications of its use for the modal updating of civil engineering structures, can be found in [Tran-Ngoc et all. – 2018] [64] and [Saada et all. – 2013] [63].

The variables to calibrated are the masonry elastic moduli E1, E2, E3 and E4, being the elastic modulus E5 the one of the materials used in the repaired regions. The objective function that considers the distance between the real dynamic behaviour and that of the numerical model is shown by the Equation (4.2-1)

$$err(e) = ln\left(1 + \left|\frac{f_{num}(e) - f_{exp}}{f_{exp}}\right| + (1 - MAC_{num,exp}(e)\right) \quad (4.2\text{-}1)$$

where:

f_{num} = natural frequency of numerical mode

f_{exp} = natural frequency of experimental mode

$MAC_{num,exp}$ = modal assurance criterion to compare the numerical modal shape with the experimental one. (4.2-2)

$e = \begin{vmatrix} E_1 \\ E_2 \\ E_3 \\ E_4 \\ E_5 \end{vmatrix}$ is the objective vector

Figure 89(a) shows the modal parameters of the calibrated model, while and Figure 89(b) the MAC matrix between the numerical and experimental mode shapes.

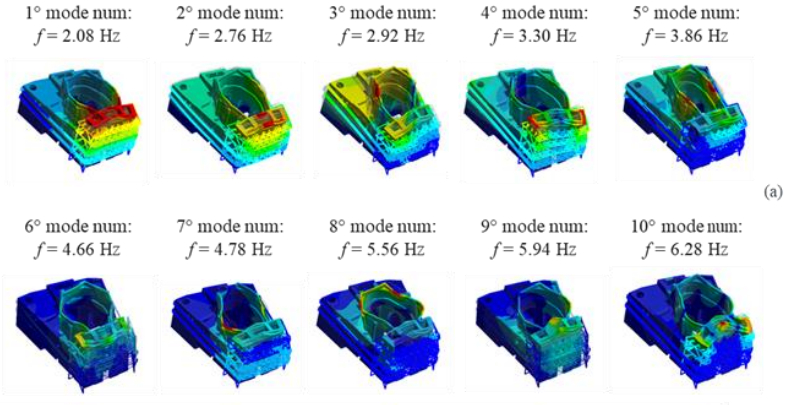

(a)

Exp. [Hz]	MAC									
2.11	0.95	0.00	0.07	0.03	0.00	0.01	0.19	0.19	0.03	0.00
2.61	0.00	0.86	0.08	0.01	0.03	0.20	0.02	0.00	0.08	0.04
3.34	0.05	0.05	0.89	0.04	0.00	0.04	0.21	0.01	0.41	0.01
3.64	0.06	0.02	0.45	0.77	0.03	0.00	0.02	0.00	0.04	0.00
3.97	0.00	0.01	0.05	0.03	0.94	0.34	0.02	0.00	0.01	0.02
4.36	0.07	0.02	0.11	0.00	0.21	0.51	0.18	0.02	0.04	0.00
5.02	0.24	0.01	0.23	0.05	0.01	0.11	0.67	0.44	0.18	0.00
5.17	0.05	0.03	0.01	0.08	0.06	0.07	0.28	0.47	0.07	0.00
5.56	0.11	0.29	0.01	0.07	0.02	0.26	0.04	0.30	0.44	0.20
5.76	0.00	0.01	0.00	0.00	0.01	0.01	0.01	0.02	0.17	0.42
Model [Hz]→	2.08	2.76	2.92	3.30	3.86	4.66	4.78	5.57	5.95	6.28
Error [%] →	1.7%	5.5%	12.6%	9.3%	2.7%	6.8%	4.9%	7.6%	7.1%	9.0%
Mode n →	**1**	**2**	**3**	**4**	**5**	**6**	**7**	**8**	**9**	**10**

(b)

Figure 89 : Results of updating (a) FEM modal shapes (b) MAC between experimental and numerical modes.

4.2.5 Optimal Sensor placement

Regarding the dynamic monitoring system, the current configuration has been optimized from the preliminary configuration characterized by only accelerometers placed on the façade (i.e., A1 e A2, Figure 90).

This sensors reorganization has been done necessarily because, from an analysis of the collected data during a training period, as it is shown in Figure 90, such configuration of accelerometers does not recognize all the vibrational modes identified in the preliminary dynamic identification test (see Figure 85(c). More in detail, it can be observed that only the 2nd vibration mode is continuously identified in every data acquisition cycle, differently from the others.

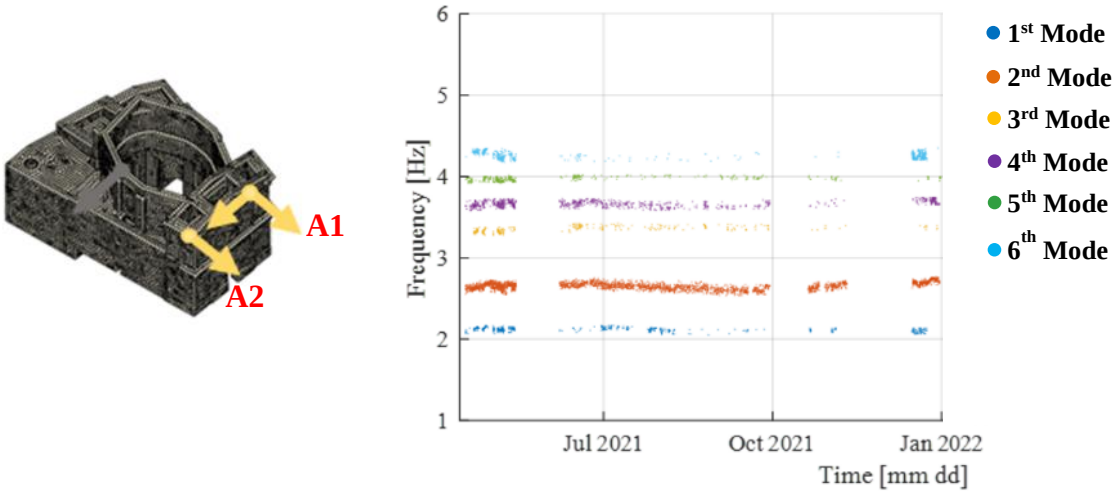

Figure 90 : frequencies identified with the preliminary Accelerometers configuration.

The Optimal Sensor Placement (OSP) procedure has been done following an approach presented by [Kammer – 1991] [65], which is called the Effective Independence (EI). This method is an iterative method where the set of candidate positions is quickly reduced to the number of available sensors. The vector $\boldsymbol{E}$ (4.2-3) represents the distribution of "Effective Independence" of a set of candidate positions and it is defined as the diagonal of the matrix

$$\boldsymbol{E} = \boldsymbol{\psi}^T \boldsymbol{\psi} \{\boldsymbol{\psi}^T \boldsymbol{\psi}\}^{-1} \boldsymbol{\psi}^T \quad (4.2\text{-}3)$$

where $\boldsymbol{\psi}$ is a matrix of finite element target modes partitioned according to a given sensor distribution. The i-th term of $\boldsymbol{E}$ represents the contribution of the sensor at the i-th position to the linear independence of the modes. If $\boldsymbol{E_i}$ is equal to 0, the sensor at that position does not contribute at the mode identification, otherwise, if $\boldsymbol{E_i}$ is equal to 1 this position must be maintained in the final sensor configuration. Different sensor positions are classified iteratively and those that do not contribute at

the identification of the modal shapes, are recognized and eliminated. The best approximation of the optimal configuration is achieved by deleting one position at a time.

In this work, the analysis has been carried out with reference to 5 modes of vibration and by considering only the DOFs on the external surfaces of the model for a total number of more than 250,000 possible DOFs. To make the analysis faster, the points to be analysed were randomly sampled to 25,000, moreover, each iteration eliminates the position that less contributes to the system's Effective Independence and the iterations end when only five positions, characterized by $\boldsymbol{E} = 1$ remain.

With the aim of limiting the number of sensors as much as possible, two of the five points identified were selected manually. Figure 91 shows the results of the OSP analysis carried out on the updated model of the church.

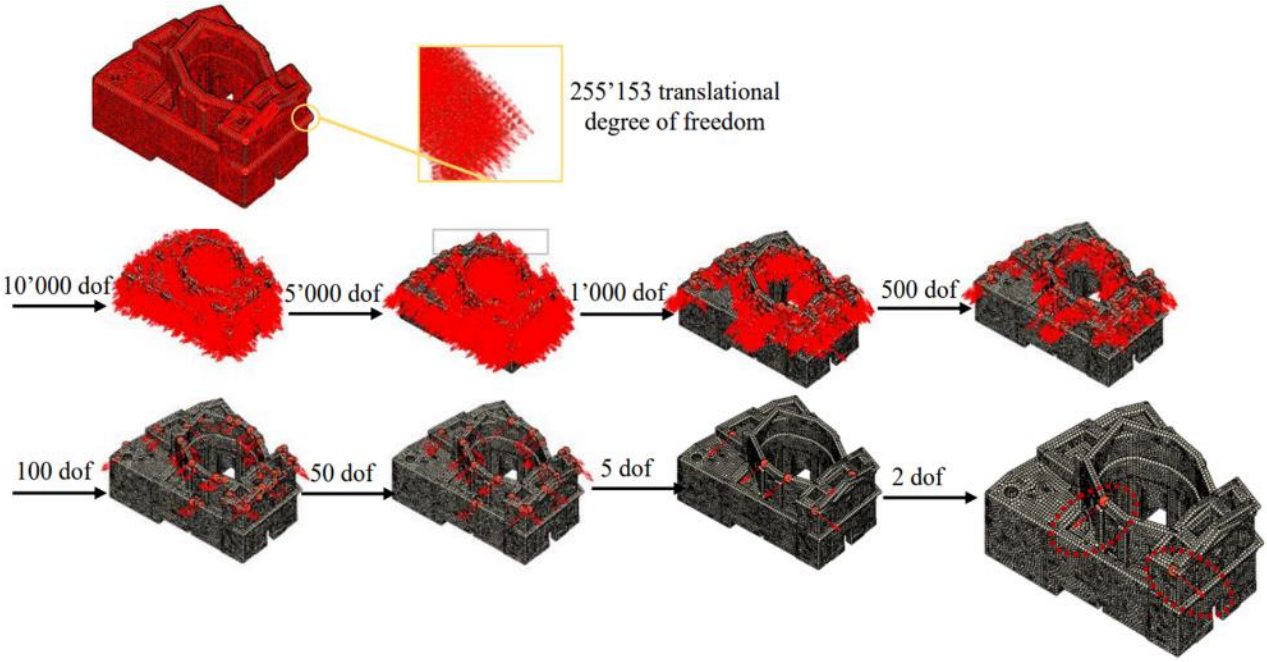

Figure 91 : Evolution of the Optimal Sensor Position procedure.

The efficiency of this OSP approach is shown in Figure 92, where the accuracy of the identified frequencies is compared between the preliminary configurations of accelerometers and the one achieved after the use of the OSP procedure, following which an accelerometer (A4) has been moved and installed on the top of lantern. It can be observed that, thanks to the presence of this new sensor, all the vibration modes are identified.

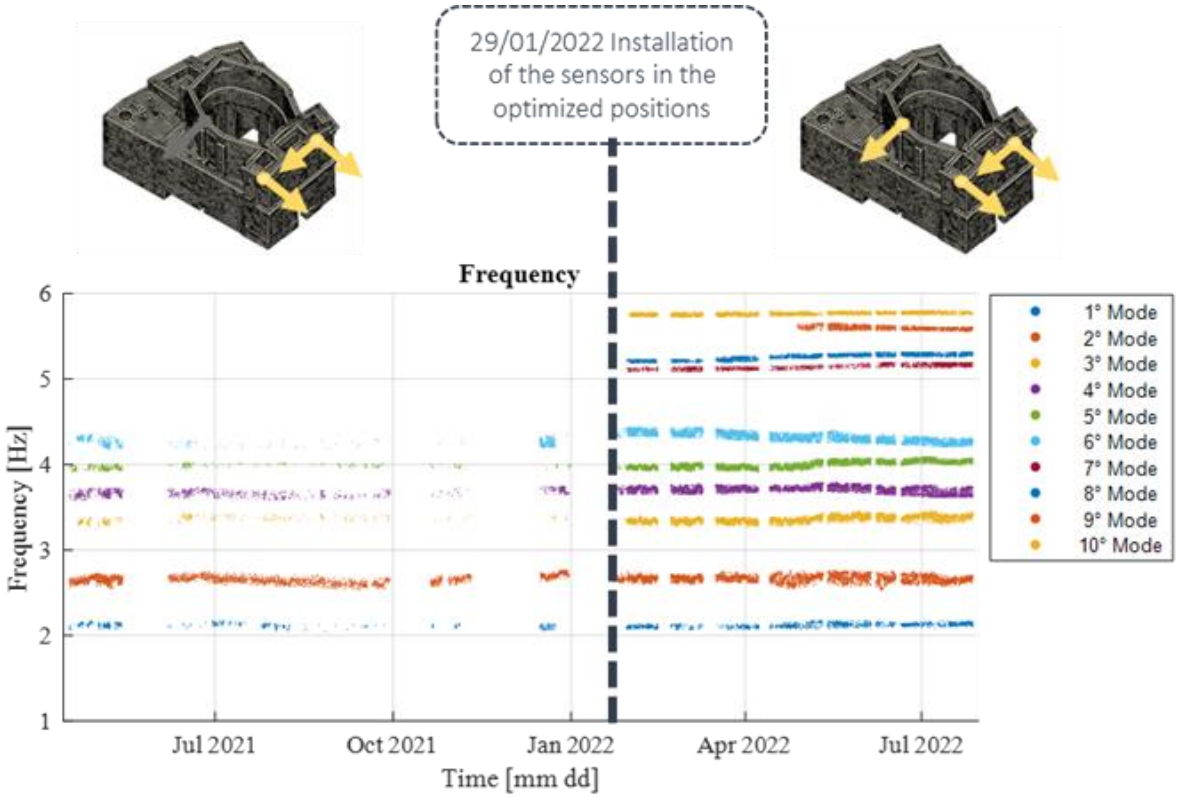

Figure 92 : Comparison of the frequencies identified before and after the OSP procedure.

4.2.6 Results of structural monitoring

In this section are summarized the results obtained by the structural monitoring. The processed data acquired by the implemented monitoring system is reported in Figure 93 Figure 93 (a) shows the natural frequencies identified over time; it can be observed that, thanks to the presence of this new sensor, all the vibration modes are identified (Region 2). In addition, the SSI/PC algorithm with the clustering analysis give a clear result for the first five modal shapes while for the remaining higher modal shapes the identification is less marked. Figure 93 (b) shown the displacements measure of the out-plane façade, acquired by D2 transducers (red line) and D1 transducer (blue line). Regarding the displacement measures, the façade initially shows a synchronous behaviour so far November 2022, subsequently it is characterized by a roto-translation behaviour. Currently the difference between the D1 and D2 transducers measure are around +/- 1.5 mm. Figure 93 (c) shows the value of the overturning façade mechanism; in detail T1 tiltmeter (blue line) and T2 tiltmeter (green line) measure the out of plane façade rotation while the T3 tiltmeter (magenta line) and T4 tiltmeter (red line) measure the in-plane façade rotation. It can be observed that T1 and T2 measure confirm the out of plane mechanism. Finally, in Figure 93 (d) are plotted the environmental conditions values, red dots are related with the external temperature while the blue line with the indoor temperature.

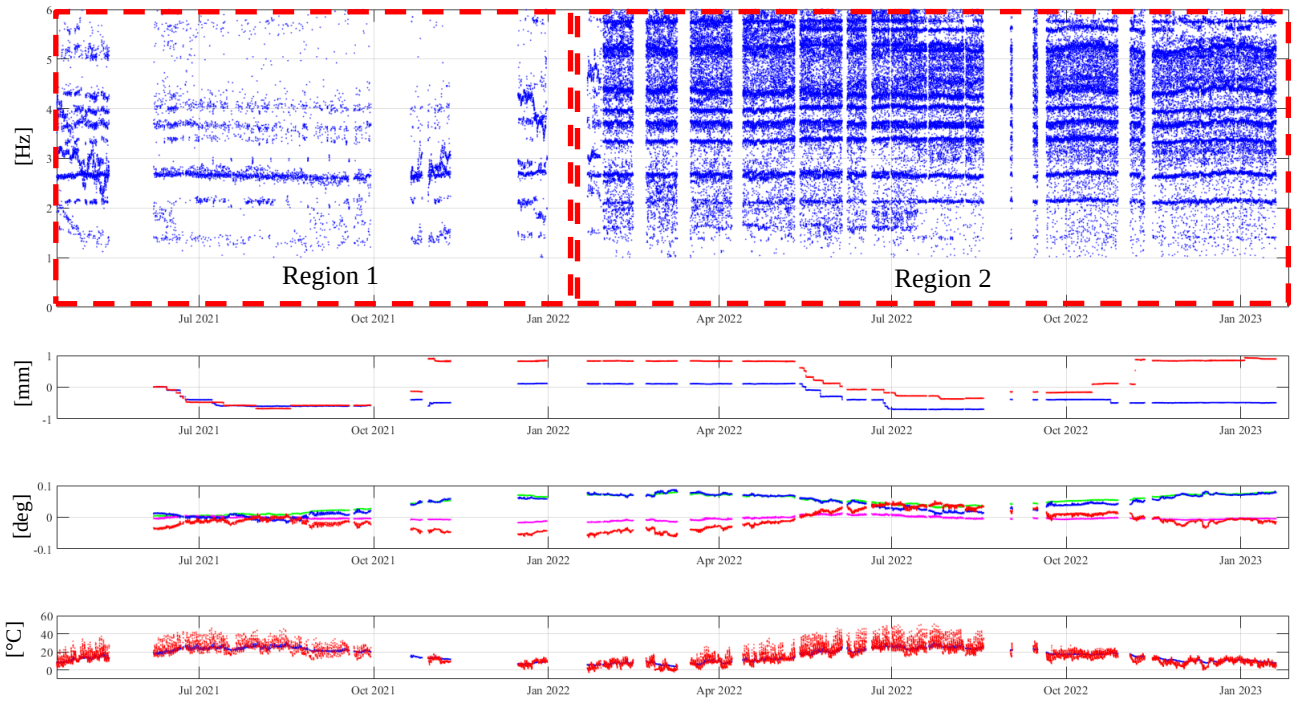

Figure 93 : Results of structural monitoring (a) natural frequencies identified, (b) out-plane façade displacement, (c) overturning façade mechanism measures and (d) external and indoor temperature.

Further detail to developed for improve the interpretation of the collected monitoring data are:

- to remove the environmental (i.e., temperature) effects on the natural frequency's values identified thought a statistical model that infer the distribution of each frequency with changes of temperature values.
- to analysed coupled effects between the church and the external retaining steel structure.
- to increase the information about the dynamical behaviour meaning that on the definition and construction of the modal shapes thanks to the inclinometer measurements.
- to reconstruct the in-elevation displacement profile with both the displacement measurements and the inclinometer measurements.

Conclusion

From the analysis of results obtained by the monitoring system designed and installed in the Portico da Varano, an architectural heritage of the Camerino city in Ducal Palace, it can be observed that the design of an idoneous SHM system for the evaluation of the response of the structure during its service life permits to improve the knowledge of the characteristic response of the buildings. Moreover, such system also allows to monitor if there is an evolution of the crack patterns occurred in the building after the seismic sequence, and to integrate the proposed approach to characterize and relate the response to low energy earthquakes happened near the site of interest, giving, this way, a complete understanding of the structural behaviour.

More in detail, the following conclusions can be drawn:

- the embedded monitoring system designed that continuously acquire data, gives a real-time control of the structure.
- the preliminary activities performed to enhance the structural knowledge, such as geometrical survey, relief of the crack patterns and ambient vibration tests, provide the basis for the design and the identification of proper sensors to be used in the embedded monitoring system. Among the choices to be done there is the numbers and types of sensors and their correct positions to control the sought-after behaviour.
- the SSI/Cov methodology has been chosen and used in the auto OMA algorithm developed to identify and to track the evolution and the fluctuation of the dynamic properties over-time, by also monitoring the environmental parameters (i.e., temperature).
- the configuration chosen to monitor the cracks on the vaults can describe the complete displacements time-history due to both the fluctuation of environmental conditions and to low energy seismic events. Additional information about cracks can be efficiently combined with dynamic monitoring to improve the response model.
- the new approach developed that is able to relate the response of the system to seismic events happened near the site give a comprehensive picture of the state of conservation of the building and of its structural behaviour. Allowing, also, to identify possible progressions of the state of damages and if there is a discrepancy between the response before and after possible further events.

References

[1] Canuti, C., Carbonari, S., Dall'Asta, A., Dezi, L., Gara, F., Leoni, G., Morici, M., Petrucci, E., Prota, A., Zona, A., 2021. Post-Earthquake Damage and Vulnerability Assessment of Churches in the Marche Region Struck by the 2016 Central Italy Seismic Sequence. International Journal of Architectural Heritage 15, 1000–1021. https://doi.org/10.1080/15583058.2019.1653403

[2] Despotaki, V., Silva, V., Lagomarsino, S., Pavlova, I., Torres, J., 2018. Evaluation of Seismic Risk on UNESCO Cultural Heritage sites in Europe. International Journal of Architectural Heritage 12, 1231–1244. https://doi.org/10.1080/15583058.2018.1503374

[3] Francesco Doglioni, Alberto Moretti, Vincenzo Petrini, 1994. Le chiese e il terremoto : dalla vulnerabilità constatata nel terremoto del Friuli al miglioramento antisismico nel restauro, verso una politica di prevenzione.

[4] Pavia, A., Scozzese, F., Petrucci, E., Zona, A., 2021. Seismic Upgrading of a Historical Masonry Bell Tower through an Internal Dissipative Steel Structure. Buildings 11, 24. https://doi.org/10.3390/buildings11010024

[5] Brincker, R., Ventura, C., 2015. Introduction to operational modal analysis. John Wiley and Sons, Inc, Chichester, West Sussex.

[6] Rainieri, C., Fabbrocino, G., 2014. Operational modal analysis of civil engineering structures: an introduction and guide for applications. Springer, New York. https://doi.org/10.1007/978-1-4939-0767-0

[7] Farrar, C.R., Worden, K., 2013. Structural health monitoring: a machine learning perspective. Wiley, Chichester, West Sussex, U.K.; Hoboken, N.J.

[8] Ewins, D.J., 2000. Modal testing: theory, practice, and application, 2nd ed. ed, Mechanical engineering research studies. Research Studies Press, Baldock, Hertfordshire, England ; Philadelphia, PA.

[9] Abd-Elhamed, A., Fathy, M., Abdelgaber, K.M., 2022. Closed-form solutions of dynamic vibration equations of seismically excited structures. Arab Journal of Basic and Applied Sciences 29, 318–329. https://doi.org/10.1080/25765299.2022.2124754

[10] Maia, N.M.M., Montalvão e Silva, J.M. (Eds.), 1997. Theoretical and experimental modal analysis, Mechanical engineering research studies. Research Studies Press ; Wiley, Taunton, Somerset, England : New York.

[11] Juang, J.-N., Pappa, R.S., 1985. An eigensystem realization algorithm for modal parameter identification and model reduction. Journal of Guidance, Control, and Dynamics 8, 620–627. https://doi.org/10.2514/3.20031

[12] Brown, D.L., Allemang, R.J., Zimmerman, R., Mergeay, M., 1979. Parameter Estimation Techniques for Modal Analysis. Presented at the 1979 Automotive Engineering Congress and Exposition, p. 790221. https://doi.org/10.4271/790221

[13] Box, G.E.P., Jenkins, G.M., Reinsel, G.C., 2008. Time Series Analysis, 1st ed, Wiley Series in Probability and Statistics. Wiley. https://doi.org/10.1002/9781118619193

[14] Gattulli, V., 2016. Implementation of Identification Methodologies on Large-Scale Structures, in: Chatzi, E., Papadimitriou, C. (Eds.), Identification Methods for Structural Health Monitoring, CISM International Centre for Mechanical Sciences. Springer International Publishing, Cham, pp. 1–34. https://doi.org/10.1007/978-3-319-32077-9_1

[15] George H. James, Thomas G. Carne, J. Laufer, 1995. The natural excitation technique (NExT) for modal parameter extraction from operating structures.

[16] Brincker, R., Amador, S., 2022. On the theory of random decrement. Mechanical Systems and Signal Processing 173, 109060. https://doi.org/10.1016/j.ymssp.2022.109060
[17] Brincker, R., Zhang, L., Andersen, P., 2001. Modal identification of output-only systems using frequency domain decomposition. Smart Mater. Struct. 10, 441–445. https://doi.org/10.1088/0964-1726/10/3/303
[18] Guillaume, P., Verboven, P., Vanlanduit, S., n.d. A Poly-Reference Implementation of the Least-Squares Complex Frequency-Domain Estimator.
[19] Lardies, J., Gouttebroze, S., 2002. Identification of modal parameters using the wavelet transform. International Journal of Mechanical Sciences 44, 2263–2283. https://doi.org/10.1016/S0020-7403(02)00175-3
[20] VanOverschee, P., De Moor, B.L.R., 1996. Subspace identification for linear systems: theory - implementation - applications. Kluwer Acad. Publ, Boston. https://doi.org/10.1007/978-1-4613-0465-4
[21] Peeters, B., De Roeck, G., 1999. REFERENCE-BASED STOCHASTIC SUBSPACE IDENTIFICATION FOR OUTPUT-ONLY MODAL ANALYSIS. Mechanical Systems and Signal Processing 13, 855–878. https://doi.org/10.1006/mssp.1999.1249
[22] Zhang, G., Tang, B., Tang, G., 2012. An improved stochastic subspace identification for operational modal analysis. Measurement 45, 1246–1256. https://doi.org/10.1016/j.measurement.2012.01.012
[23] Magalhães, F., Cunha, Á., 2011. Explaining operational modal analysis with data from an arch bridge. Mechanical Systems and Signal Processing 25, 1431–1450. https://doi.org/10.1016/j.ymssp.2010.08.001
[24] Filipe Manuel Rodrigues Leite de Magalhães, 2010. OPERATIONAL MODAL ANALYSIS FOR TESTING AND MONITORING OF BRIDGES AND SPECIAL STRUCTURES.
[25] Pastor, M., Binda, M., Harčarik, T., 2012. Modal Assurance Criterion. Procedia Engineering 48, 543–548. https://doi.org/10.1016/j.proeng.2012.09.551
[26] Cabboi, A., Magalhães, F., Gentile, C., Cunha, Á., 2017. Automated modal identification and tracking: Application to an iron arch bridge: Automated Modal Identification and Tracking. Struct. Control Health Monit. 24, e1854. https://doi.org/10.1002/stc.1854
[27] Magalhães, F., Cunha, Á., Caetano, E., 2009. Online automatic identification of the modal parameters of a long span arch bridge. Mechanical Systems and Signal Processing 23, 316–329. https://doi.org/10.1016/j.ymssp.2008.05.003
[28] Ubertini, F., Gentile, C., Materazzi, A.L., 2013. Automated modal identification in operational conditions and its application to bridges. Engineering Structures 46, 264–278. https://doi.org/10.1016/j.engstruct.2012.07.031
[29] Novoselsky, A., Kagan, E., 2021. An introduction to cluster analysis. https://doi.org/10.13140/RG.2.2.25993.57448/1
[30] Saxena, A., Prasad, M., Gupta, A., Bharill, N., Patel, O.P., Tiwari, A., Er, M.J., Ding, W., Lin, C.-T., 2017. A review of clustering techniques and developments. Neurocomputing 267, 664–681. https://doi.org/10.1016/j.neucom.2017.06.053
[31] Talabis, M.R.M., McPherson, R., Miyamoto, I., Martin, J.L., Kaye, D., 2015. Analytics Defined, in: Information Security Analytics. Elsevier, pp. 1–12. https://doi.org/10.1016/B978-0-12-800207-0.00001-0

[32] Marrongelli, G., Gentile, C., 2019. DEVELOPMENT AND APPLICATION OF AUTOMATED OMA ALGORITHMS.
[33] Gentile, C., Ruccolo, A., Canali, F., 2019. Continuous monitoring of the Milan Cathedral: dynamic characteristics and vibration-based SHM. J Civil Struct Health Monit 9, 671–688. https://doi.org/10.1007/s13349-019-00361-8
[34] Masciotta, M.-G., Ramos, L.F., Lourenço, P.B., 2017. The importance of structural monitoring as a diagnosis and control tool in the restoration process of heritage structures: A case study in Portugal. Journal of Cultural Heritage 27, 36–47. https://doi.org/10.1016/j.culher.2017.04.003
[35] Morici, M., Canuti, C., Dall'Asta, A., Leoni, G., 2020. Empirical predictive model for seismic damage of historical churches. Bull Earthquake Eng 18, 6015–6037. https://doi.org/10.1007/s10518-020-00903-2
[36] Ubertini, F., Cavalagli, N., Kita, A., Comanducci, G., 2018. Assessment of a monumental masonry bell-tower after 2016 Central Italy seismic sequence by long-term SHM. Bull Earthquake Eng 16, 775–801. https://doi.org/10.1007/s10518-017-0222-7
[37] Kita, A., Cavalagli, N., Ubertini, F., 2019. Temperature effects on static and dynamic behavior of Consoli Palace in Gubbio, Italy. Mechanical Systems and Signal Processing 120, 180–202. https://doi.org/10.1016/j.ymssp.2018.10.021
[38] Ramos, L.F., Aguilar, R., Lourenço, P.B., Moreira, S., 2013. Dynamic structural health monitoring of Saint Torcato church. Mechanical Systems and Signal Processing 35, 1–15. https://doi.org/10.1016/j.ymssp.2012.09.007
[39] Cabboi, A., Gentile, C., Saisi, A., 2017. From continuous vibration monitoring to FEM-based damage assessment: Application on a stone-masonry tower. Construction and Building Materials 156, 252–265. https://doi.org/10.1016/j.conbuildmat.2017.08.160
[40] Foti, D., Diaferio, M., Giannoccaro, N.I., Mongelli, M., 2012. Ambient vibration testing, dynamic identification and model updating of a historic tower. NDT & E International 47, 88–95. https://doi.org/10.1016/j.ndteint.2011.11.009
[41] Ramos, L.F., Marques, L., Lourenço, P.B., De Roeck, G., Campos-Costa, A., Roque, J., 2010. Monitoring historical masonry structures with operational modal analysis: Two case studies. Mechanical Systems and Signal Processing 24, 1291–1305. https://doi.org/10.1016/j.ymssp.2010.01.011
[42] Saisi, A., Gentile, C., Guidobaldi, M., 2015. Post-earthquake continuous dynamic monitoring of the Gabbia Tower in Mantua, Italy. Construction and Building Materials 81, 101–112. https://doi.org/10.1016/j.conbuildmat.2015.02.010
[43] Cavalagli, N., Kita, A., Ubertini, F., 2017. The role of dynamic monitoring for seismic assessment of monumental heritage buildings : an application to Palazzo dei Consoli in Gubbio.
[44] Lorenzoni, F., Casarin, F., Caldon, M., Islami, K., Modena, C., 2016. Uncertainty quantification in structural health monitoring: Applications on cultural heritage buildings. Mechanical Systems and Signal Processing 66–67, 268–281. https://doi.org/10.1016/j.ymssp.2015.04.032
[45] Gharehbaghi, V.R., Noroozinejad Farsangi, E., Noori, M., Yang, T.Y., Li, S., Nguyen, A., Málaga-Chuquitaype, C., Gardoni, P., Mirjalili, S., 2022. A Critical Review on Structural Health Monitoring: Definitions, Methods, and Perspectives. Arch Computat Methods Eng 29, 2209–2235. https://doi.org/10.1007/s11831-021-09665-9

[46] Akaike, H., 1998. Information Theory and an Extension of the Maximum Likelihood Principle, in: Parzen, E., Tanabe, K., Kitagawa, G. (Eds.), Selected Papers of Hirotugu Akaike, Springer Series in Statistics. Springer New York, New York, NY, pp. 199–213. https://doi.org/10.1007/978-1-4612-1694-0_15

[47] Baker, J.W., 2015. Efficient Analytical Fragility Function Fitting Using Dynamic Structural Analysis. Earthquake Spectra 31, 579–599. https://doi.org/10.1193/021113EQS025M

[48] Baker, J.W., n.d. Introduction to Probabilistic Seismic Hazard Analysis.

[49] Sabetta, F., Pugliese, A., n.d. Estimation of Response Spectra and Simulation of Nonstationary Earthquake Ground Motions.

[50] Scordilis, E.M., 2006. Empirical Global Relations Converting M S and m b to Moment Magnitude. J Seismol 10, 225–236. https://doi.org/10.1007/s10950-006-9012-4

[51] Cipriani, L., Morici, M., Zona, A., Leoni, G., Dall'Asta, A., 2023. Preliminary results in the automated detection of operational modal properties of the Portico Varano in the Camerino Ducal Palace. Procedia Structural Integrity 44, 2106–2113. https://doi.org/10.1016/j.prostr.2023.01.269

[52] Döhler, M., Reynders, E., Magalhães, F., Mevel, L., Roeck, G.D., Cunha, Á., 2011. Pre- and Post-identification Merging for Multi-Setup OMA with Covariance-Driven SSI, in: Dynamics of Bridges, Volume 5, Conference Proceedings of the Society for Experimental Mechanics Series. Springer New York, New York, NY, pp. 57–70. https://doi.org/10.1007/978-1-4419-9825-5_7

[53] Reynders, E., Magalhães, F., Roeck, G.D., Cunha, Á., n.d. Merging Strategies for Multi-setup Operational Modal Analysis: Application to the Luiz I Steel Arch Bridge.

[54] Bokaian, A., 1990. Natural frequencies of beams under tensile axial loads. Journal of Sound and Vibration 142, 481–498. https://doi.org/10.1016/0022-460X(90)90663-K

[55] Duvnjak, I., Ereiz, S., Damjanović, D., Bartolac, M., 2020. Determination of Axial Force in Tie Rods of Historical Buildings Using the Model-Updating Technique. Applied Sciences 10, 6036. https://doi.org/10.3390/app10176036

[56] Gentile, C., Poggi, C., Ruccolo, A., Vasic, M., 2017. Dynamic assessment of the axial force in the tie-rods of the Milan Cathedral. Procedia Engineering 199, 3362–3367. https://doi.org/10.1016/j.proeng.2017.09.442

[57] Gentilini, C., Marzani, A., Mazzotti, M., 2013. Nondestructive characterization of tie-rods by means of dynamic testing, added masses and genetic algorithms. Journal of Sound and Vibration 332, 76–101. https://doi.org/10.1016/j.jsv.2012.08.009

[58] Kim, B.H., Park, T., 2007. Estimation of cable tension force using the frequency-based system identification method. Journal of Sound and Vibration 304, 660–676. https://doi.org/10.1016/j.jsv.2007.03.012

[59] Resta, C., Chellini, G., De Falco, A., 2020. Dynamic Assessment of Axial Load in Tie-Rods by Means of Acoustic Measurements. Buildings 10, 23. https://doi.org/10.3390/buildings10020023

[60] Arezzo, D., Nicoletti, V., Leonardo, C., Carbonari, S., Leoni, G., Gara, F., n.d. First results of the monitoring of the façade damage mechanism of the "Santa Maria in Via" Church in Camerino following the 2016 Central Italy Earthquake.

[61] Arezzo, D., Quarchioni, S., Nicoletti, V., Carbonari, S., Gara, F., Leonardo, C., Leoni, G., 2023. SHM of historical buildings: The case study of Santa Maria in Via church in Camerino (Italy). Procedia Structural Integrity 44, 2098–2105. https://doi.org/10.1016/j.prostr.2023.01.268

[62] Kennedy, J., Eberhart, R., 1995. Particle swarm optimization, in: Proceedings of ICNN'95 - International Conference on Neural Networks. Presented at the ICNN'95 - International

Conference on Neural Networks, IEEE, Perth, WA, Australia, pp. 1942–1948. https://doi.org/10.1109/ICNN.1995.488968

[63] Saada, M.M., Arafa, M.H., Nassef, A.O., 2013. Finite element model updating approach to damage identification in beams using particle swarm optimization. Engineering Optimization 45, 677–696. https://doi.org/10.1080/0305215X.2012.704026

[64] Tran-Ngoc, H., Khatir, S., De Roeck, G., Bui-Tien, T., Nguyen-Ngoc, L., Abdel Wahab, M., 2018. Model Updating for Nam O Bridge Using Particle Swarm Optimization Algorithm and Genetic Algorithm. Sensors 18, 4131. https://doi.org/10.3390/s18124131

[65] Kammer, D.C., 1991. Sensor placement for on-orbit modal identification and correlation of large space structures. Journal of Guidance, Control, and Dynamics 14, 251–259. https://doi.org/10.2514/3.20635

[66] Keshmiry, A., Hassani, S., Mousavi, M., Dackermann, U., 2023. Effects of Environmental and Operational Conditions on Structural Health Monitoring and Non-Destructive Testing: A Systematic Review. Buildings 13, 918. https://doi.org/10.3390/buildings13040918

[67] Sohn, H., 2007. Effects of environmental and operational variability on structural health monitoring. Phil. Trans. R. Soc. A. 365, 539–560. https://doi.org/10.1098/rsta.2006.1935

[68] Cabboi, A., Gentile, C., Saisi, A., 2017. From continuous vibration monitoring to FEM-based damage assessment: Application on a stone-masonry tower. Construction and Building Materials 156, 252–265. https://doi.org/10.1016/j.conbuildmat.2017.08.160

[69] García-Macías, E., Ubertini, F., 2020. Automated operational modal analysis and ambient noise deconvolution interferometry for the full structural identification of historic towers: A case study of the Sciri Tower in Perugia, Italy. Engineering Structures 215, 110615. https://doi.org/10.1016/j.engstruct.2020.110615

[70] Mario Azzara, R., De Roeck, G., Girardi, M., Padovani, C., Pellegrini, D., Reynders, E., 2018. The influence of environmental parameters on the dynamic behaviour of the San Frediano bell tower in Lucca. Engineering Structures 156, 175–187. https://doi.org/10.1016/j.engstruct.2017.10.045

[71] Ubertini, F., Cavalagli, N., Kita, A., Comanducci, G., 2018. Assessment of a monumental masonry bell-tower after 2016 Central Italy seismic sequence by long-term SHM. Bull Earthquake Eng 16, 775–801. https://doi.org/10.1007/s10518-017-0222-7

[72] Ceravolo, R., Coletta, G., Miraglia, G., Palma, F., 2021. Statistical correlation between environmental time series and data from long-term monitoring of buildings. Mechanical Systems and Signal Processing 152, 107460. https://doi.org/10.1016/j.ymssp.2020.107460

[73] García-Macías, E., Ubertini, F., 2022. Least Angle Regression for early-stage identification of earthquake-induced damage in a monumental masonry palace: Palazzo dei Consoli. Engineering Structures 259, 114119. https://doi.org/10.1016/j.engstruct.2022.114119

[74] Gentile, C., Ruccolo, A., Canali, F., 2019. Long-term monitoring for the condition-based structural maintenance of the Milan Cathedral. Construction and Building Materials 228, 117101. https://doi.org/10.1016/j.conbuildmat.2019.117101

[75] Kita, A., Cavalagli, N., Ubertini, F., 2019. Temperature effects on static and dynamic behavior of Consoli Palace in Gubbio, Italy. Mechanical Systems and Signal Processing 120, 180–202. https://doi.org/10.1016/j.ymssp.2018.10.021

[76] Zonno, G., Aguilar, R., Boroschek, R., Lourenço, P.B., 2019. Analysis of the long and short-term effects of temperature and humidity on the structural properties of adobe buildings using

continuous monitoring. Engineering Structures 196, 109299. https://doi.org/10.1016/j.engstruct.2019.109299

[77] Erazo, K., Sen, D., Nagarajaiah, S., Sun, L., 2019. Vibration-based structural health monitoring under changing environmental conditions using Kalman filtering. Mechanical Systems and Signal Processing 117, 1–15. https://doi.org/10.1016/j.ymssp.2018.07.041

[78] Worden, K., Sohn, H., Farrar, C.R., 2002. NOVELTY DETECTION IN A CHANGING ENVIRONMENT: REGRESSION AND INTERPOLATION APPROACHES. Journal of Sound and Vibration 258, 741–761. https://doi.org/10.1006/jsvi.2002.5148

[79] Benjamin, J.R., Cornell, C.A., 2014. Probability, statistics, and decision for civil engineers, Dover edition. ed. Dover Publications, Inc, Mineola, New York.

Acknowledgments

First of all the person deserving the greatest gratitude is myself, for the perseverance shown day after day despite all the obstacles that life has thrown in my path.

A big thank you goes to my friend and colleague, Eng. Davide Arezzo PhD, who three years ago put my name forward when Prof. Fabrizio Gara was searching, on behalf of Prof. Andrea Dall'Asta, for potential candidates for the doctoral course.

So, a huge thank you goes to Prof. Andrea Dall'Asta for the opportunity he provided me to become part of his wonderful research group, composed of Prof. Graziano Leoni, Prof. Alessandro Zona, Prof. Michele Morici, Eng. Laura Gioiella PhD, Eng. Fabrizio Scozzese PhD, and Eng. Fabio Micozzi PhD. Thanks to all of you for the support and valuable teachings; you are fantastic individuals with a high scientific calibre.

Especially, I thank Prof. Michele Morici for the invaluable support given to me both in the development and critical analysis of the topic I tackled, enabling me to grasp its various facets. I also express my gratitude to Eng. Laura Gioiella PhD for her valuable advice.

A few words of thanks also go to my PhD fellow students Eng. Lucia Barchetta PhD, Eng Claudia Canuti PhD, Eng. Nicola Ceccolini, Eng. Lorenzo Principi, Eng. Alberto Poeta study friends and various outbursts.

Finally, I want to thank you Prof. Fabrizio Gara and his research team, in particular the monitoring group composed Eng. Davide Arezzo PhD, and Eng. Vanni Nicoletti PhD both for the meeting days done about the structural monitoring with the idea sharing target and the cooperation on the work done in the Santa Maria in Via church.